

VYSOKÉ UČENÍ TECHNICKÉ V BRNĚ

BRNO UNIVERSITY OF TECHNOLOGY



FAKULTA CHEMICKÁ
ÚSTAV CHEMIE MATERIÁLŮ

FACULTY OF CHEMISTRY
INSTITUTE OF MATERIALS SCIENCE

MOLECULAR MODELLING - STRUCTURE AND PROPERTIES OF CARBENE-BASED CATALYST

MOLEKULOVÉ MODELOVÁNÍ - STRUKTURA A VLASTNOSTI KATALYZÁTORŮ NA BÁZI
KARBENŮ

DIPLOMOVÁ PRÁCE

MASTER'S THESIS

AUTOR PRÁCE

AUTHOR

Bc. EVA KULOVANÁ

VEDOUCÍ PRÁCE

SUPERVISOR

RNDr. LUKÁŠ RICHTERA, Ph.D.

BRNO 2012



Brno University of Technology
Faculty of Chemistry
Purkyňova 464/118, 61200 Brno 12

Master's thesis Assignment

Number of master's thesis: **FCH-DIP0639/2011** Academic year: **2011/2012**
Institute: Institute of Materials Science
Student: **Bc. Eva Kulovaná**
Study programme: Chemistry, Technology and Properties of Materials (N2820)
Study field: Chemistry, Technology and Properties of Materials (2808T016)
Head of thesis: **RNDr. Lukáš Richtera, Ph.D.**
Supervisors:

Title of master's thesis:

Molecular modelling - Structure and Properties of carbene-based catalyst

Master's thesis assignment:

Several models of carbene compounds will be formed using software for molecular modelling. Geometry optimization and some spectroscopic properties (UV/Vis spectra) will be computed, possibly prediction of RA, IR and NMR spectra will be performed. Data from optimized structures like bond lengths and angles will be compared with those gained from CCDC (Cambridge Crystallographic Data Centre).

Deadline for master's thesis delivery: 11.5.2012

Master's thesis is necessary to deliver to a secretary of institute in three copies and in an electronic way to a head of master's thesis. This assignment is enclosure of master's thesis.

Bc. Eva Kulovaná
Student

RNDr. Lukáš Richtera, Ph.D.
Head of thesis

prof. RNDr. Josef Jančář, CSc.
Head of institute

In Brno, 15.1.2012

prof. Ing. Jaromír Havlica, DrSc.
Dean

ABSTRACT

By using molecular modelling it is possible to predict the behaviour of new compounds and to help interpreting of the experimental data. The objective of the thesis was the prediction of selected properties of polymerization catalysts based on carbenes, the prediction of their structures and spectral characteristics and the study of the mechanism of the ring-opening polymerization of lactide.

To confirm the behaviour of carbenes and their precursors based on chlorides selected characteristics of a molecule were studied. The calculation of selected molecular orbitals and electrostatic potential maps was made. Subsequently, bond distances and bond angles of selected imidazole and imidazoline compounds, "free" carbenes and their possible hydrolysis products were obtained by using computer programs. Data of structural similar compounds, which have already been characterized, were obtained from CCDC (Cambridge Crystallographic Data Centre) and were compared with the calculated data. Infrared and Raman spectra of the imidazole salt and the infrared spectrum of the appropriate carbene were measured. The measured spectra were compared with the predicted ones. For the better spectra interpretation the spectra of possible hydrolysis products were calculated. Subsequently, the mechanism of the ring-opening polymerization of lactide was investigated. Based on calculated energies of stationary points the novel mechanism of polymerization was suggested.

ABSTRAKT

Pomocí molekulového modelování je možné předpovídat chování nových látek a napomáhá při jinak obtížné interpretaci experimentálních dat. Cílem práce byla predikce vybraných vlastností polymeračních katalyzátorů na bázi karbenů, predikce jejich struktur a spektrálních charakteristik a studie mechanismu polymerace za otevření kruhu laktidu.

K ověření chování karbenů a jejich prekurzorů ve formě chloridů byly studovány vybrané charakteristiky molekuly. Byl proveden výpočet vybraných molekulových orbitalů a elektrostatických map. Následně pomocí počítačových programů byly získány teoretické vazebné délky a úhly vybraných imidazolových a imidazolinových sloučenin, karbenů a jejich možných produktů hydrolyzy. Data strukturně podobných, již charakterizovaných sloučenin, byla získána z CCDC (Cambridge Crystallographic Data Centre) a následně byla konfrontována s vypočítanými daty. Byla změřena infračervená a Ramanova spektra imidazolové soli a infračervené spektrum příslušného karbenu. Tato spektra byla konfrontována s napredikovanými. Pro lepší interpretaci spekter byla spočítána spektra možných produktů hydrolyzy. Následně byl studován mechanismus polymerace za otevření kruhu laktidu. Na základě spočítaných energií stacionárních bodů byl navržen nový mechanismus polymerace.

KEYWORDS

N-heterocyclic carbenes, *ab initio* methods, DFT methods, FTIR spectroscopy, Raman spectroscopy, transition states

KLÍČOVÁ SLOVA

N-heterocyclické karbeny, *ab initio* metody, DFT metody, FTIR spektroskopie, Ramanova spektroskopie, tranzitní stavy

KULOVANÁ, E. *Molecular modelling – structure and properties of carbene-based catalyst*. Brno: Vysoké učení technické v Brně, Fakulta chemická, 2012. 58 p. Vedoucí diplomové práce RNDr. Lukáš Richtera, Ph.D.

DECLARATION

I declare that the diploma thesis has been worked out by myself and that all the quotations from the used literary sources are accurate and complete. The content of diploma thesis is the property of the Faculty of Chemistry of Brno University of Technology and all commercial uses are allowed only if approved by both the supervisor and the dean of the Faculty of Chemistry, BUT.

.....
student's signature

ACKNOWLEDGMENTS

I would like to thank RNDr. Lukáš Richtera, Ph.D. and Mgr. Soňa Hermanová, Ph.D. for valuable advice and comments and Mgr. Jan Grůza, Ph.D. for help with calculations.

CONTENTS

1	Introduction	7
2	Theoretical part	8
2.1	Definition and classification of carbenes	8
2.2	N-heterocyclic carbenes	9
2.2.1	General properties of NHCs	11
2.2.2	NHCs as nucleophilic catalysts	12
2.2.3	Basicity	13
2.2.4	Mechanism of ring-opening polymerization	14
2.2.4.1	Monomer-activated mechanism	15
2.2.4.2	Chain-end-activated mechanism	17
2.2.5	Carbene precursors	18
2.3	Molecular modelling	20
2.3.1	General terms	20
2.3.1.1	Coordinate systems	20
2.3.1.2	Common units	20
2.3.1.3	Potential energy surfaces	21
2.4	Quantum mechanics	21
2.4.1	Approximations of <i>ab initio</i> methods	21
2.4.2	Electron correlation	22
2.4.3	Basis sets	23
2.4.4	Using <i>ab initio</i> methods	24
2.4.5	Semi-empirical methods	25
2.4.6	Density functional theory	25
2.5	Molecular mechanics	25
2.6	Geometry optimization	26
2.7	Infrared and Raman spectroscopy	26
2.7.1	Harmonic oscillator approximation	27
2.7.2	Principle of IR and RA spectroscopy	27
2.7.3	Prediction of spectra	28
2.8	Computer programs	29
2.8.1	Operating ArgusLab and PC GAMESS/Firefly	29
2.8.2	Operating Titan and Spartan	32
3	Experimental part	35
3.1	Studied compounds	35
3.2	Softwares and computational methods	35
3.2.1	Fundamental calculations	35
3.2.2	Geometry optimization	36
3.2.3	Spectra prediction	36
3.2.3	Study on the mechanism of ROP of lactide	36
3.3	Gained data	36
3.3.1	Databases	36
3.3.2	Measurement	37
3.3.2.1	FTIR spectra	37
3.3.2.2	RA spectra	37
4	Results and discussion	38

4.1	Fundamental calculations	38
4.1.1	Orbitals	38
4.1.2	Electrostatic potential maps	39
4.2	Geometry optimization.....	40
4.2.1	Carbenes and their precursors.....	40
4.2.2	Hydrolysis products.....	42
4.3	Spectra prediction	43
4.4	Study on the mechanism of the ROP of lactide	48
4.4.1	Simulation of the ring-opening of lactide.....	50
5	Conclusion.....	52
6	References	53
7	List of abbreviations	57
8	Nomenclature list.....	58
9	Appendix	

1 INTRODUCTION

Molecular modelling has made a significant progress together with the development of the computer technology. It utilizes the results of theoretical chemistry as inputs into efficient computer programs to calculate the structures and properties of molecules. First, computational quantum chemistry has been developed. The advancement of computer softwares has continued in many research groups. John Pople, who made the methods more efficient and made their application more popular, was awarded the Nobel Prize¹ in 1998.

On the basis of *ab initio* methods, which were proved to be competent for the prediction of molecular geometry, the carbene (methylene) intermediate in the gas-phase has been studied. In 1970, by using of Hartree-Fock calculations by Bender and Schaeffer it was investigated that the molecule of methylene is bent. This fact was proved in the next years by experiments. Nowadays, the accuracy of these methods is similar or better to that of most experimental methods¹.

2 THEORETICAL PART

2.1 Definition and classification of carbenes

The simplest representative of carbenes is methylene ($\text{H}_2\text{C}:$). Generally, carbenes with the formula of $\text{RR}'\text{C}:$ (Fig. 1) are neutral compounds containing a divalent carbon with only six valence electrons. They are classified as singlet and triplet carbenes differing significantly in chemical reactivity pattern. Singlet carbenes behave like zwitterions. Triplet carbenes participate in chemical reactions similarly like free radicals. Most carbenes have a nonlinear triplet ground state; however they have very short life-time.

Carbenes bonded as ligands to the transition metal centre, could be classified into two types: Fischer and Schrock carbenes. The Fischer carbenes are electrophilic at the carbene carbon atom and they are in singlet state. On the other hand, the Schrock carbenes have more nucleophilic carbene centre.

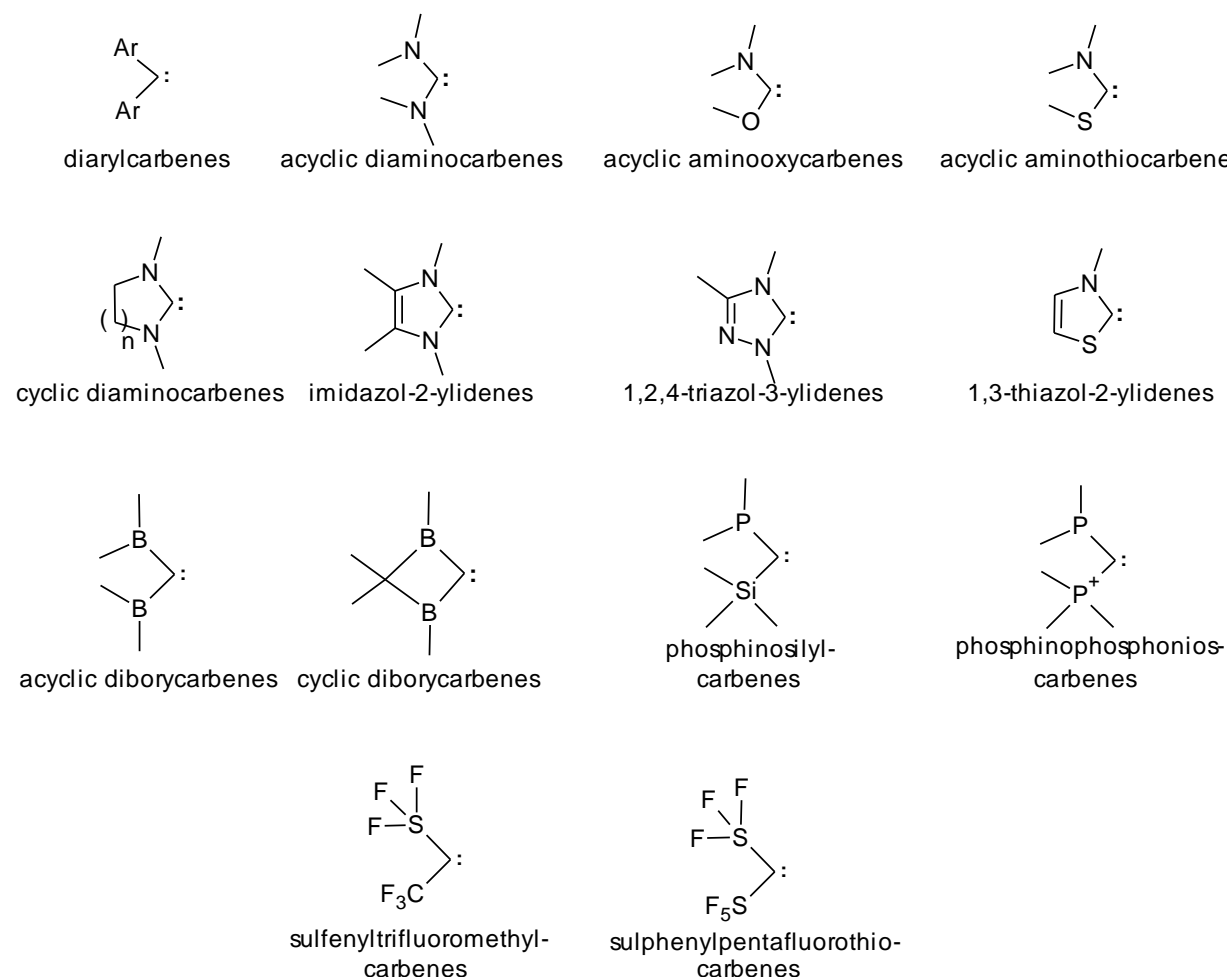


Fig. 1 Prepared types of carbenes

Heterocyclic carbenes contain at least one atom of carbon and at least one heteroatom such as oxygen, sulphur or nitrogen in the cycle. Heteroatom donor groups on carbene centre render the originally degenerate orbitals on carbon unequal in energy. Consequently, both the nucleophilicity of the carbon atom and the thermodynamic stability of the carbene compound

are increased. Although several combinations of heteroatoms in carbene ring are possible, only singlet carbenes with two nitrogen atoms (N-heterocyclic carbenes) were isolated as crystalline compounds² till 1997.

N-heterocyclic carbene structures were studied by Wanzlick *et al.*³ in the early 1960s - unfortunately without the successful preparation of stable “free” carbenes. Arduengo *et al.*⁴ succeed in preparation of “free” carbene by deprotonation of imidazolium ion in 1991 (Fig. 2).

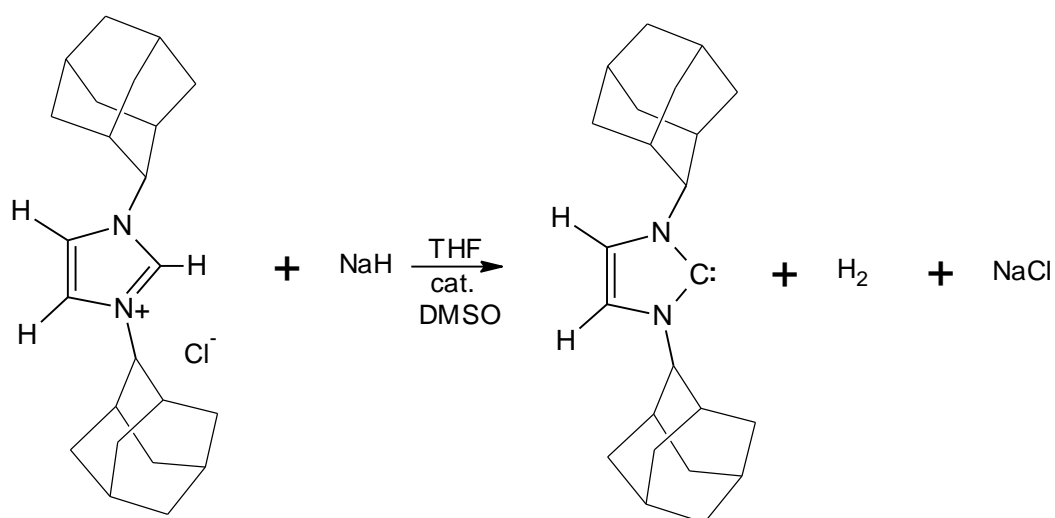


Fig. 2 Deprotonation of imidazolium salt

2.2 N-heterocyclic carbenes

N-heterocyclic carbenes (NHCs) are classified into the four main types: imidazol-2-ylidenes, imidazolin-2-ylidenes, 1,2,4-triazol-3-ylidenes and 1,3-thiazol-2-ylidenes (Fig. 3).

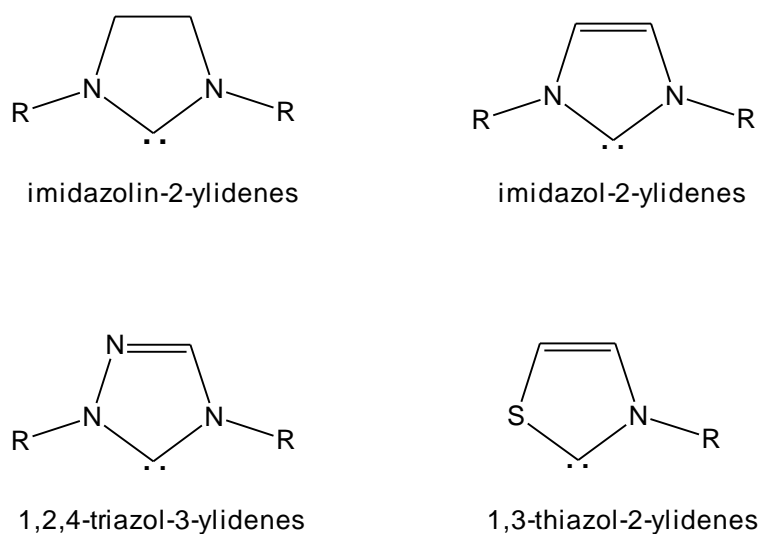


Fig. 3 Types of stable N-heterocyclic carbenes

NHCs could be synthesized by a variety of ways, for example by deprotonation of imidazolium salts⁴ (Fig. 2), by the elimination of methanol with 5-methoxy-1,3,4-triphenyl-4,5-dihydro-1H-1,2,4-triazol at higher temperature⁵ (Fig. 4a) or by reduction of thiones with potassium in boiling THF⁶ (Fig. 4b).

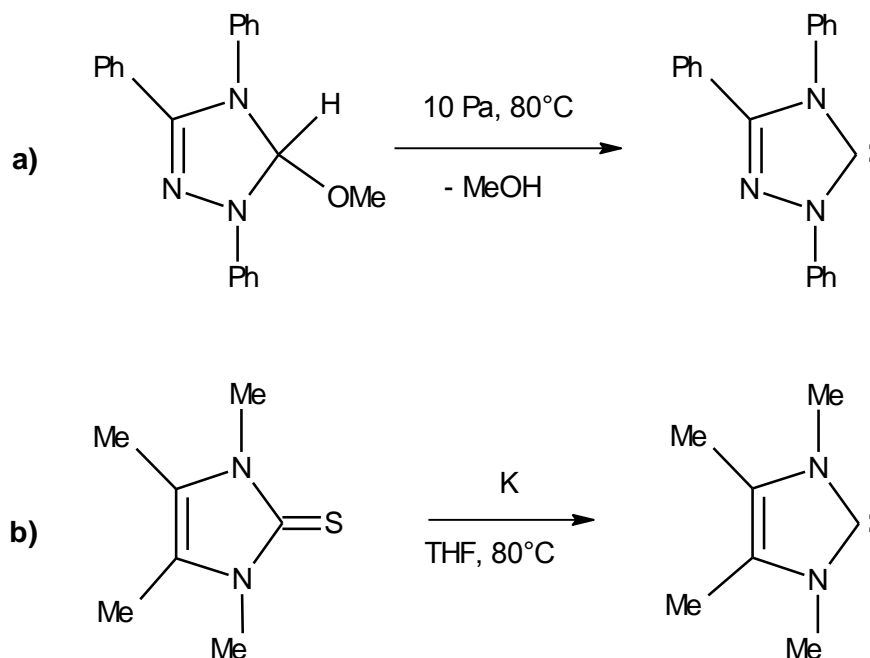


Fig. 4 The examples of the synthesis of *N*-heterocyclic carbenes

The carbenes that can be isolated as stable crystalline compounds at room temperature are also known as Arduengo carbenes. NHCs are often colourless crystals thermodynamically stable in the absence of oxygen and moisture⁴. In presence of air moisture imidazoline-2-ylidenes hydrolyze to ring-opened product^{7,8}, while imidazole-2-ylidenes can hydrolyze to two tautomeric ring-opened forms⁸. The reaction of an imidazole-2-ylidene with water in aqueous solution formed a stable solution of the corresponding imidazolium-hydroxide. On the other hand the hydrolysis of the carbene in a mainly aprotic environment with only traces of moisture yields a hydrogen-bridged carbene-water complex that converts slowly to two tautomeric ring opened forms⁸ (Fig. 5). Moreover, some carbenes are stable only in the form of solution⁹.

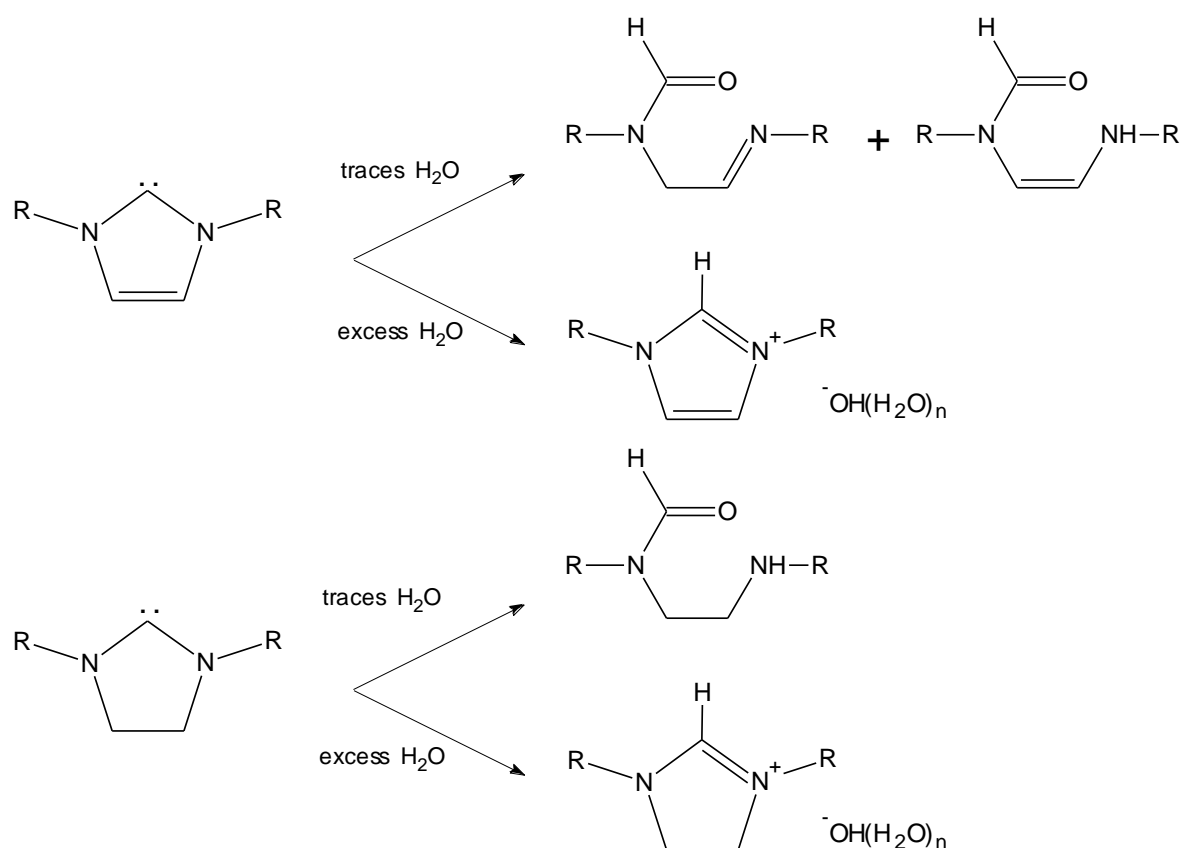


Fig. 5 The scheme of hydrolysis of imidazole-2-ylidenes and imidazoline-2-ylidenes

2.2.1 General properties of NHCs

NHCs have a pronounced low-energy of HOMO (highest occupied molecular orbital) and a high-energy of LUMO (lowest unoccupied molecular orbital)¹⁰. Due to the small HOMO-LUMO gaps carbenes are very reactive. They are stronger electron-pair donors (Lewis bases) than amines because of the lower electronegativity of carbon atom. Their electron-accepting capabilities are more significant than those of boranes. NHCs properties benefit from a “push-pull” effect, because the amino groups are π -donating (mesomeric effect) and σ -withdrawing (inductive effect)².

The stability of NHCs results mainly from electronic effects (mesomeric +M as well as inductive -I effects), although the steric hindrance plays an important role as well. In the imidazol-2-ylidenes the nitrogen lone pairs and the C=C double bonds ensure the kinetic stability because of their high electron density and π -donation from nitrogen lone pairs plays a minor role. The aromatic character of these carbenes is less pronounced than that of imidazolium salts precursors, but it brings an additional stabilization of $\sim 109 \text{ kJ}\cdot\text{mol}^{-1}$ ($\sim 26 \text{ kcal}\cdot\text{mol}^{-1}$)¹¹.

Generally, the kinetic stability of compounds is crucial for preparative chemistry. Stable NHCs are investigated for several reasons. The attention is paid to the structure, reactivity and theoretical understanding of these highly Lewis basic (one of the strongest known bases) and nucleophilic molecules. Moreover, stable “ylidene” carbenes are used for preparation of main group and transitional metal complexes. It is worth mentioning that several “*in situ*” methods for syntheses of metal “ylidene” complexes without the necessity of “free carbenes” or their equivalents isolation have also been developed².

2.2.2 NHCs as nucleophilic catalysts

NHCs belong to naturally occurring nucleophilic catalysts and have found also various catalytic applications in synthetic chemistry². Some of them are utilized in important organic synthesis, for example in the formoin condensation reactions converting C2 to C6 carbohydrates, in oxidative benzoin condensation of aldehydes, alcohols and aromatic nitro compounds to yield esters, in the Michael-Stetter reaction yielding 1,4-dicarbonyl derivatives and in the benzoin condensation of aldehydes to α -hydroxyketones¹² (Fig. 6). Chiral triazolium salts as catalyst precursors are used in asymmetric variants of ylide-catalyzed benzoin condensations and Michael-Stetter reaction¹³.

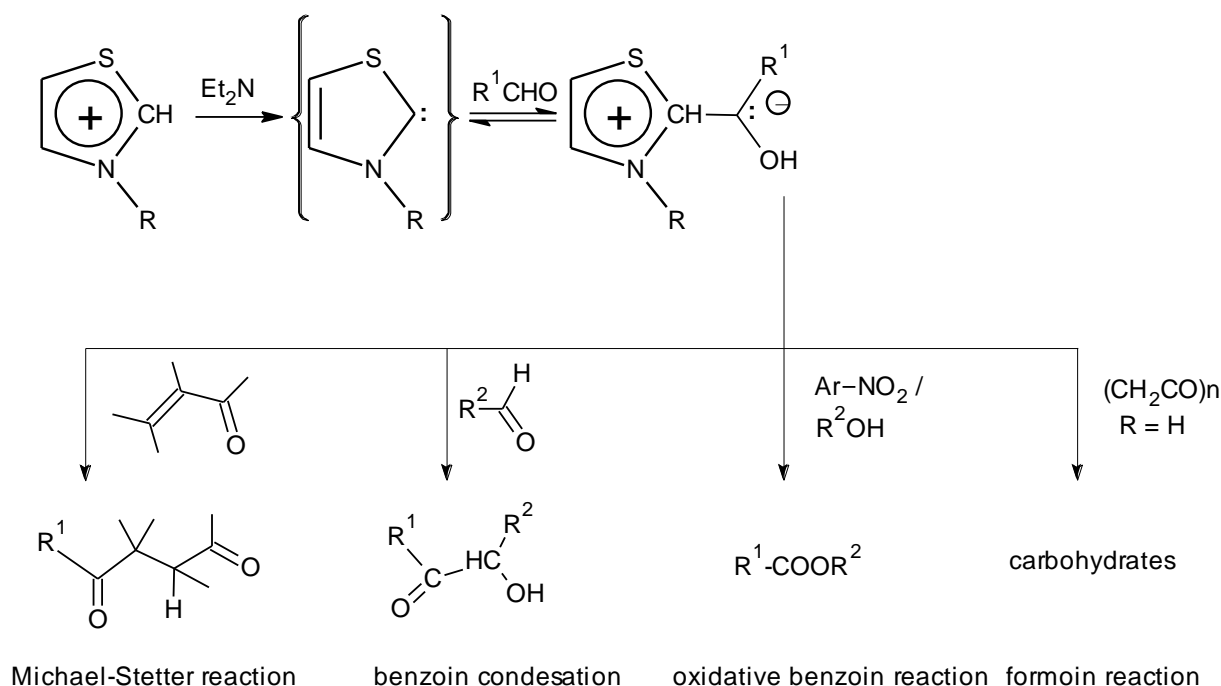


Fig. 6 Organic transformations of aldehydes catalysed by N-heterocyclic ylidenes

N-heterocyclic carbenes can catalyze transesterification reactions with a high efficiency for a variety of phosphorus esters¹⁴ and carboxylic acid esters¹⁵. Among them, the catalysed synthesis yielding the commercially important polyester poly(ethylene terephthalate) (PET) is significant¹⁶. It should be reminded that the nature of both the alcohol and carbene is crucial for efficiency of transesterification reactions. The N-aryl substituted carbenes are less effective than the N-alkyl substituted carbenes, especially for secondary alcohols¹⁵. The high transesterifications catalytic reactivity of N-heterocyclic carbenes was found out in the case of the step-growth polycondensations¹⁵ as well as depolymerizations¹⁶ of engineering thermoplastics.

NHCs are able to catalyze the ring-opening polymerization (ROP) of cyclic esters as well. In 2001, the catalyzed living ROP of lactones was reported. The formed polylactones had controlled molecular weight and narrow polydispersity¹⁷. Since this first report, the wide platform based on structural and electronic diversity of N-heterocyclic carbenes for the ROP of different monomers including lactides, lactones, carbonates, and silyl ethers, has been developed. Examples of effective catalysts of ROP are presented in Fig. 7¹⁸.

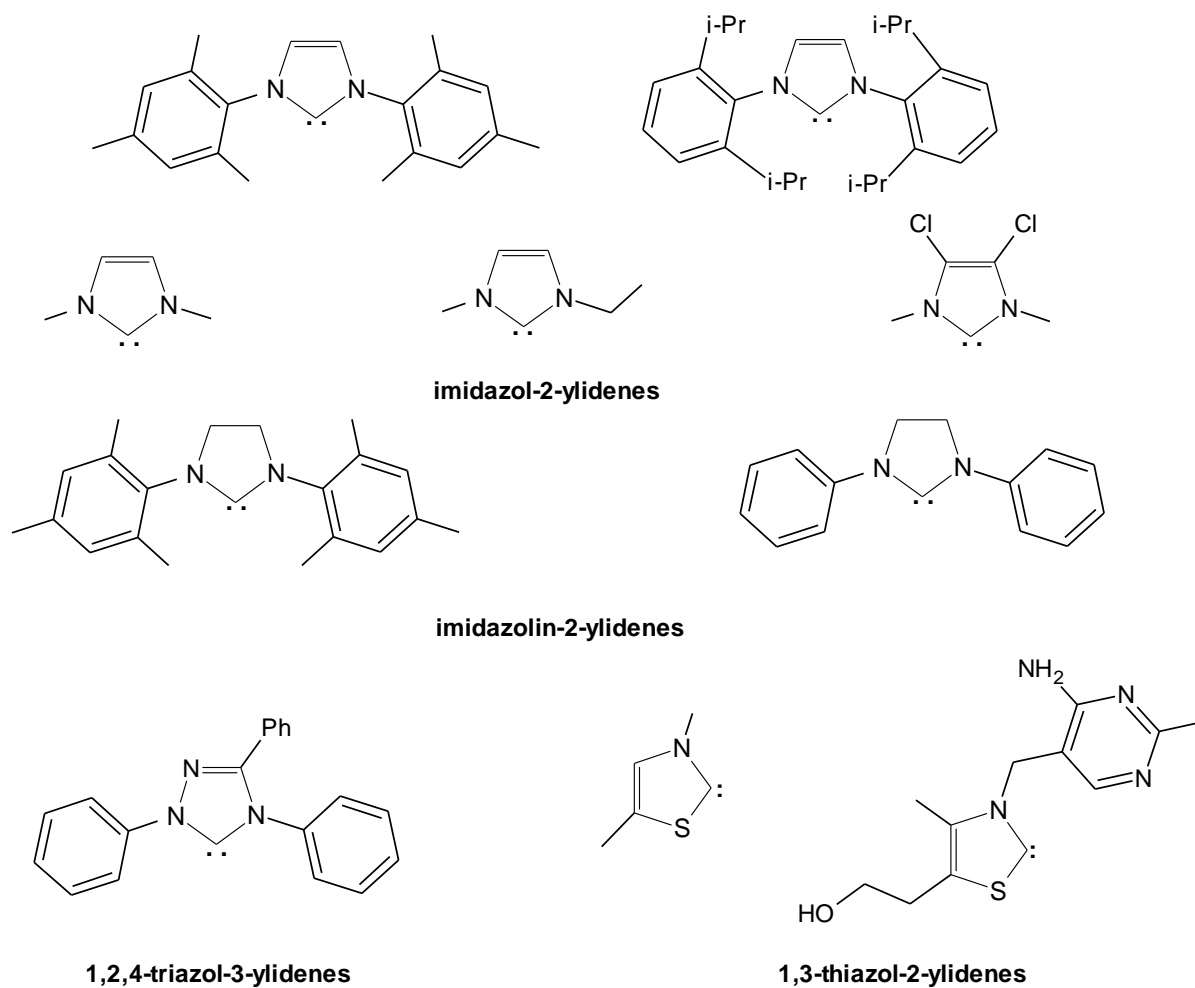


Fig. 7 Examples of *N*-heterocyclic carbenes for ROP

2.2.3 Basicity

N-heterocyclic carbenes are very strong Lewis bases. In 2002 Denk *et al.*¹⁹ suggested that the basicity of NHCs could be related to their catalytic activity. In 2004 Magill *et al.*²⁰ predicted values of pK_a's of nucleophilic NHCs in dimethyl sulfoxide (DMSO) and acetonitrile (MeCN). The substitution at the 4 and 5 position of imidazol-2-ylidene ring with electron-withdrawing groups significantly reduces the basicity while that with electron-donating groups increases the basicity. The aryl-substituents at nitrogen drastically decrease the basicity in comparison with alkyl-substituents. Saturated carbene analogue possesses slightly increased a basicity²⁰. The values of pK_a's were summarized in the table, which is presented in Appendix.

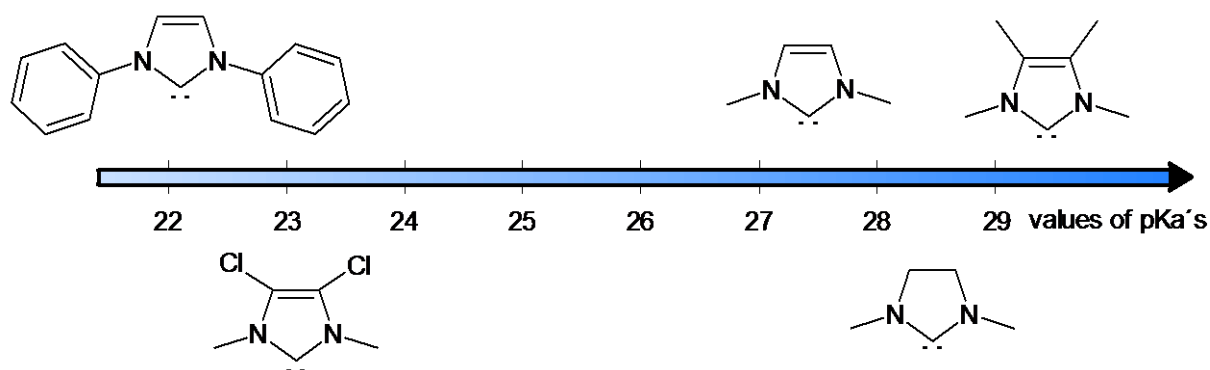


Fig. 8 Values of pK_a 's of NHCs in water (pK_a 's of NH_3 is ~ 35)

2.2.4 Mechanism of ring-opening polymerization

The ROP is fundamentally a transesterification reaction, therefore two possible mechanisms could be assumed: a monomer-activated mechanism mediated by the nucleophilic attack of the carbene on the lactide and a chain-end-activated mechanism where the carbene activates the alcohol toward nucleophilic attack¹⁸.

Based on the analogy with the known behaviour of pyridine derivatives in acylation reactions²¹ and bensoin and formoin condensation reactions²² nucleophilic mechanism was postulated. Moreover, on the bases of relative pK_a 's it was found out that the alcohol was unlikely able to protonate the 1,3-dimesitylimidazol-2-ylidene (IMes) and to initiate an anionic polymerization from the alkoxide¹⁷. On the other hand, it was supposed that hydrogen bonding (H-bonding) between the carbene and the alcohol could activate the alcohol toward nucleophilic attack^{23,24}. For ROP it corresponds to the chain-end-activated mechanism. According to theoretical calculation done for transesterification reactions it was predicted that alcohol activation pathway (via H-bonding) has a lower barrier than the nucleophilic mechanism²⁴. Consequently chain-end-activated mechanism can be sometimes called as H-bonding alcohol activation mechanism²⁵.

The mechanistic competition between the nucleophilic and general-base mechanism is a topic of discussion in the case of nucleophilic/basic organic catalysis. For the mechanism of ROP, the nature of the catalyst, the monomer, as well as alcohol is essential. Recently, regarding the calculations of ROP pathway catalysed by 4-(dimethylamino)pyridine (DMAP)^{25,26} it has been predicted that both two types of mechanism are energetically possible. In the gas phase or in polar aprotic solvents the basic (H-bonding) pathway was proposed to be more favourable than the nucleophilic mechanism²⁶ (Fig. 9). On the other hand, if alcohol initiators are absent or at present low concentration (high monomer/initiator ratio) nucleophilic pathway can compete²⁵.

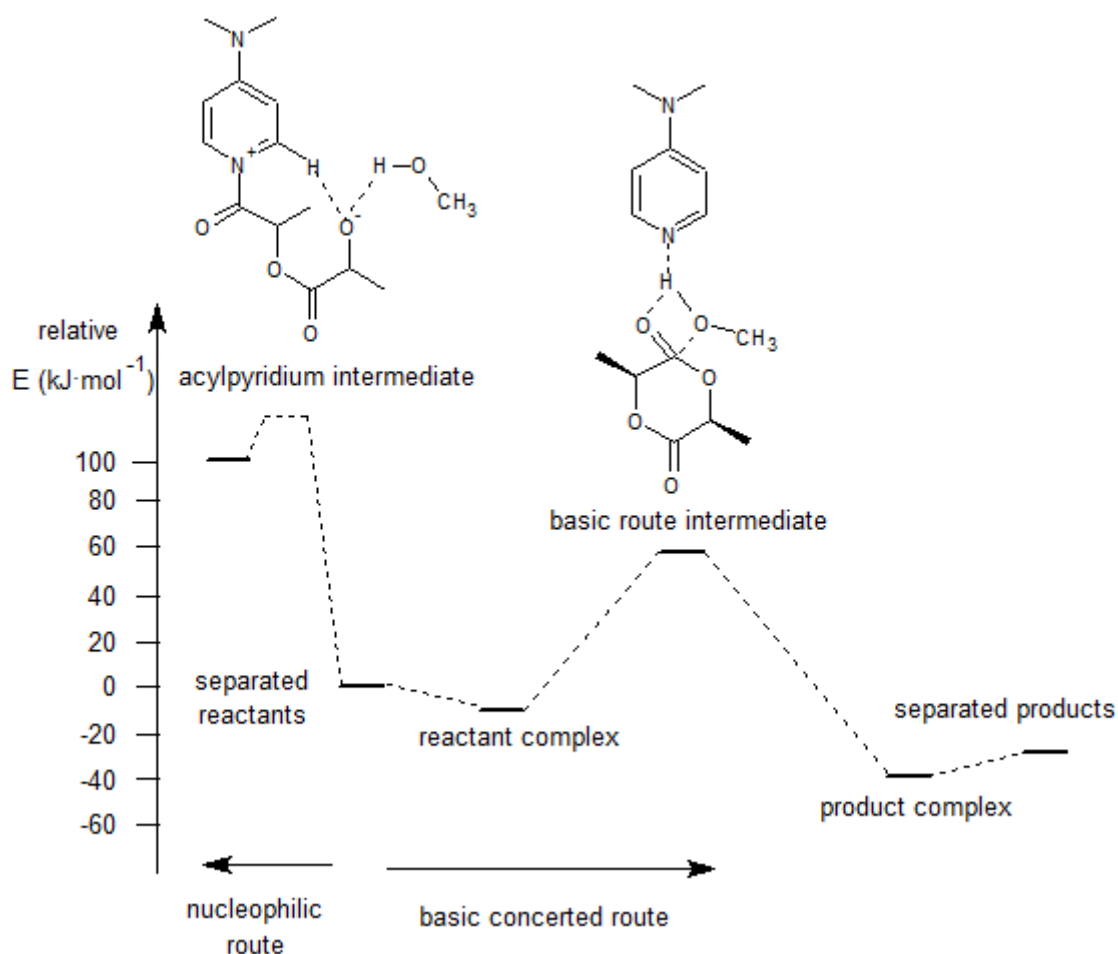


Fig. 9 Nucleophilic and basic (concerted) routes of DMAP-catalyzed ring-opening of lactide predicted at B3LYP/6-31G(d) level in dichloromethane

2.2.4.1 Monomer-activated mechanism

The crucial feature of nucleophilic mechanism is the formation of a zwitterionic intermediate, which is generated after the nucleophilic attack of the carbene on the lactide. After that the ring-opening of the tetrahedral intermediate follows and the acylimidazolium alkoxide zwitterion is formed (Fig. 10). Protonation of the alkoxide of the zwitterion by the initiating or end-chain terminated alcohol yields an alkoxide which esterificates the acylimidazolium to form the open-chain ester and carbene. The activated monomer (in the form of zwitterion) adds the activated monomer to the growing polymer chain. All chains grow at the same rate, which is a kinetic characteristic of living polymerization¹⁸.

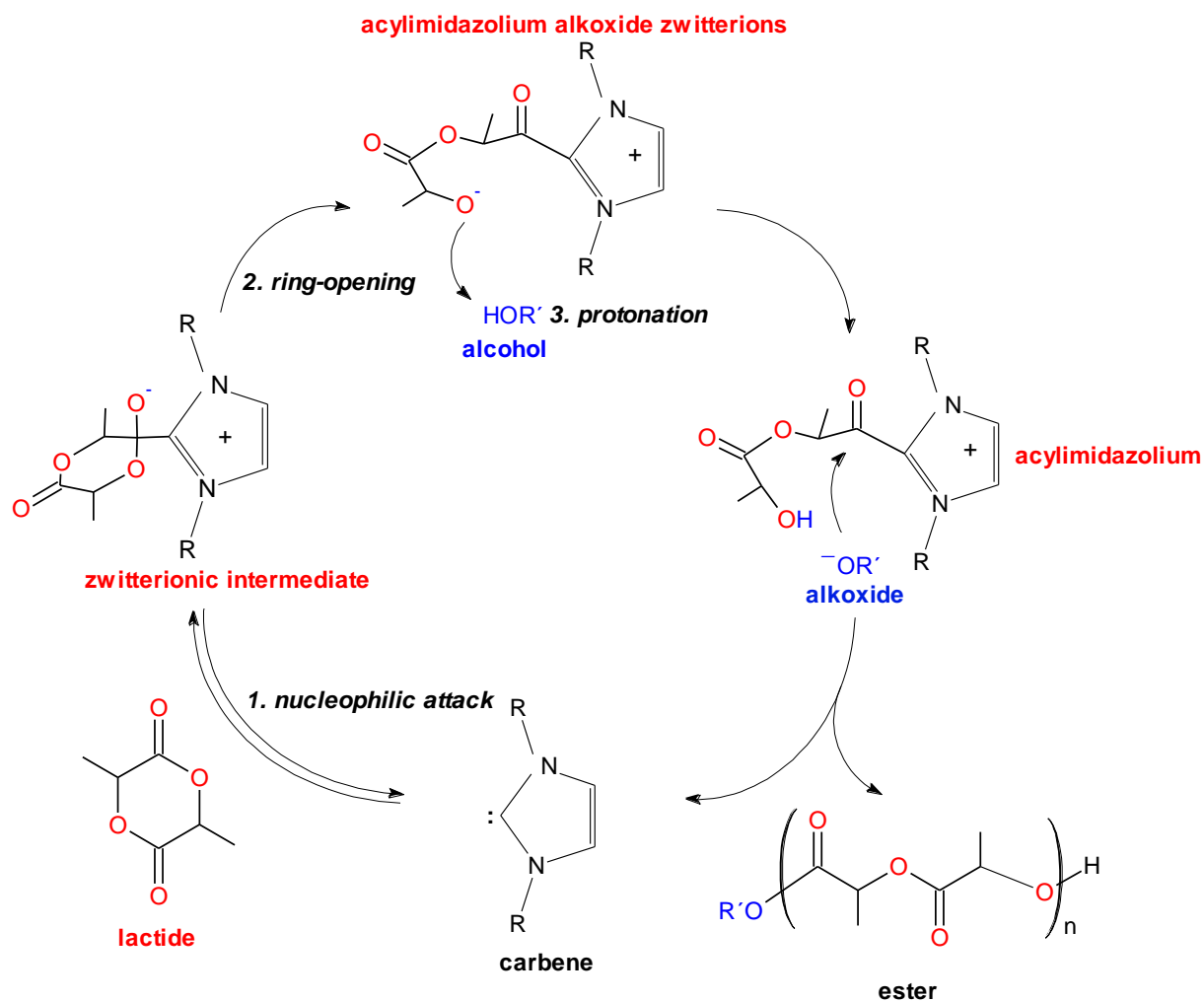


Fig. 10 Scheme of nucleophilic monomer-activated mechanism of ROP

To understand the role of zwitterionic intermediates in ROP, the polymerization of lactide without alcohol initiators was investigated and cyclic poly(lactide)s of defined molecular weight were obtained (Fig. 11). These NHC-mediated zwitterionic polymerizations showed a considerable degree of control and exhibit features of living polymerization²⁷.

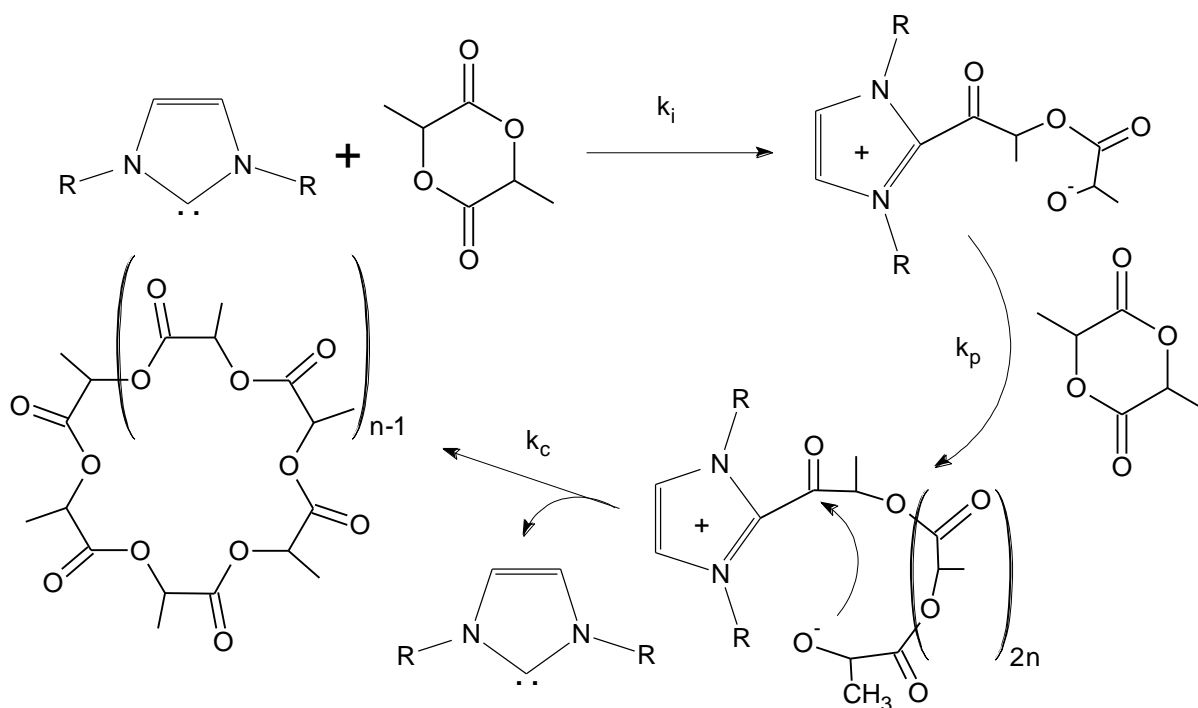


Fig. 11 Scheme of the mechanism of NHC-mediated zwitterionic polymerization of lactide

2.2.4.2 Chain-end-activated mechanism

The chain-end-activated mechanism has similar features as a classical anionic polymerization. During the anionic mechanism the strong base initially reacts with the alcohol initiator (or chain end), which is activated by deprotonation to form an alkoxide. In the next step the attack of the alkoxide on the carbonyl carbon of the monomer is followed by acyl-oxygen bond scission. Subsequently the ester end group and an active alcoholate species (which reacts with the further monomer) are generated²⁵.

Milder general bases can activate the alcohol initiator or chain end via H-bonding, which causes that bases enhance the nucleophilicity of the initiating or propagating alcohol. Subsequently the nucleophilic attack on the lactone monomer is more facile^{24,25} (Fig. 12).

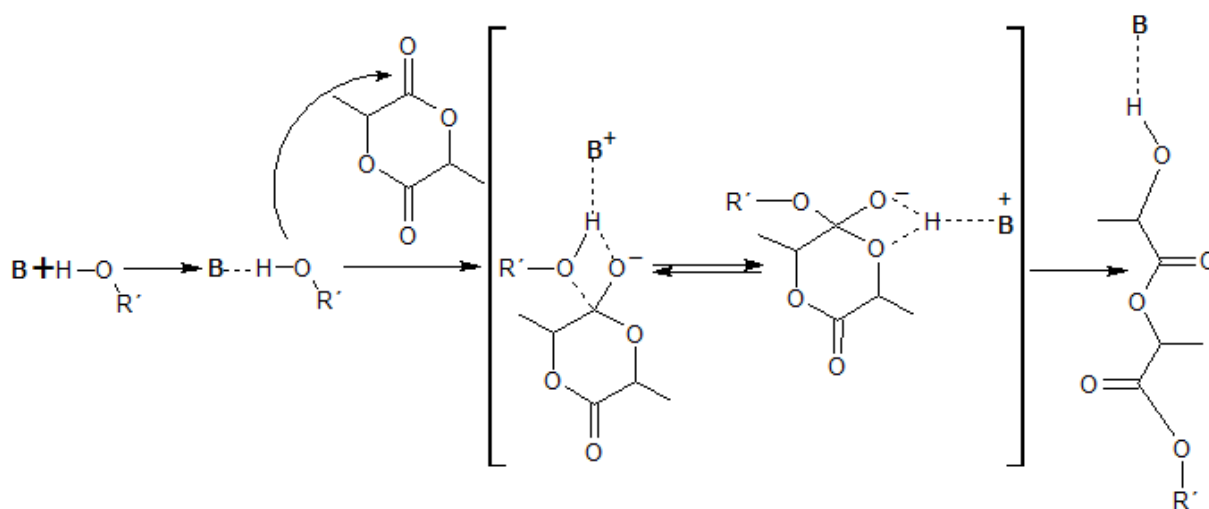


Fig. 12 Scheme of the general chain-end-activated mechanism of ROP

2.2.5 Carbene precursors

Because of difficulty in the synthesis of “free” NHCs which are moisture (oxygen) sensitive, a lot of techniques for the generation of carbenes from more readily available precursors have been reported. The common method is *in situ* deprotonation²⁸ of thiazolium, imidazolium or triazolium salts. Neat imidazolium-derived ionic liquids²⁹ are used as catalyst sources and solvents for transesterification and ROP. THF/ionic liquid mixtures in which a biphasic polymerization proceeds serve as a catalysts reservoir¹⁸ (Fig. 13).

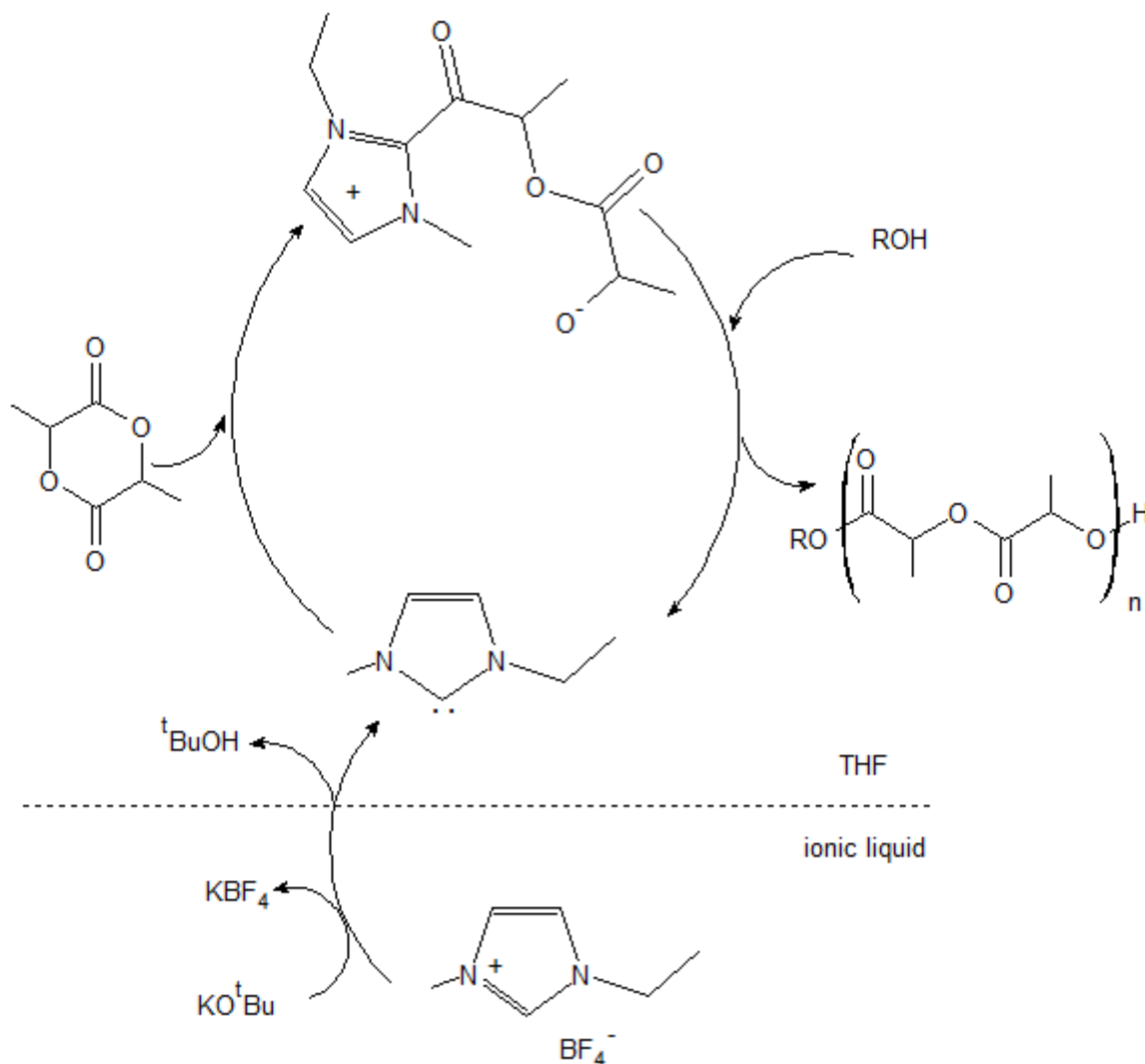


Fig. 13 Polymerization using a biphasic ionic liquid-NHC system

The other precursors able to generate “free” carbene are silver(I) NHC complexes³⁰, chloroform and fluoro-substituted arene NHC adducts³¹ and alcohol adducts³². NHCs could be generated from alcohol adducts by thermolysis⁵ (Fig. 4a). Alcohol adducts act as single-component catalyst/initiators for ROP of lactide at room temperature (Fig. 14). Adducts can be prepared and isolated simply by the mixing of primary or secondary alcohols with the isolated carbene. Moreover, two *in situ* procedures that eliminate the need for isolation of the “free” carbene were developed³² (Fig. 15).

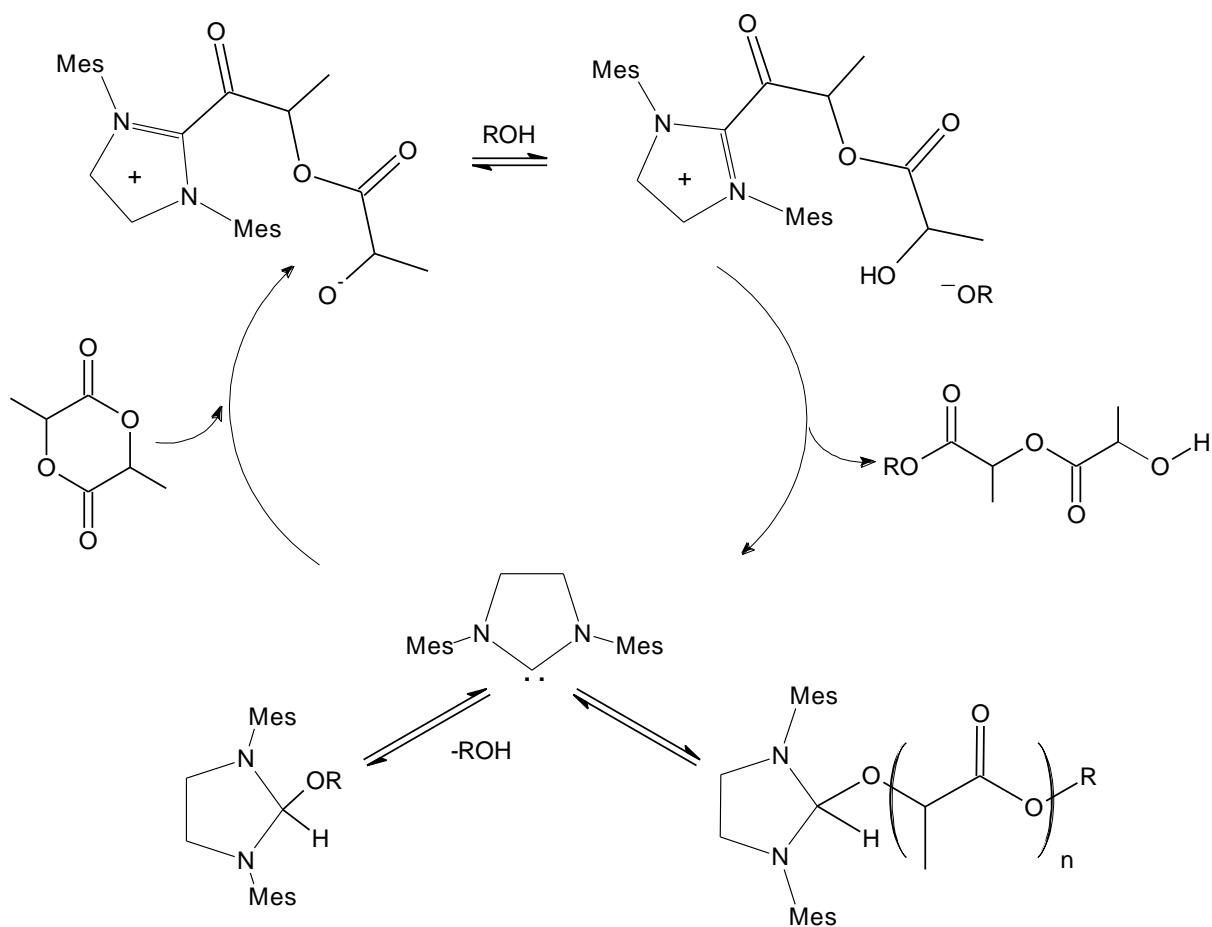


Fig. 14 Proposed nucleophilic mechanism for ROP of lactide with alcohol adducts

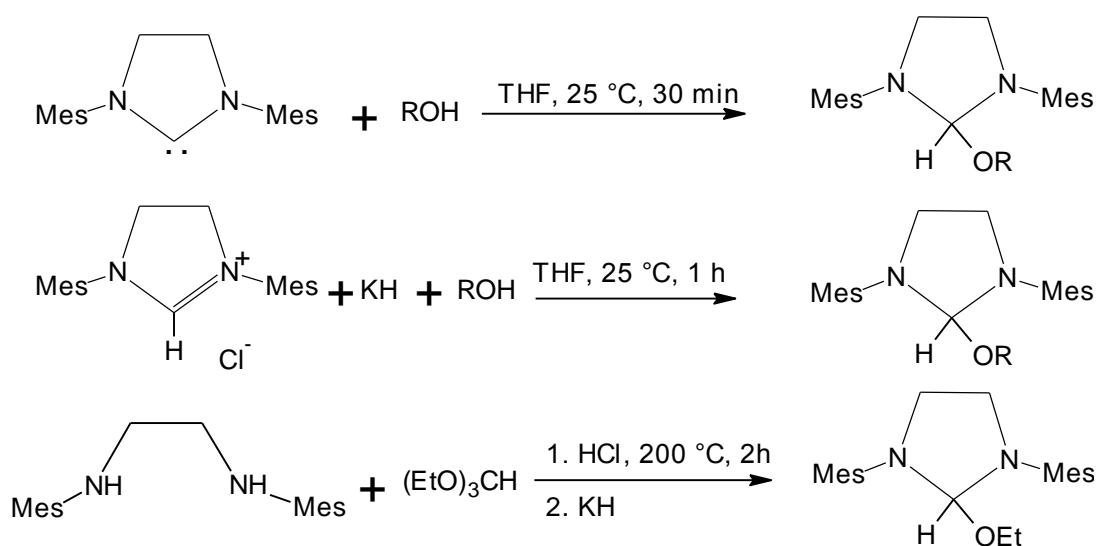


Fig. 15 Scheme of the preparation of alcohol adducts

2.3 Molecular modelling

Molecular modelling includes all theoretical and computational methods used to model the behaviour of molecules, hence for molecular modelling terms as “theoretical chemistry” or “computational chemistry” are used³³. Molecular modelling started a fast progress with development in the computing area. Today molecular modelling plays a significant role in many research laboratories and enables to predict the behaviour of the new compounds, design of new drugs and materials and helps to interpret experimental data. The term “*in silico*” was introduced for research using computer calculations and simulations as an analogy to Latin terms “*in vivo*”, “*in vitro*” and “*in situ*” used primarily in biology. Today three main methods of molecular modelling are distinguished: molecular mechanics, quantum mechanics and simulation methods. In a principle simulation methods use both quantum mechanics and molecular mechanics, so they will not be discussed.

2.3.1 General terms

2.3.1.1 Coordinate systems

The specification of the position of atoms or molecules in the system to a modelling program is one of the most crucial point in molecular modelling. There are two common ways. The simpler way is to specify the Cartesian coordinates (x, y, z) of all atoms present. The second way is using of *internal coordinates*, in which the position of each atom is described relative to other atoms in system. These coordinates are usually written as a Z -matrix and are commonly used as input to many quantum mechanics programs. But it is necessary mentioned that many programs can convert Cartesian coordinates to internal and vice versa³³.

2.3.1.2 Common units

For molecular modelling it is usual to work with atomic units because properties of atomic particles as electrons, protons and neutrons are expressed too small values. In other way the values must be multiplied by several powers of 10. Relations between the atomic units and SI units (International System of Units) are expressed in Tab. 1:

Tab. 1 Relations between the atomic units and SI units

Physical quantity	Atomic units	SI units
Charge	1	$ e =1.60219 \cdot 10^{-19}$ C
Length	1	$a_0 = 5.29177 \cdot 10^{-11}$ m (1 Bohr)
Mass	1	$m_e = 9.10593 \cdot 10^{-31}$ kg
Energy	1	$E_a = 4.35981 \cdot 10^{-18}$ J (1 Hartree)

Non-SI units Ångströms (Å) or picometers (pm) are very often used for bond lengths, whereas non-SI units kilocalories (kcal) or kilojoules (kJ) are very often used for energies³³. Relations are given in Tab. 2.

Tab. 2 Units of length and energy

Length	1 Å	10^{-10} m	100 pm
Energy	1 Hartree	2627.34 kJ·mol ⁻¹	627.5095 kcal·mol ⁻¹

2.3.1.3 Potential energy surfaces

Changes in the energy of a system can be specified by movements on a multidimensional surface. This surface is called the potential energy surface (PES) and is mathematical relationship related molecular structure and the resultant energy. For the simplest molecule (diatomic) it is a two-dimensional curve. For a system with N atoms the potential energy surface is $3N$ -dimensional (Cartesian coordinates) or $(3N - 6)$ -dimensional (internal coordinates)^{33,34}.

The most significant points on the potential energy surface are stationary points (the first derivative of the energy is zero). One type of stationary points is minimum that can be global, local, or saddle point. Global minimum is the lowest point anywhere on the potential surface, on the other hand local minimum is the lowest point in some limited region of the potential energy surface. Global minimum represents the most stable conformation or structural isomer, whereas local minimum represents less stable conformations or structural isomers. The saddle point is maximum in one direction and minimum in the other. This point corresponds to a transition structure connecting with two equilibrium structures³⁴.

2.4 Quantum mechanics

All quantum mechanics methods are based on the solution of the Schrödinger equation. The well-know form of this equation is:

$$\hat{H}\Psi = E\Psi \quad (2.4-1)$$

However, this equation can be exactly solved only for one-electron system (*i. e.* the hydrogen atom), therefore approximations need to be made. According to the nature of approximations methods of quantum mechanics can be classified into semi-empirical methods, *ab initio* methods and density functional theory (DFT)^{33,34,35}. All methods will be briefly discussed. Mathematical concepts were described in detail in the previous work³⁶.

2.4.1 Approximations of *ab initio* methods

How it was said the Schrödinger equation cannot be solved exactly for any molecular systems, hence the Born-Oppenheimer approximation were established. This approximation separates the motion of the electrons from the motion of the nuclei because the masses of the nuclei are circa 1800 times heavier than masses of the electron and they move slower. Using of the Born-Oppenheimer approximation the Schrödinger equation is solved for the electrons alone in the field of the nuclei, however for polyelectronic systems further approximations are required.

First formulation of the wavefunction (orbital) for a polyelectronic system is known as a *Hartree product*, but it does not fulfil the antisymmetry principle. Slater determinant can be used to satisfy the antisymmetry principle and is the simplest form of an orbital wavefunction. The major problem for the solution of the Schrödinger equation is the presence of interactions between the electrons. Fock assumed that each electron moves in a fixed field including the nuclei and the other electrons, thus the Hartree-Fock equations express a single electron in the spin orbital in the field of the nuclei and the other electrons in their fixed spin orbital. However the solutions of Hartree-Fock equations are not unique. The general strategy to solve these equations is called as a *self-consistent-field* (SCF) procedure. The individual electronic solutions correspond to lower and lower total energy until results for all electrons are unchanged. SCF approaches also include density functional procedures.

Furthermore, for the solution of Hartree-Fock equations for molecules we must agree to an alternative approach and express the molecular orbitals. The most common way is linear combination of atomic orbitals (LCAO). The lowest energy of system is determined by using *Roothaan-Hall* equations, which is often written as matrix equation^{33,35}.

2.4.2 Electron correlation

The most essential disadvantage of Hartree-Fock method is that it does not involve the electrons correlation. The electrons are assumed to be moving in an average potential of the other electrons. However in reality, the motions of electrons are correlated and they tend to “avoid” each other. The difference between the Hartree-Fock energy and the exact energy is called the correlation energy. If the electron correlation is neglected, we can get some clearly anomalous results. The inclusion of the correlation effect is warranted, although Hartree-Fock geometries are often in good agreement with experiment. The electron correlation is crucial in the study of dispersive effects. It is often discussed in *ab initio* methods, but effects of electron correlation are involving in the semi-empirical methods³³.

The position of Hartree-Fock models is illustrated in Fig. 16, where all possible theoretical models are placed. The horizontal axis depicted the extent of the separation of electron motions (in context the separation of electron motions means that the method is uncorrelated). Hartree-Fock models are placed at the extreme left, while fully-correlated models are placed at the extreme right. Practical correlated models are found somewhere in between. The vertical axis shows the basis set. A minimal basis set is located at the top and contains the fewest possible functions (the basis sets will be discussed in the next section), while a “complete” basis set is located at the bottom and in Hartree-Fock models is called as Hartree-Fock limit³⁵.

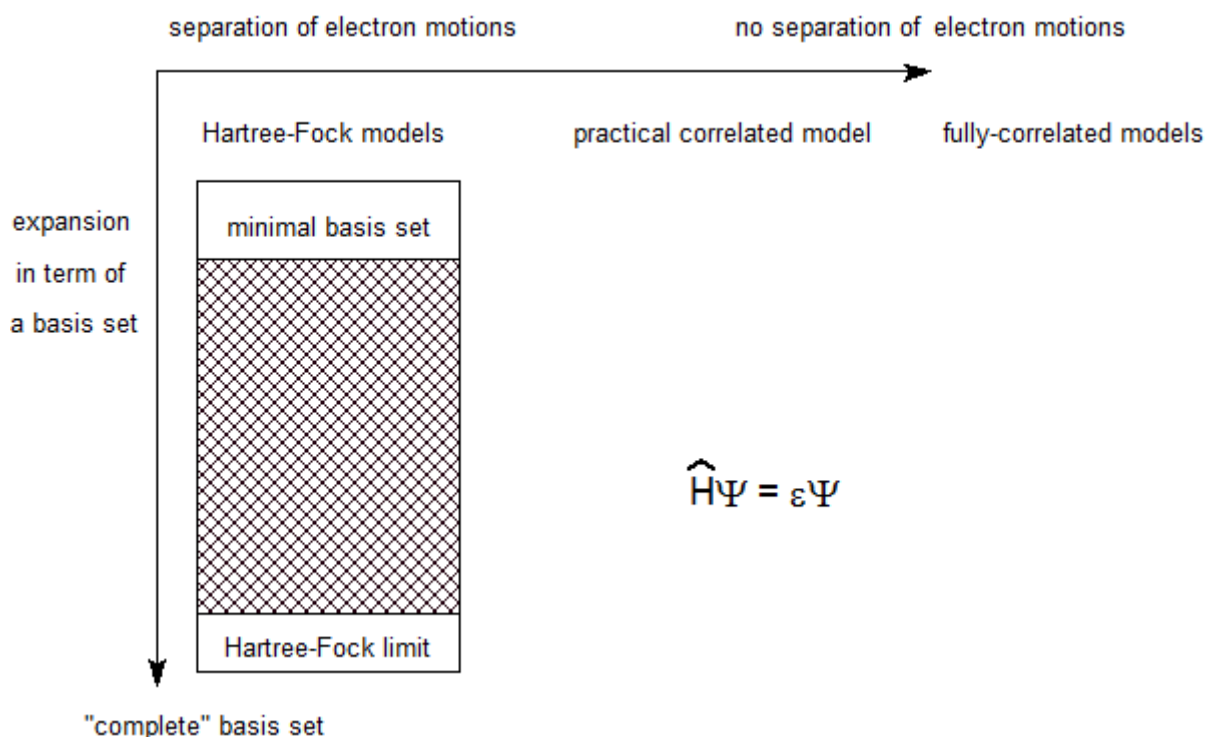


Fig. 16 The two-dimensional diagram of all possible theoretical methods

2.4.3 Basis sets

The basis sets consist of atomic orbitals, which are used to form molecular orbitals. At first the Slater type orbitals (STOs) were used. However with these types of orbitals it is difficult to solve three- and four-centre integrals, if the atomic orbitals are located on different atoms. Hence the Slater orbitals were replaced by Gaussian type orbitals (GTOs). The advantage of these functions is fact that the product of two Gaussians can be expressed as a single Gaussian, which is located along the line joining the centres of two Gaussians. For quantum mechanics methods a linear combination of Gaussian functions is used³³.

The simplest possible atomic orbital representation is a minimal basis set that involves the minimum number of functions required to accommodate all the filled orbitals in each atom. They contain only one contraction per atomic orbital. The most common minimal basis set is STO-nG (Slater type orbital), where n Gaussian functions are used to represent each orbital.

A double zeta valence basis set (DZV) doubles the number of functions in the minimal basis set. The SCF method calculates automatically the basis set coefficients of the contracted and the diffuse functions^{33,36}.

A split valence basis uses a single function for inner shells, but doubles the number of functions which are used to describe the valence electrons. The core orbitals do not influence chemical properties very much in contrast to the valence orbitals. These basis sets are noted as 3-21G. It means that three Gaussians describe the core orbitals and other three Gaussians describe electrons orbitals, where the contracted part represents two Gaussians and the diffuse part represents one Gaussians. The most common split valence basis set is 6-31G.

Other type of basis sets is a basis with polarisation functions that has higher angular quantum number and corresponds to d orbitals for the first- and second-row elements and p orbitals for hydrogen. A polarization function is denoted by the asterisk * or by (d) at the end

of a basis set. 6-31G* or 6-31G(d) is a 6-31G basis with polarisation functions on heavy atoms. Two asterisks ** or (d,p) denotes polarisation functions on hydrogen and helium atom in addition to 6-31G(d) or 6-31G*.

A basis with diffuse functions deals with cations, anions and molecules included lone pairs. This basis set is denoted using +. The basis set is denoted using ++, if the diffuse functions are included for hydrogen as well as for heavy metals^{33,35,36}.

For correlated models Dunning's cc-pVDZ, cc-pVTZ and cc-pVQZ basis sets are commonly used. These basis sets converge systematically to complete-basis-set limit using empirical extrapolation techniques. The cc-pVDZ, cc-pVTZ and cc-pVQZ basis sets mean "correlation consistent-polarized Valence Double (Triple, Quadruple) Zeta" basis sets. They involve larger shells of polarization functions and can be augmented with diffuse functions by adding the aug- prefix (aug-cc-pVDZ)^{35,36}.

2.4.4 Using *ab initio* methods

In the *ab initio* methods we do use no empirical data in their calculations. The term *ab initio* means that the calculation is from first principles. This method is based on the laws of quantum mechanics and on the values of a small number of physical constants:

1. The masses and charges of electrons and nuclei
2. The speed of light
3. Planck's constant

The *ab initio* calculation offers high quality quantitative predictions for many systems, however takes on the order of one to a few days, hence is often expensive. It is usual for several tens of atoms³⁴. The most popular *ab initio* methods can be classified into three main groups: the Hartree-Fock methods, post-Hartree-Fock methods and multi-reference methods. The post-Hartree-Fock methods incorporate correlation effects. The most popular approaches Configuration interaction (CI) models and Møller-Plesset perturbation theory (MP2, MP3 or MP4) extend the Hartree-Fock model by mixing ground-state and excited-state wavefunctions. On the other hand they are more expensive than Hartree-Fock models and are impractical (they can be used only for the smallest systems)^{34,35}. Multireference methods can be divided into Multi-configurational self-consistent field (MCSCF), Multireference single and double configuration interaction (MRDCI) and N-electron valence state perturbation theory (NEVPT). For our calculations we will use only Hartree-Fock methods, which involve Restricted Hartree Fock (RHF), Unrestricted Hartree Fock (UHF) and Restricted open shell Hartree Fock (ROHF) calculation^{33,34,35}.

This method can be used for the simple single point calculation as well as for geometry optimization, frequency calculation, electric multipoles, total electron density distribution and molecular orbitals or thermodynamic properties. The most common calculation but the most exacting is geometry optimization, which is a starting step of other calculations. The electron density can be visualised as a solid object, whose the surface connects points of equal density. On this surface the electrostatic potential or other properties can be mapped. Using the electron density distribution of individual molecular orbitals we can determine and plot HOMO and LUMO, which influence reactivity of molecules³³.

2.4.5 Semi-empirical methods

Semi-empirical methods solve an approximate form of the Schrödinger equations because consider only valence electrons of the system (electrons associated with the core are ignored). The basis set is restricted to a minimal valence representation³⁵. Further, semi-empirical methods use parameters derived from experimental data to simplify the calculation. The most popular semi-empirical methods are MNDO (modified neglect of diatomic overlap), AM1 (Austin Model 1) and PM3 (the name is derived from the fact that it is the third parameterization of MNDO)³³. The AM1 and PM3 methods use the same approximations but differ in their parameterization. Moreover PM3 method is parametrised for transition metals³⁵. In contrast to *ab initio* methods they are relative inexpensive and very large molecules can be calculated. We can first calculate semi-empirical optimization to obtain a starting structure for Hartree-Fock or Density Functional Theory optimization. These methods can quickly calculate molecular orbitals or vibrational normal modes. However they have some problems with systems including hydrogen bonding, transitional structures and with molecules containing atoms for which they are poor parametrized³⁴.

2.4.6 Density functional theory

Density functional theory is similar to *ab initio* methods. The essential difference is that DFT calculates with the general functionals of the electron density instead of the many-electron wavefunction. Both models use the same basis set as well as the SCF approach³⁵. Moreover, DFT includes the effects of electron correlation. DFT methods are generally less expensive than Hartree-Fock methods RHF, furthermore they achieve greater accuracy. The electronic energy is a sum of the kinetic energy, the electron-nuclear interaction, the Coulomb repulsion and the exchange-correlation energy. The most popular functionals are pure density functionals and hybrid functionals. The pure density functionals treat the exchange and correlation components. Both exponents can be of two types: local functionals depend on the electron density, while gradient-corrected depend on the electron densities and their gradient. The well-known BLYP functional connects Becke's gradient-corrected exchange functional with the gradient-corrected correlation functional of Lee, Yang and Parr. The hybrid functionals include a mixture of Hartree-Fock exchange and DFT exchange along with DFT correlation. The popular B3LYP functional is Becke-style three-parameter functional³⁴. In Appendix you can see examples of functionals and their descriptions³⁸.

2.5 Molecular mechanics

Molecular mechanics is based on Newtonian mechanics to predict the structures and properties of molecules. The potential energy of all systems is calculated using force fields, which include these components:

1. A set of equations describing the change of the potential energy of a molecule with the location of its component atoms
2. A series of atom types describing characteristics of an element with specific chemical context
3. One or more parameter sets that fit the equations and atom types to experimental data

Bonded interactions are treated as "springs" with an equilibrium distance equal to the experimental or calculated bond length. These calculations perform computations based upon

the interactions among the nuclei. Electronic effects are implicitly involved in force fields through parameterization. Hence, molecular mechanics calculations are quite inexpensive computationally, and can be used for very large systems (thousands of atoms). Although, it carries several limitations as well³⁴. Molecular mechanics methods differ in the number and specific nature of the terms and the parameterization. The most popular methods are SYBYL, MMFF or AMBER^{33,35}.

2.6 Geometry optimization

An isolated molecule in vacuum is usually taken into account for geometry optimization (equilibrium geometry). The crucial point of geometry optimization is the finding of the conformation with the lowest energy. A *minimalisation algorithm* is used to identify geometries of the system that correspond to minimum points on the energy surface. Using of geometry optimization we can search as well as the saddle points that correspond to the transition structures. For quantum mechanics other methods are used than for molecular mechanics. Most minimisation algorithms can only go downhill on the energy surface; hence they can only locate the nearest minimum to the starting point. When we search the global minimum, we must create different starting points and minimise each point³³.

In real molecular modelling applications it is impossible to find the exact location of minima or saddle points. Hence an approximation of these points is found. The energy is monitored from one iteration to the next and the process is stopped when the difference in energy between successive steps falls below a specified threshold that is called the convergence criteria. A second method is to monitor the change in coordinates and a third method is to calculate the root-mean-square gradient. We can distinguish two groups of minimisation algorithms: those which use derivatives of the energy with respect to the coordinates and those which do not³³. Both algorithms were discussed in previous work³⁶.

2.7 Infrared and Raman spectroscopy

Infrared (IR) and Raman (RA) spectroscopy provide information about vibrational motions of a molecule and is used to identify compounds and study their structure. A common laboratory instrument that uses this technique is a Fourier transform infrared (FTIR) spectrometer. For the description of infrared and Raman spectra the approximations were established as well. A first approximation separates the total energy into the energy of the motion of the electrons in the molecule, the energy of the vibrations of the atoms and energy of the rotation of the molecule. If the molecule absorbs energy, the electronic, the rotational and vibrational states can change. A transfer of energy will occur, when Bohr's frequency condition is satisfied:

$$\Delta E = E_2 - E_1 = h\nu \quad (2.7-1)$$

The transition is allowed, if the selection rules are valid. In IR (Infrared) and RA (Raman) spectra vibrational and rotational states change, however the rotational transitions have a little signification and they can be measured mainly in the gaseous state. Vibrational transitions appear in the 10^2 - 10^4 cm^{-1} region and originate from vibrations of nuclei, while rotational transitions principally appear in the 1 - 10^2 cm^{-1} region (microwave region) because rotational levels are relatively close to each other. Below each electronic level there is "zero-point

energy” which must exist even at a temperature of absolute zero as a result of Heisenberg’s uncertainty principle:

$$E_0 = \frac{1}{2} h\nu \quad (2.7-2)$$

In the Born-Oppenheimer and harmonic oscillator approximations the resonance frequencies are determined by the normal modes corresponding to the molecular electronic ground state potential energy surface³⁹.

2.7.1 Harmonic oscillator approximation

For the description of vibrations of diatomic molecule the harmonic oscillator approximation was introduced. The frequency of vibration depends on force constant and reduced mass. For the harmonic oscillator a potential curve is parabolic, however the actual potential curve differs, hence the wavenumber of normal vibration is corrected for anharmonicity. This anharmonicity causes the appearance of overtones and combination vibration, which are forbidden in the harmonic oscillator³⁹.

In polyatomic molecules the situation is more complicated because all nuclei perform their own harmonic oscillators. Extremely complicated vibrations of the molecule can be represented as a superposition of a number of normal vibrations³⁹. The mathematical background was mentioned in previous work³⁶.

Nonlinear molecules have $3N-6$ degrees of vibrational modes (called vibrational degrees of freedom), because six coordinates describe the translational and rotational motion of the molecule as a whole. In contrast linear molecules have $3N-5$ degrees of vibrational modes, because no rotational freedom exists around the molecular axis. When all the normal vibrations are independent of each other, the consideration may be limited to a special case in which only one normal vibration is excited. So in the normal vibration, all the nuclei move with the same frequency and in phase.

As result of all approximations we solve the matrix secular equation:

$$|GF - E\lambda| = 0 \quad (2.7-3)$$

where G is matrix elements, F is hessian matrix of the force constant and E is the unit matrix. We obtain the wavelengths that are converted to the wavenumbers. If the order of the secular equation is higher than three, it is too difficult to solve it. Symmetry of a molecule can significantly simplify the calculations³⁹.

2.7.2 Principle of IR and RA spectroscopy

The principle of IR spectroscopy is the absorption of infrared radiation by molecules. Three regions of IR spectroscopy can be distinguished: near-infrared $14000-4000 \text{ cm}^{-1}$, mid-infrared $4000-400 \text{ cm}^{-1}$ (most common) and far-infrared ($400-10 \text{ cm}^{-1}$). The energy of IR radiation is not enough for changes electronic ground states, but it causes changes of rotational-vibrational states of the molecule, however the vibrational transitions predominate.

Raman spectra originate in the electronic polarization caused by ultraviolet, visible and near-IR light. Raman spectroscopy uses the scattering of the monochromatic light (laser) and spectra are represented as shifts of the incident frequency in ultraviolet, visible and near-IR region³⁹.

The vibrations can be divided into two basic groups: stretching and bending vibrations. The examples of vibration are depicted in Fig. 17. The stretching vibrations appear in region 4000-1500 cm^{-1} (sometimes called the group frequency region), while bending vibrations appear in region 1500-400 cm^{-1} (called finger print region). This region includes a very complicated series of absorptions and it is more difficult to choose individual bonds, however every organic compound produces a unique pattern in this part of the spectrum.

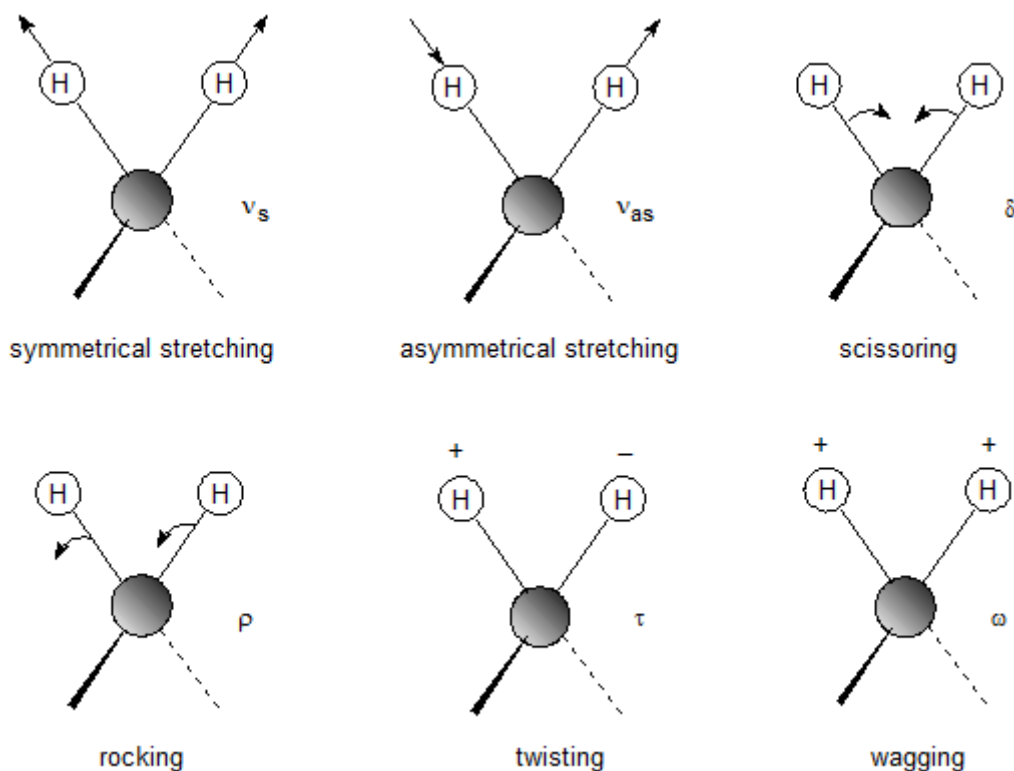


Fig. 17 Vibrations of a CH₂ group

The vibrational mode in molecule is IR active, when it is related with changes in the dipole moment, whereas the vibrational mode in molecule is Raman active, when it is related with changes in the polarization. Symmetrical stretching and bending will be Raman active and IR inactive, while asymmetrical stretching and bending will be IR active and Raman inactive in molecules with a centre of symmetry. Each vibrational mode may be IR active, Raman active, both, or neither for molecules without a centre of symmetry⁴⁰.

2.7.3 Prediction of spectra

Spectra are usually predicted in gaseous phase at 298.15 K. Calculations use an idealized view of nuclear position, however in reality, the nuclei in molecules are constantly in motion. These vibrations are regular and predictable in equilibrium states. Programs are able to compute the vibrational spectra of molecules in their ground and excited states, describe the displacements a system and predict the direction and magnitude of the nuclear displacement that occurs when a system absorbs a quantum of energy.

Molecular frequencies and the distinguishability between minima (discussed in Section 2.6) depend on the second derivative of the energy with respect to the nuclear positions. Programs calculate analytic second derivatives for the HF and DFT. Frequency calculations are valid only at stationary points on the potential energy surface, hence must be done on optimized structures³⁴. Computed frequencies at the Hartree-Fock level contain well-known systematic errors because of the neglect of electron correlation. Computed frequencies at DFT level include the effect of electron correlation, however they contain well-known systematic errors as well. Hence it is usual to scale frequency by empirical factors⁴¹.

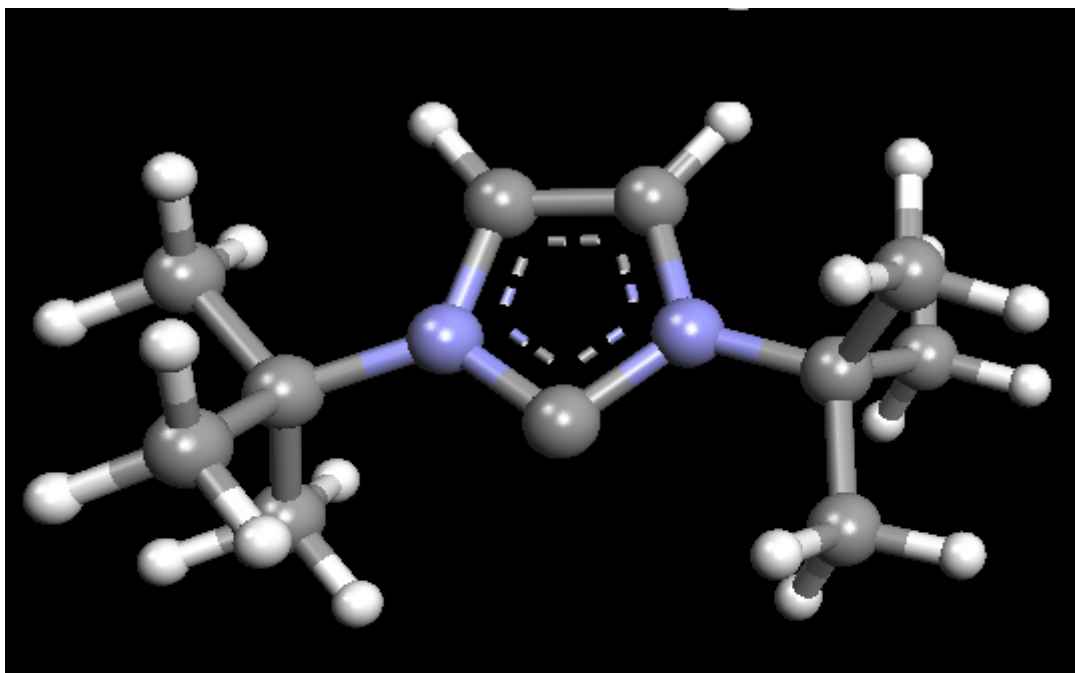
2.8 Computer programs

A variety of computer programs are utilized to calculate the structures and properties of molecules. Efficient *ab initio* computer programs are GAUSSIAN, PC GAMESS/Firefly, GAMESS (US), GAMESS (UK), MOLCAS, MOLPRO and Spartan. Furthermore they usually contain density functional theory (DFT), molecular mechanics or semi-empirical methods.

We will use PC GAMESS/Firefly^{42,43}, ArgusLab⁴⁴, Titan⁴⁵ and Spartan⁴⁶. PC GAMESS/Firefly is based on GAMESS (US). GAMESS abbreviates General Atomic and Molecular Electronic Structure System. It is able to calculate single-point energies, geometry optimizations or predictions of IR and Raman intensities. It does not include a graphical user interface, hence softwares for the creating of input files and for the visualization of results were used. For that reasons ArgusLab, Titan or Gabedit⁴⁷ can be perform. Gabedit can graphically display many calculation results as molecular orbitals, surfaces from the electron density, electrostatic potential or NMR shielding density and UV-Vis, IR and Raman spectra. In contrast to Gabedit, ArgusLab and Titan allow simple calculations or pre-optimizations. They can calculate and display molecular orbitals or electrostatic potential-mapped electron density surfaces. Titan is the older version of Spartan that is the complex program. In addition to simple calculations Spartan allows to study of reactions.

2.8.1 Operating ArgusLab and PC GAMESS/Firefly

In ArgusLab⁴⁴ structures of studied compounds were formed and pre-optimized at AM1 level (Fig. 18). The coordinates obtained by ArgusLab were edited in any text editor, where in the next step the input file for PC GAMESS/Firefly^{42,43} was created. The coordinates were set up into PC GAMESS/Firefly format, thus the name of method, the symmetry, the name of atom and the nuclear charge was added. Subsequently, these groups were defined: \$CONTRL, \$SYSTEM, \$SCF, \$GUESS, \$BASIS, \$ZMAT and \$STATPT according to PC GAMESS/Firefly documentation³⁸. The example of the input file for PC GAMESS/Firefly is given in Appendix.



```

Geometry Search using BFGS update
Cycle  Energy[au]  deE [au]  Grad Norm  |Max Grad[i]|  alpha
*****
start -77.013049  0.0000e+000  0.000317  0.000095
  1  -77.013049  -3.9284e-008  0.000303  0.000091  4.0000e-001
  2  -77.013049  -3.0711e-007  0.000213  0.000068  4.0000e-001
Geometry optimization converged !!
Calculating Properties
Calculation Finished

```

Fig. 18 *The optimized structure of carbene at AM1 level in ArgusLab*

The input file for PC GAMESS/Firefly was opened in RUNpcg⁴⁸ and the calculation was run. Subsequently, from the output file of the geometry optimization the ENT file was generated. This file was opened in ArgusLab and the selected bond distances and angles were measured (Fig. 19).

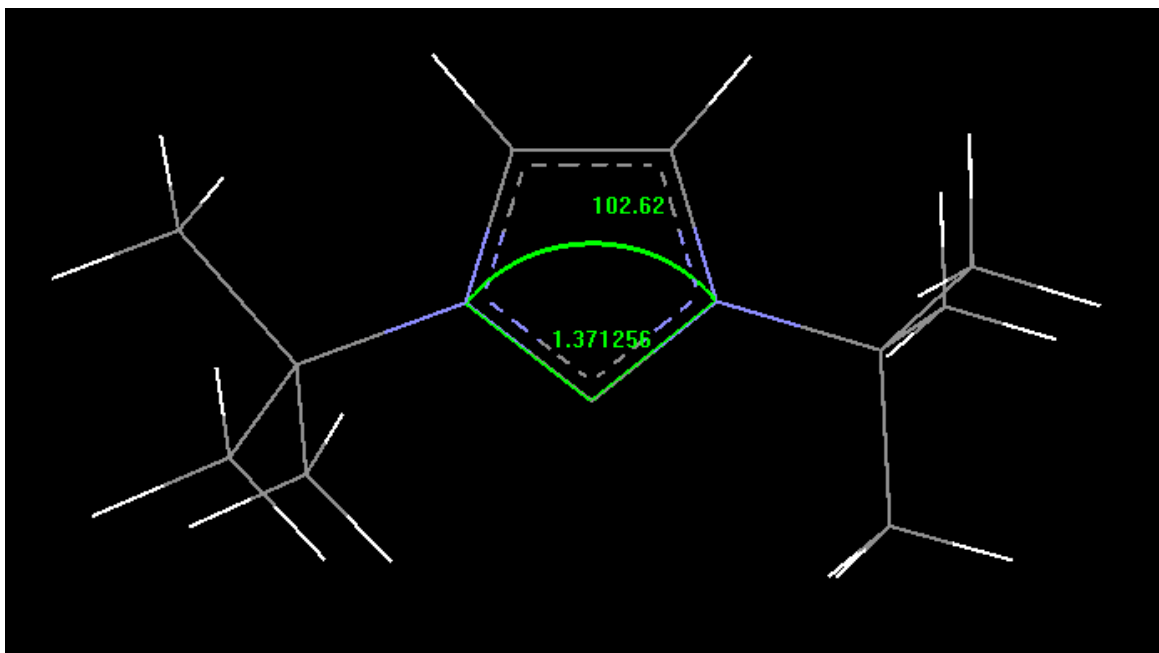


Fig. 19 The measurement of bond distances and bond angles

Then the input file of spectra prediction was created from the output file of the geometry optimization. Spectra calculations were run in RUNpcg as well. Output file was read, visualized and converted into XY format in Gabedit⁴⁷ (Fig. 20). Subsequently, spectra were set up in Excel⁴⁹.

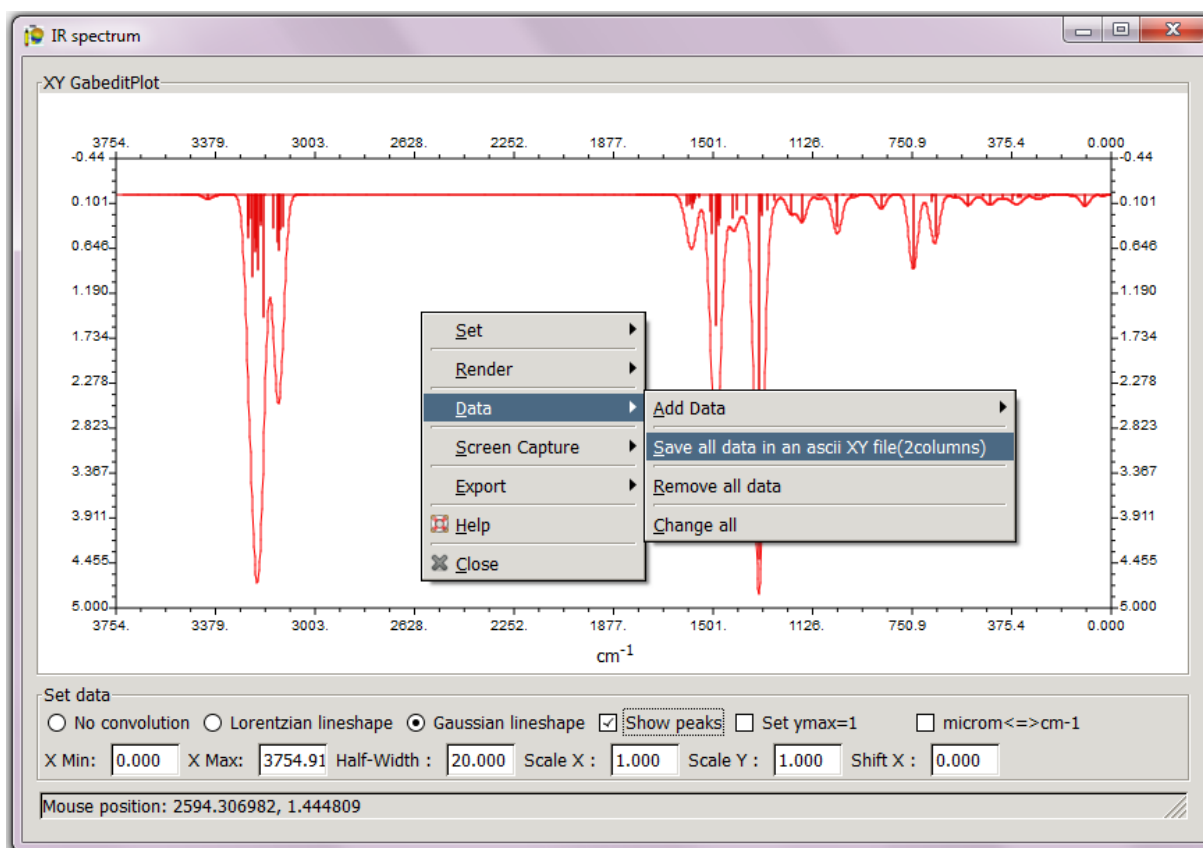



Fig. 20 The visualisation and the conversion of the output file

Program WinSCP⁵⁰ was used to transfer input files in the INP format between a local and a remote computer, while program PuTTY⁵¹ was used to run a calculation by using the command line. Program WinSCP can serve as freeware FTP (File Transfer Protocol) and SFTP (Secure File Transfer Protocol) client, while program PuTTY can act as a client for SSH (Secure Shell) or raw TCP (Transmission Control Protocol) computing protocol. For more detail you can see previous work³⁶.

2.8.2 Operating Titan and Spartan

How it was mentioned, Titan⁴⁵ is the older version of Spartan⁴⁶, hence both programs have similar operations. Both programs include graphical user interface, so they do not need to form the input file as PC GAMESS/Firefly. In Titan the structures of carbenes was built as well to compare with ones from ArgusLab. The molecule was constructed from atomic segments that specify atom type and local environmental (tetrahedral carbon in Fig. 21). Subsequently, the structure was minimized at molecular mechanics level by clicking on the icon .

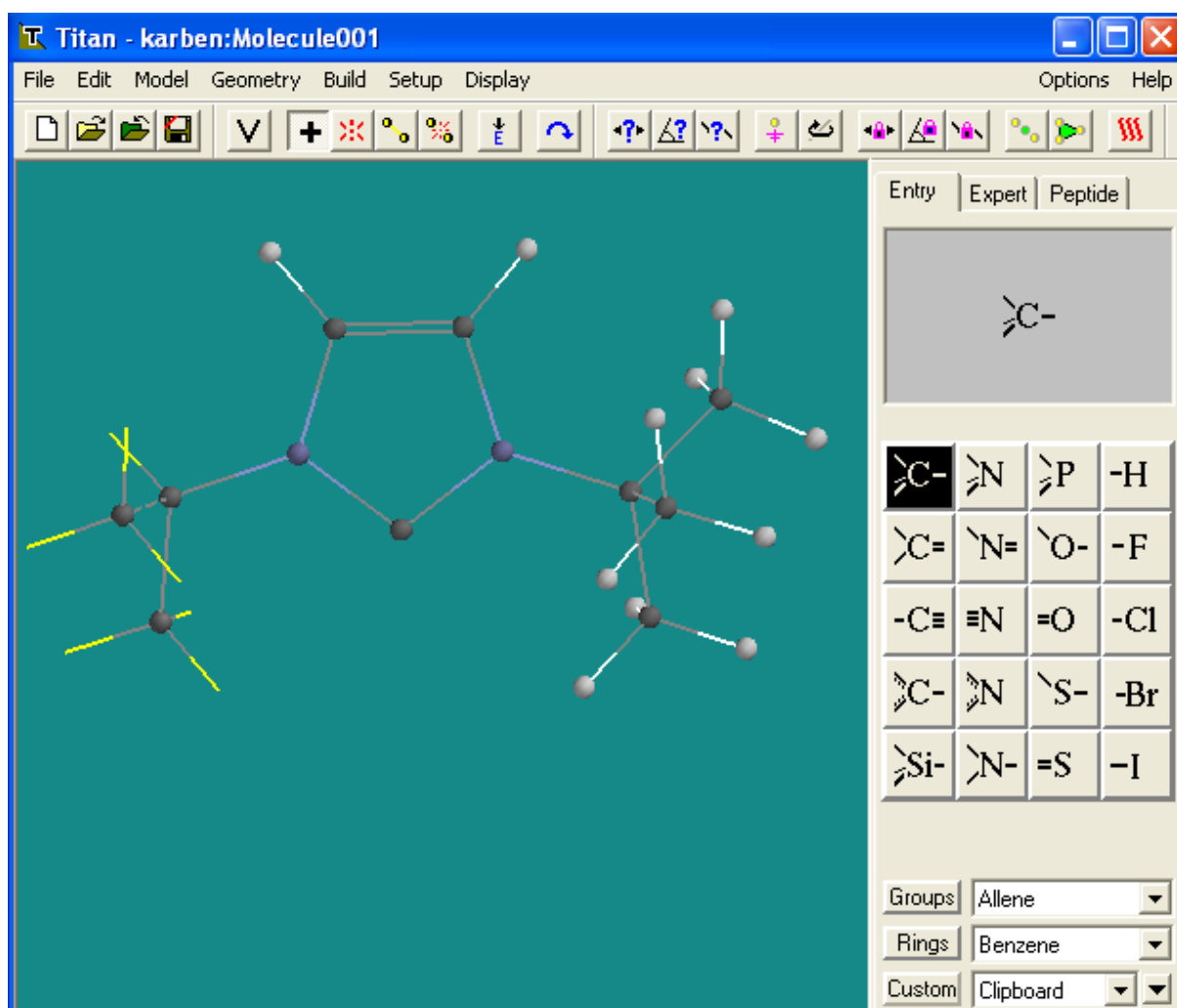


Fig. 21 The construction of the molecule in Titan (tetrahedral carbon in model kit is marked black)

After that Calculations dialog from Setup menu was opened, the type of calculation was selected (Fig. 22) and the job was submitted. At first the molecule was optimized at semi-empirical level, then at RHF and DFT (B3LYP) level.

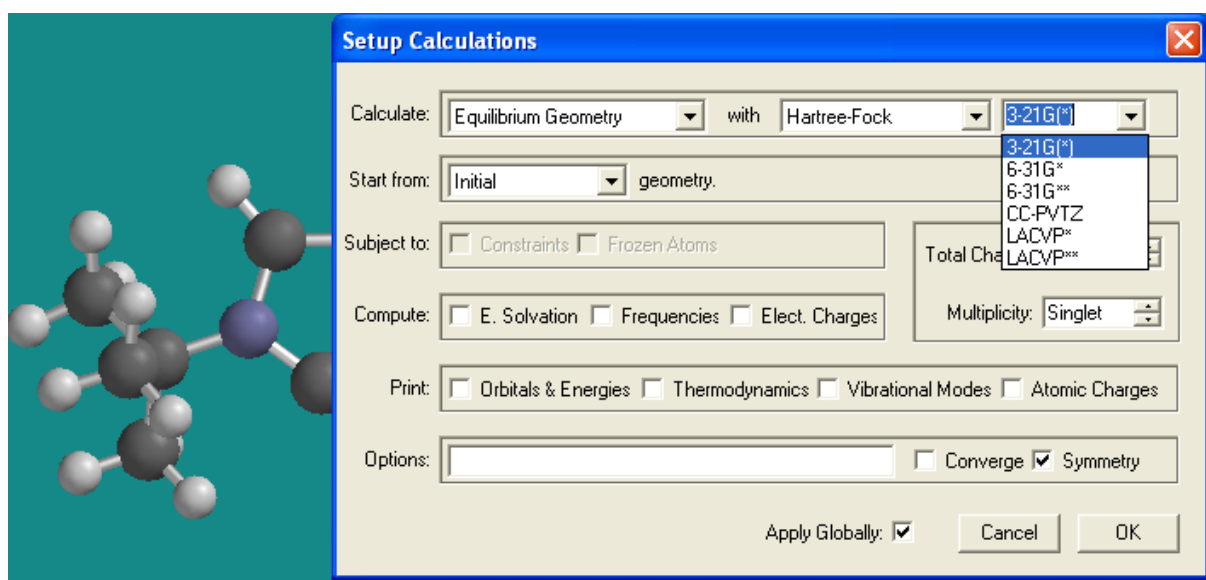


Fig. 22 *The selection of type of calculation*

In Titan it is possible to calculate vibrational frequencies as well. The option of frequencies to right of “Compute” was selected in Calculations dialog from Setup menu and calculation was run. Then Vibration List from Display menu was opened (Fig. 23). After the clicking on frequency in the Vibration List an individual motion was animated. Furthermore, in Spartan calculated and measured spectra can be compared.

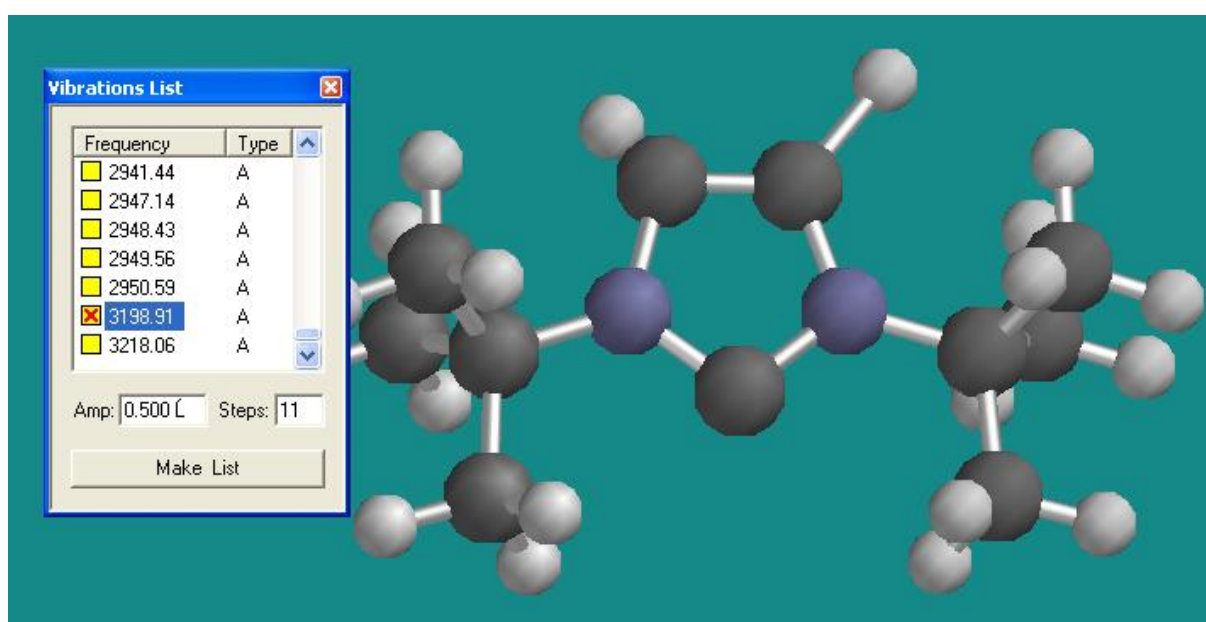

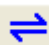



Fig. 23 *The animation of vibrational frequencies*

Titan and Spartan are able to study interactions, reactions and their mechanisms. In this point the generation of an interaction between the carbene and the alcohol (H-bond) will be discussed. In the beginning molecules of the carbene and of the alcohol were constructed in other files and both structures were optimized at AM1 level. Subsequently, both optimized structures were inserted into the same file (in Titan both structures must be constructed and optimized in the same file). The icon  was used and alcohol hydrogen atom and carbene carbon atom were selected. The transition state at molecular mechanics level was generated (Fig. 24) by clicking on the icon  (in Spartan the icon ). The proposed transition state was optimized at AM1 level.

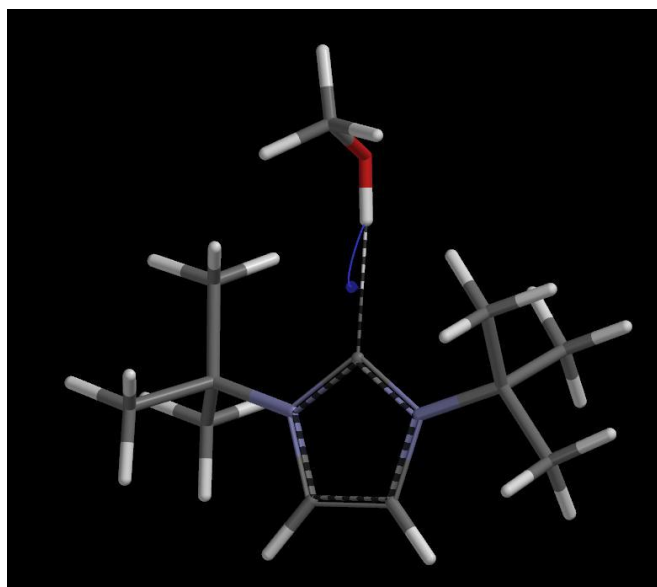


Fig. 24 *The generation (blue arrow) of transition state at molecular mechanics level in Spartan*

3 EXPERIMENTAL PART

3.1 Studied compounds

The study was focused on a 1,3-di-*tert*-butylimidazolium chloride **NC₁H-Cl**, 1,3-di-*tert*-butylimidazol-2-ylidene **NC₁** as “free” carbene, its possible hydrolysis products *N*-*tert*-butyl-*N*-[(2*E*)-2-(*tert*-butylimino)ethyl]formamide (1,4-di(*tert*-butyl)-4-formyl-1,4-diaza-but-1-ene) **N=C-CA** and *N*-*tert*-butyl-*N*-[(2*Z*)-2-(*tert*-butylamino)ethenyl]formamide **N-C=CA** and their saturated analogues; 1,3-di-*tert*-butyl-imidazolinium chloride **NC₂H-Cl**, 1,3-di-*tert*-butylimidazolin-2-ylidene **NC₂** and *N*-*tert*-butyl-*N*-[2-(*tert*-butylamino)ethyl]formamide (*N*-formyl-*N,N'*-di-*tert*-butylethylenediamine) **N-C-CA** (Fig. 25). **NC₁H-Cl** was kindly donated by Dr. Gerard Mignani from Rhodia Operations – Centre de Recherches de Lyon, France. “Free” carbene **NC₁** was prepared from **NC₁H-Cl** according to the published procedure using butyllithium¹⁰. Other compounds were studied only at theoretical level by using computational studies. **N=C-CA** was confirmed as a product of hydrolysis which proceeded slowly for a period of days and explains the “air sensitivity” of respective carbene⁷. Recently, the possible formation of two ring-opening isomers as the products of the imidazol-2-ylidene hydrolysis has been reported⁸.

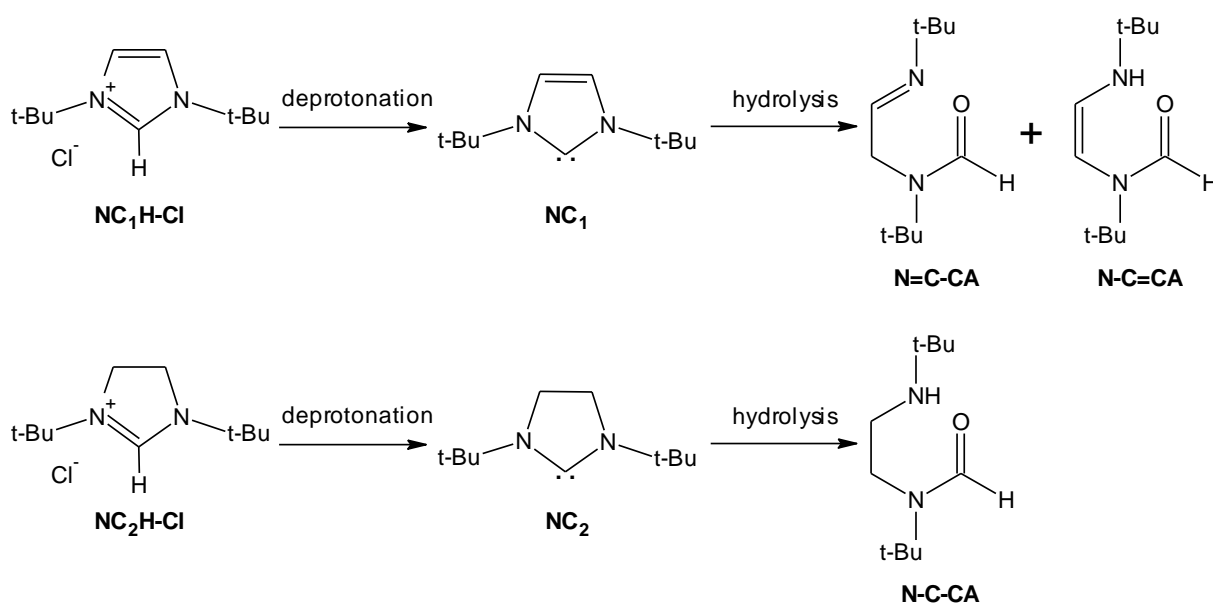


Fig. 25 Studied compounds

3.2 Softwares and computational methods

3.2.1 Fundamental calculations

Calculations were done in ArgusLab⁴⁴ and Titan. In ArgusLab methods of molecular mechanics (UFF, AMBER) and semi-empirical methods (MNDO, AM1, PM3) were used, whereas in Titan⁴⁵ methods of molecular mechanics (MMFF, SYBYL), semi-empirical methods (MNDO, AM1, PM3), RHF/6-31G(d) and B3LYP/6-31G(d) methods were used. For calculations only one isolated molecule in vacuum was taken into account.

3.2.2 Geometry optimization

Calculations were performed in PC GAMESS/Firefly^{42,43}. In previous work³⁶ bond distances and bond angles were calculated at RHF and DFT (B3LYP functional) level with 6 different basis sets. Based on previous calculations different functionals of DFT method with 6-31G(d) basis set were investigated. Atoms were numbered according to Fig. 26. Energy gradients were calculated analytically with the optimization tolerance set to $1 \cdot 10^{-5}$ Hartree/Bohr. Since calculations on the computer were too slow (sometimes a number of days), the most calculations were continued on the BUT server monkey2.ro.vutbr.cz. Programs WinSCP⁵⁰ and PuTTY⁵¹ were used for the manipulation on the server (discussed in Section 2.8.2). Moreover, a structure of **NC**₁ was optimized also at AM1, RHF/6-31G(d) and B3LYP/6-31G(d) levels in Spartan⁴⁶ for comparison with PC GAMESS/Firefly. For calculations only one isolated molecule in vacuum was taken into account.

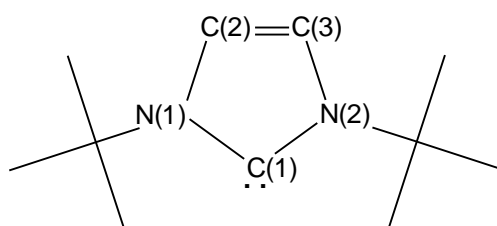


Fig. 26 The numbering of atoms

3.2.3 Spectra prediction

Calculations were computed in PC GAMESS/Firefly^{42,43} and B3LYP/6-31G(d) level was mainly used. For the comparison of spectra other functionals (O3LYP, BHLYP and PBE0) were used. Computed frequencies contain known systematic errors, therefore it is usual to scale frequency⁴¹ predicted at B3LYP/6-31G(d) level by empirical factor of 0.9613, at O3LYP/6-31(d) level by empirical factor of 0.9617, at BHLYP level by empirical factor of 0.9244 and PBE0 level by empirical factor of 0.9512. The most calculations were calculated on the BUT server monkey2.ro.vutbr.cz. For the comparison the spectrum of **NC**₁ was calculated and compared with the measured one in Spartan⁴⁶. For calculations only one isolated molecule in gaseous phase at 298.15 K was assumed.

3.2.3 Study on the mechanism of ROP of lactide

Calculations were done in Spartan. For the generation of transition state methods of molecular mechanics were used. All stationary points were optimized at AM1 and B3LYP/6-31G(d) levels. The functions of Transition States, Freeze Center, Constrain Distance and Set Torsion were used. Structures were optimized in gaseous phase in vacuum.

3.3 Gained data

3.3.1 Databases

Data of already characterized compounds including **NC**₁⁷, **NC**₂⁵², **N-C-CA**⁷ and similar precursors (**NC**₁**H-F**₃**CSO**₃⁵³, **NC**₂**H-SCN**⁵⁴) were gained from CCDC (Cambridge Crystallographic Data Centre) and were used for the comparison with calculated data.

3.3.2 Measurement

3.3.2.1 FTIR spectra

FTIR spectra of $\text{NC}_1\text{H-Cl}$ and FTIR spectra of NC_1 in the region $400\text{-}4000\text{ cm}^{-1}$ were recorded on a Bruker TENSOR 27 as KBr pellets prepared in dry a box under nitrogen atmosphere.

3.3.2.2 RA spectra

RA spectra of $\text{NC}_1\text{H-Cl}$. RA spectra, which in the region $100\text{-}3500\text{ cm}^{-1}$ were measured on a Bruker EQUINOX IFS 55/S equipped with a Raman module FRA 106/S. The excitation line was $1\ 064\text{ nm}$ of a Nd:YAG laser. The solids samples were placed in a Schlenk flask under nitrogen atmosphere.

4 RESULTS AND DISCUSSION

4.1 Fundamental calculations

Initially, selected molecular orbitals and electrostatic potential maps were computed. In previous work³⁶ calculations were done in ArgusLab⁴⁴ with the semi-empirical methods, now these calculations were compared with calculations in Titan and were extended by RHF and DFT level.

4.1.1 Orbitals

Since generally, both the symmetry and the energy of HOMO and LUMO (highest occupied and lowest unoccupied molecular orbitals) have a significant influence on the mechanisms of reactions of molecules, the energies of molecular orbitals of $\text{NC}_1\text{H-Cl}$, NC_1 , $\text{NC}_2\text{H-Cl}$, NC_2 were initially computed. Selected molecular orbitals and electrostatic potential maps were calculated at AM1 and PM3 levels in ArgusLab⁴⁴ and subsequently at the same levels and B3LYP/6-31G(d) level in Titan⁴⁵. Due to the small band gap both the studied carbenes NC_1 and NC_2 are very reactive. How it was supposed, calculated molecular orbitals at the equal level had the same character in both programs (Fig. 27, Fig. 28). The difference between predicted HOMO at AM1 level against PM3 level was noticeable (Fig. 28, Fig. 29), on the other hand LUMO showed the same character at both levels. The differences are caused different experimental sets of data that are included in computational methods (discussed in Section 2.4.5). Further, it was illustrated that LUMO predicted at more complicated level (B3LYP/6-31G(d)) was almost identical (Fig. 30).

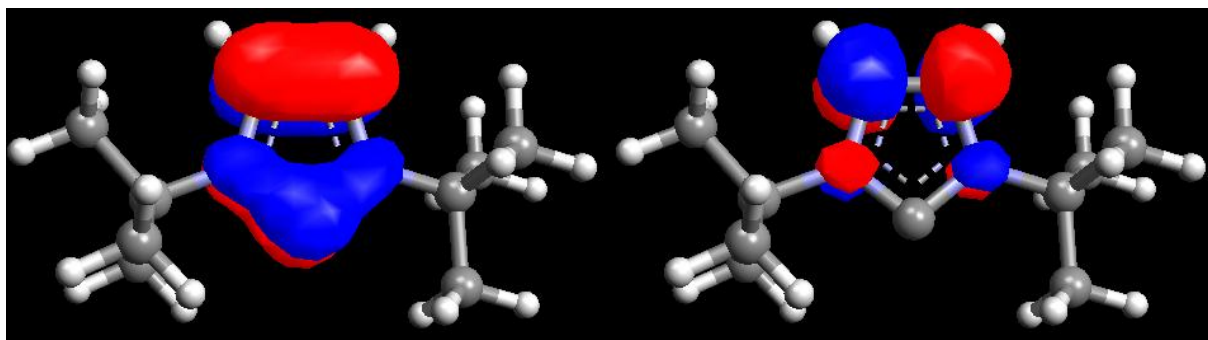


Fig. 27 The calculation of HOMO (left) and LUMO (right) of NC_1 at AM1 level in ArgusLab

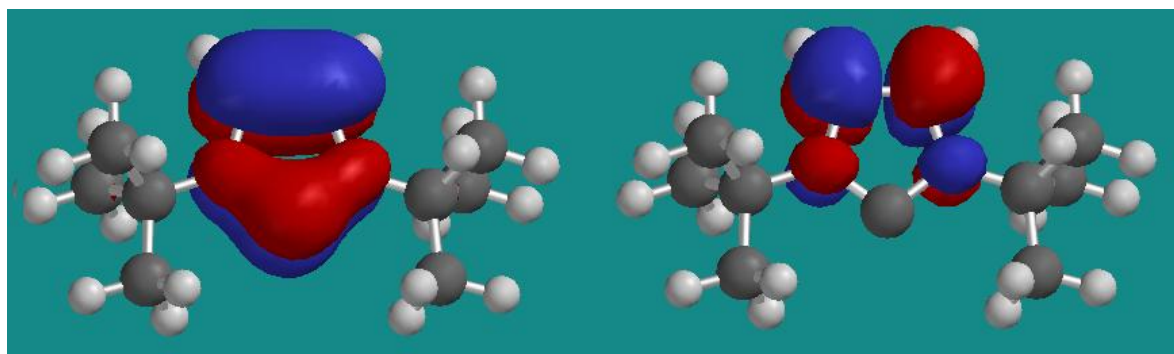


Fig. 28 The calculation of HOMO (left) and LUMO (right) of NC_1 at AM1 level in Titan

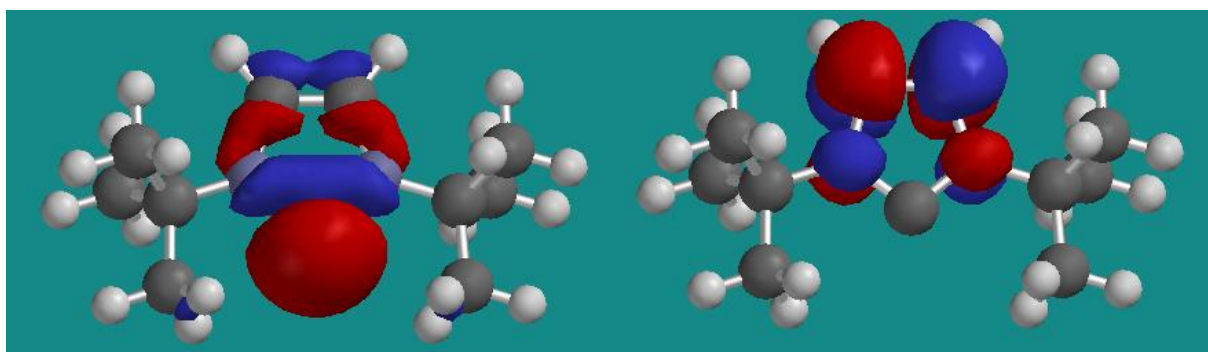


Fig. 29 The calculation of HOMO (left) and LUMO (right) of NC_1 at PM3 level in Titan

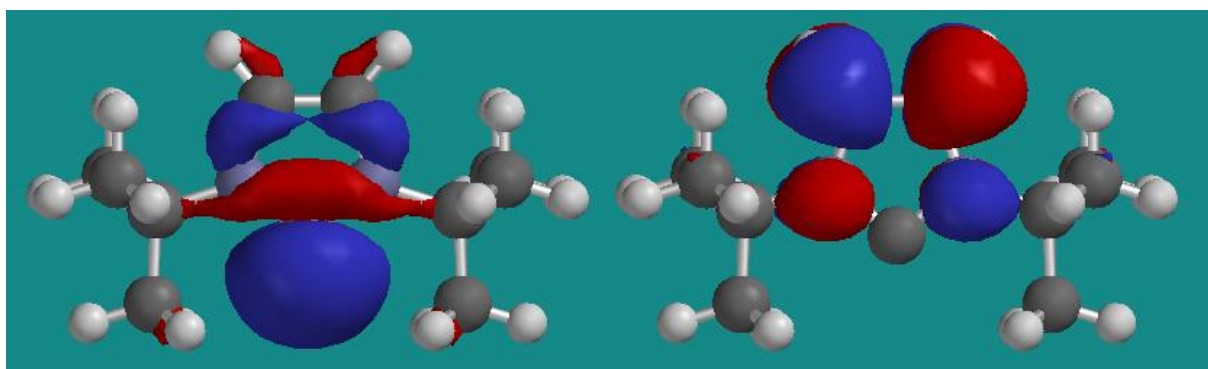


Fig. 30 The calculation of HOMO (left) and LUMO (right) of NC_1 at B3LYP/6-31G(d) level in Titan

4.1.2 Electrostatic potential maps

From the electrostatic potential maps (Fig. 39) it was possible to notice that the electrostatic potential on the carbene centre was bigger onto unsaturated carbene than onto saturated analogue. This fact could be correlated with catalytic activity. In 2005, Lai *et al.*²³ reported that imidazol-2-ylidene against imidazolin-2-ylidene has better catalytic capacity because of less activation barrier for transesterification reactions. On the other hand the electrostatic potential on the carbene centre of corresponding chlorides NC_1H-Cl , NC_2H-Cl was lower.

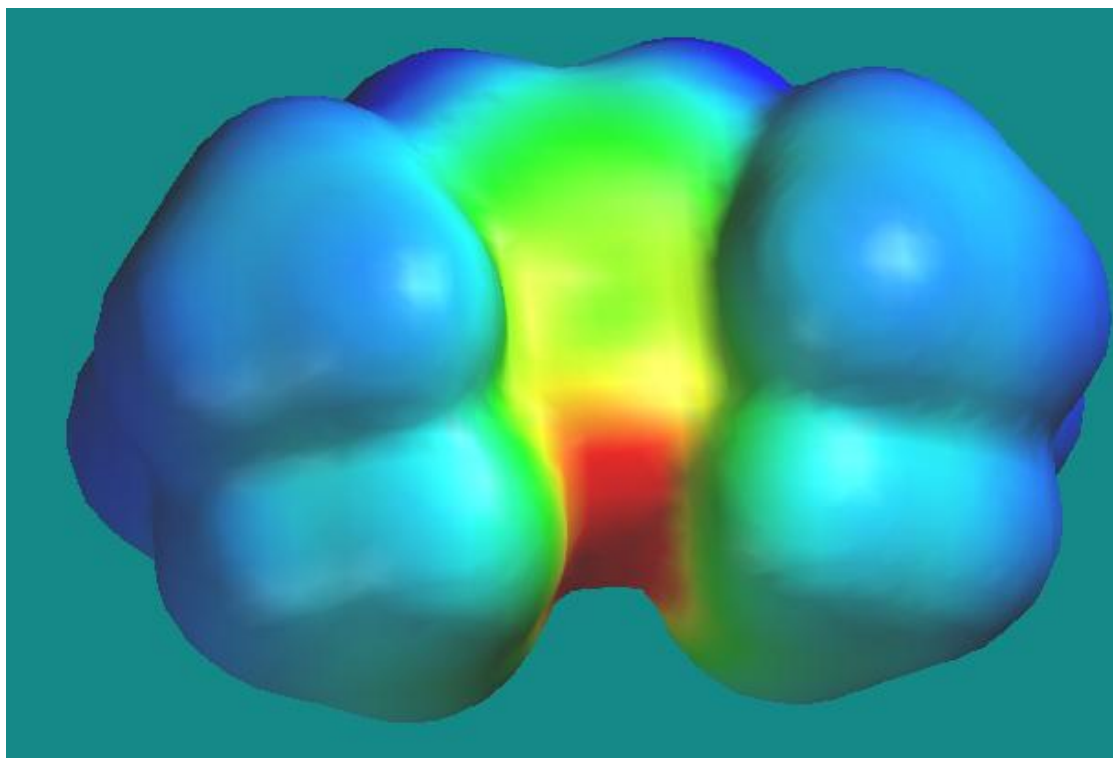


Fig. 31 *The electrostatic potential maps of NC₁ predicted at AM1 level in Titan*

4.2 Geometry optimization

4.2.1 Carbenes and their precursors

Best predictions of selected bond distances and bond angles of **NC₁**, **NC₁H-Cl**, **NC₂** and **NC₂H-Cl** are summarized in Appendix. Moreover predicted structures of **NC₁** and **NC₂** are compared with data from CCDC, therefore their tables contain average relative errors E_{\emptyset} . In Fig. 32 the optimized structure of **NC₂H-Cl** was presented. Best calculations were presented at 5th meeting on Chemistry and Life 2011⁵⁵. Bond distances and relative errors of **C(1)-N(1)** bond of **NC₁** calculated by different functionals were depicted in Fig. 33. This bond distance was best predicted by PBE0, PBE1PW91 and B3PW91 functionals. Based on all calculations it was investigated, that the best results of **NC₁** were obtained at O3LYP/6-31G(d) level. Good results were achieved with SVWN5 and BHLYP functionals aspect to CPU time. In contrast, the worse results were obtained with BLYP functional aspect to big average relative error and long CPU time. In summary good results were reached with all hybrid functionals. On the other hand only some types of exchange-correlation functionals (SVWN5 functional) were successful. **NC₁** was optimized also at AM1, RHF/6-31G(d) and B3LYP/6-31G(d) levels in Spartan⁴⁶. Moreover, in Spartan the symmetry of the molecule can be easily include in calculations. Results are summarized in Appendix. The structure with the symmetry C_{2v} is about 2.55 kJ·mol⁻¹ more stable than with symmetry C_s at B3LYP/6-31G(d) level, which is in agreement with the fact that according to CCDC⁷ the known symmetry of **NC₁** is C_{2v} . For **NC₂** the similar trends were noticed. **C(1)-N(1)** bond distance was best predicted by PBE0, PBE1PW91 and B3PW91 functionals as well. The best results of **NC₂** were obtained at PBE0/6-31G(d) level. Good results were achieved with SVWN5 functional as well, while the worse results were obtained by GLYP functional.

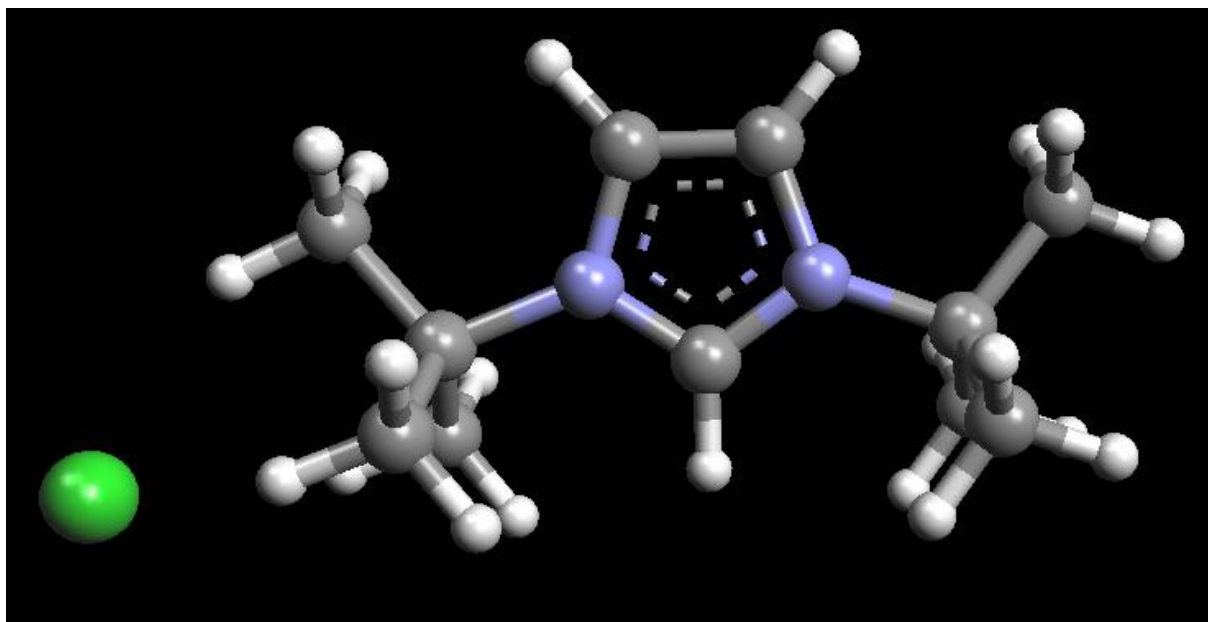


Fig. 32 The structure of $\text{NC}_2\text{H-Cl}$ optimized at B3LYP/6-31G(d) in ArgusLab

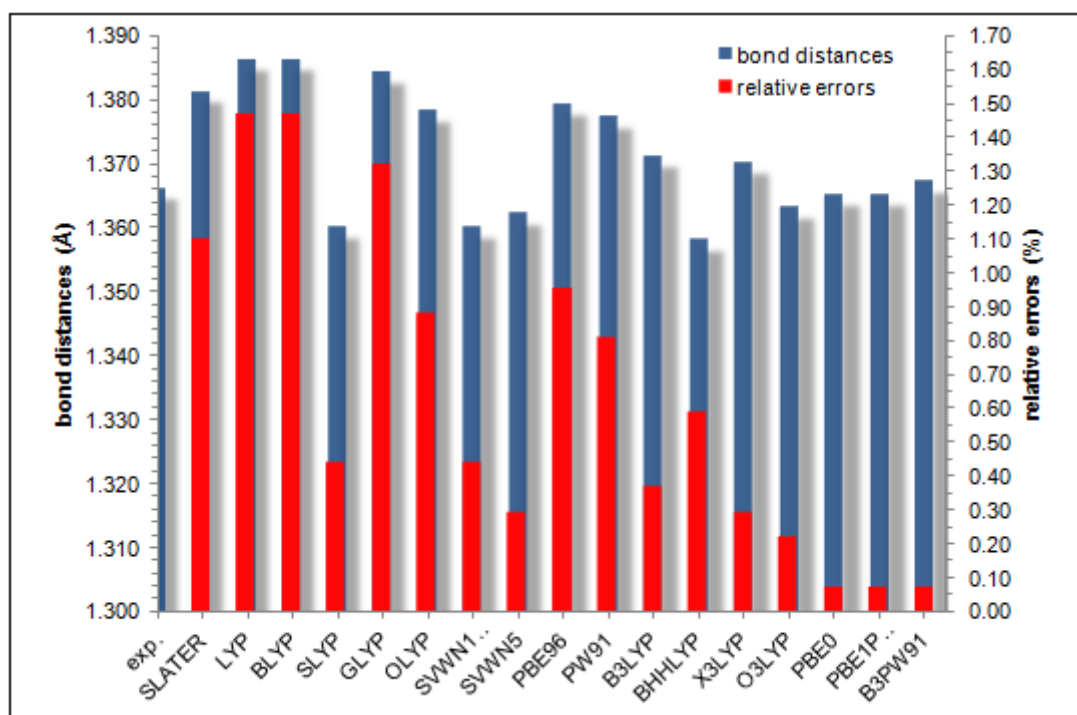


Fig. 33 Bond distances and relative errors of $\text{C}(1)\text{-N}(1)$ bond of NC_1 calculated by different functionals

Calculated data of chloride precursors could not be compared directly, because up till now any structural data of these compounds have not been published yet. Therefore selected bond distances and bond angles of other known precursors ($\text{NC}_1\text{H-F}_3\text{CSO}_3$, $\text{NC}_2\text{H-SCN}$) were computed. Best predictions of $\text{NC}_1\text{H-F}_3\text{CSO}_3$ and $\text{NC}_2\text{H-SCN}$ are summarized in Appendix. Bond distances and relative errors of $\text{C}(1)\text{-N}(1)$ bond of $\text{NC}_1\text{H-F}_3\text{CSO}_3$ calculated by

different functionals were depicted in Fig. 34. This bond distance was best predicted by B3LYP and X3LYP functionals. Based on all calculation it was noticed, that the best results of $\text{NC}_1\text{H-F}_3\text{CSO}_3$ were obtained with X3LYP functional, whereas the best results of $\text{NC}_2\text{H-SCN}$ were achieved with SVWN5 functional. Aspect to these results it could be supposed that the best functional for unsaturated salts ($\text{NC}_1\text{H-Cl}$) is X3LYP functional, whereas for saturated salts ($\text{NC}_2\text{H-Cl}$) is SVWN5 functional. Moreover calculations of precursors compared to carbenes took more CPU time.

In summary it was calculated that bonds C(1)-N(1) and N(1)-C(2) cut down against bonds of the appropriate carbenes, on the other hand the bond C(2)-C(3) elongated and the angle N(1)-C(1)-N(2) increased. The deviation could be the consequence of taking one isolated molecule in vacuum into account for the calculation. Compared to previous calculation³⁶ the best predictions achieved smaller deviations. To reach a better accuracy the using of the better method (MP2, CI) or the better basis set (cc-pVDZ, aug-cc-pVDZ) represents one of possible ways.

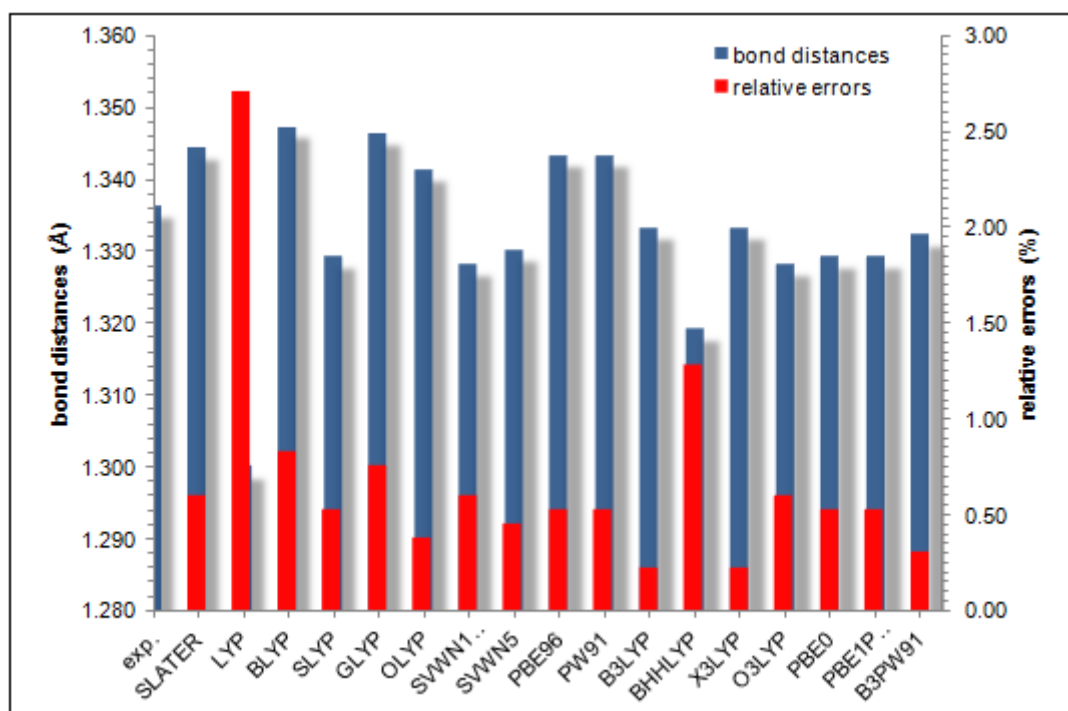


Fig. 34 Bond distances and relative errors of C(1)-N(1) bond of $\text{NC}_1\text{H-F}_3\text{CSO}_3$ calculated by different functionals

4.2.2 Hydrolysis products

Geometry optimization of hydrolysis products were done due to the enhancement of spectra interpretation. Best predictions of selected bond distances and bond angles are summarized in Appendix. In Fig. 35 the optimized structure of N-C-CA was depicted. Based on the results of calculations the best results of N-C-CA were obtained at B3PW91/6-31G+(d,p) level. It was found out that N=C-CA is more stable than N-C=CA due to the fact that N=C-CA is located

about $7.8 \text{ kJ}\cdot\text{mol}^{-1}$ lower in energy which agrees well with Denk's⁷ and Holloczki's⁸ works. Further, it was calculated that the bond length **N(1)-C(2)** of **N=C-CA** is shortened by 0.04 \AA in comparison with that of the corresponding tautomer **N-C=CA**, whereas the bond **C(2)-C(3)** by 0.17 \AA . On the other hand, bond length **C(3)-N(2)** is elongated by 0.12 \AA and angle value is increased by 1.39° . Calculated bonds lengths **N(1)-C(2)**, **C(2)-C(3)** and **C(3)-N(2)** of **N-C-CA** were the longest ones, which is in the agreement with the fact that single bonds are longer than double bonds.

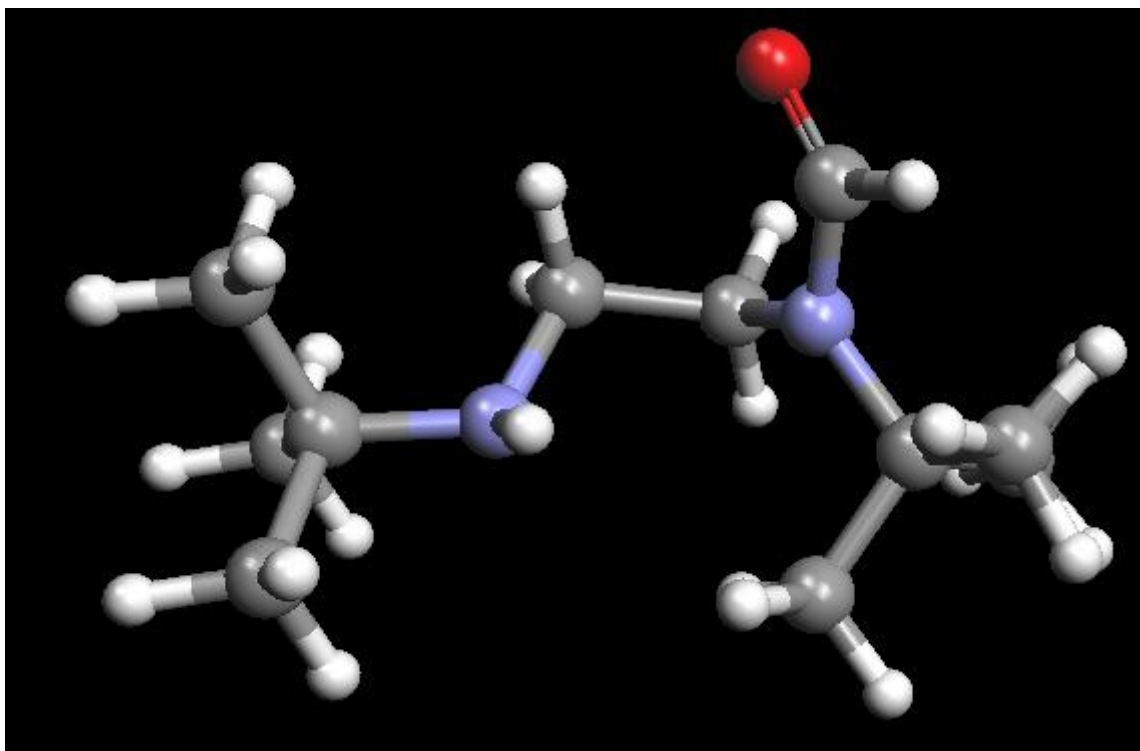


Fig. 35 The structure of **N-C-CA** optimized at **B3PW91/6-31G(d)** in **ArgusLab**

4.3 Spectra prediction

IR and than RA spectra of **NC₁H-Cl** (Fig. 36) and **NC₁** (Fig. 37) were obtained from data of geometry optimization. For the prediction of spectra **B3LYP/6-31G(d)** level was mainly used. The comparison of the spectra predictions at different levels is available in Appendix. All predicted spectra had the similar character, however differed in wavenumbers. The calculated spectra were compared with measured ones. Further, both measured IR spectra of **NC₁** (Fig. 38) were confronted with published Leites' data⁵⁶. These IR spectra did not correspond completely, therefore spectra of possible hydrolysis products (**N=C-CA**, **N-C=CA**) were calculated (Fig. 39). In the IR spectrum of the carbene **NC₁** synthesised according to Denk⁷ (1st synthesis) the presence of weak absorption band at 1686 cm^{-1} was revealed. Based on the calculated vibrational frequency of 1696 cm^{-1} belonging to $\nu_{C=O}$, the presence of the hydrolysis product **N=C-CA** in studied carbene **NC₁** is suggested. Our

measured (2nd synthesis) IR spectrum corresponded with Leites' IR spectrum⁵⁶. The table with compared wavenumbers is available in Appendix.

We did not find well correlation between calculated and measured (2nd synthesis) IR spectra (Fig. 40), but it is necessary to mention, that for predictions only one isolated molecule in gaseous phase was assumed. On the contrary, for the measurement the compound in solid state was taken. In Fig. 41 the example of the comparison of both spectra in Spartan⁴⁶ is presented. To get deeper insight into this field further research will be done.

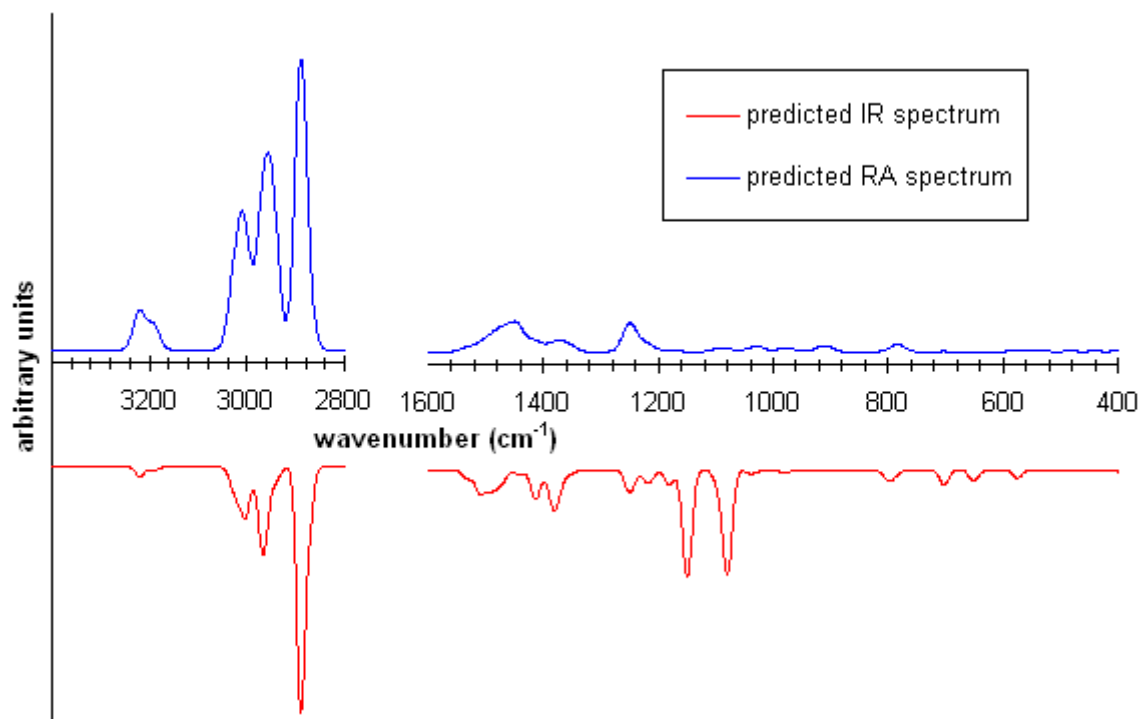


Fig. 36 The predicted IR spectrum of NC_1H-Cl at B3LYP/6-31(d) level ν (cm^{-1}): 573 (vw), 651 (vw), 677 (vw), 731 (vw), 799 (vw), 914 (vw), 982 (vw), 1037 (vw), 1081 (m), 1152 (m), 1180 (vw), 1217 (vw), 1252 (vw), 1383 (vw), 1415 (vw), 1490 (vw), 1508 (vw), 1532 (vw), 2892 (vs), 2967 (w), 3007 (w), 3219 (vw) and the predicted RA spectra of NC_1H-Cl at B3LYP/6-31(d) level ν (cm^{-1}): 575 (vw), 782 (vw), 909 (vw), 982 (vw), 1028 (vw), 1097 (vw), 1249 (vw), 1369 (vw), 1415 (vw), 1455 (vw), 2890 (vs), 2958 (m), 3010 (w), 3192 (vw), 3217 (vw)

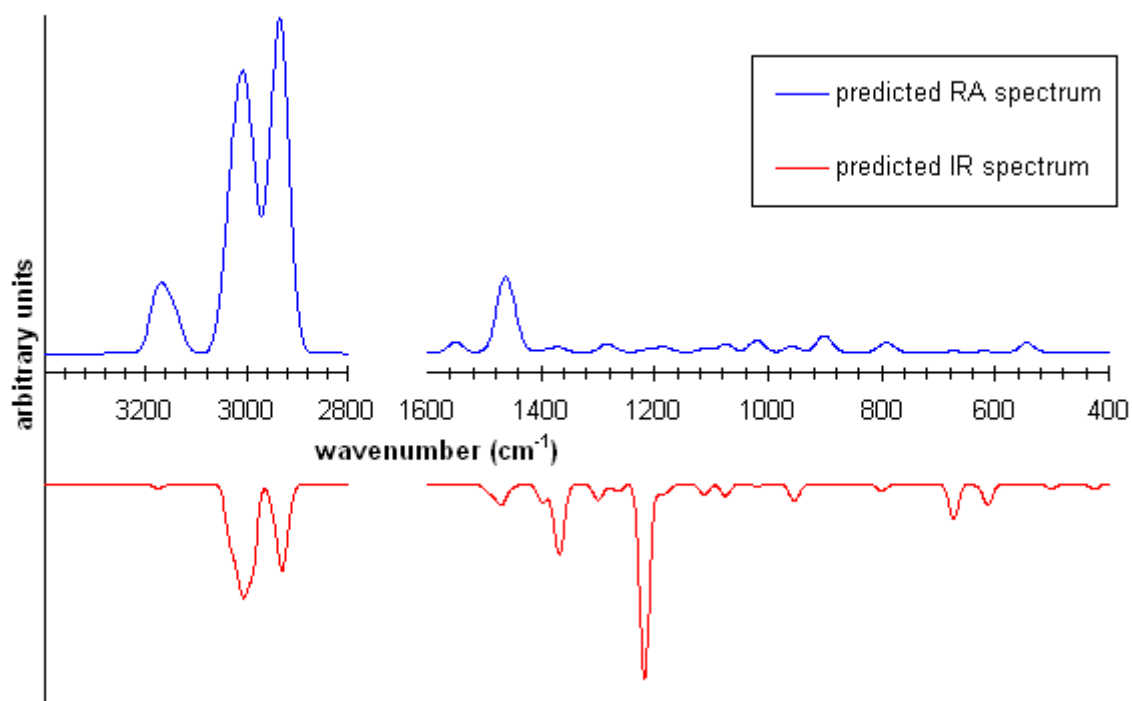


Fig. 37 The predicted IR spectrum of NC_1 at B3LYP/6-31(d) level ν (cm^{-1}): 425 (vw), 500 (vw), 546 (vw), 614 (vw), 673 (vw), 800 (vw), 907 (vw), 955 (vw), 1021 (vw), 1076 (vw), 1115 (vw), 1183 (vw), 1218 (s), 1265 (vw), 1301 (vw), 1366 (w), 1397 (vw), 1470 (vw), 2931 (m), 3009 (m), 3180 (vw) and the predicted RA spectrum of NC_1 at B3LYP/6-31(d) level ν (cm^{-1}): 543 (vw), 789 (vw), 902 (vw), 959 (vw), 1021 (vw), 1075 (vw), 1139 (vw), 1193 (vw), 1285 (vw), 1374 (vw), 1462 (w), 1549 (vw), 2935 (vs), 3008 (vs), 3170 (w)

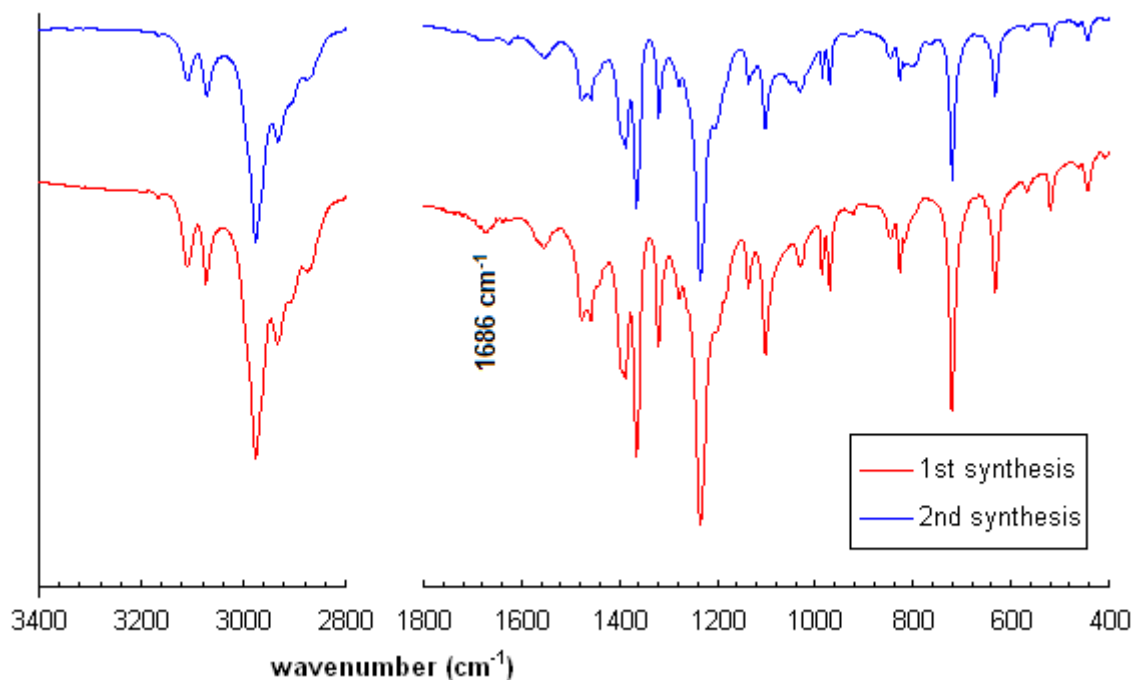


Fig. 38 The measured IR spectrum (1st synthesis) of NC_1 (KBr) ν (cm^{-1}): 444 (vw), 519 (vw), 567 (vw), 633(w), 719 (s), 816 (w), 827 (w), 847 (w), 922 (vw), 970 (w), 986 (w), 1031 (w), 1101 (m), 1136 (w), 1202 (m), 1234 (vs), 1277 (m), 1319 (m), 1366 (vs), 1387 (s), 1458 (m), 1476 (m), 1555 (w), 1657 (w), 1672 (w), 1686 (w), 2876 (w), 2909 (m), 2932 (m), 2976 (vs), 3073 (w), 3109 (w) and the measured IR spectrum (2nd synthesis) of NC_1 (KBr) ν (cm^{-1}): 444 (vw), 462 (vw), 519 (vw), 567 (vw), 633(w), 719 (s), 816 (w), 827 (w), 847 (w), 922 (vw), 970 (w), 985 (w), 1031 (w), 1101 (m), 1136 (w), 1186 (sh), 1203 (m), 1234 (vs), 1279 (w), 1319 (w), 1365 (s), 1387 (m), 1458 (w), 1475 (w), 1555 (vw), 2875 (w), 2901 (sh), 2931 (m), 2976 (vs), 3072 (w), 3109 (w)

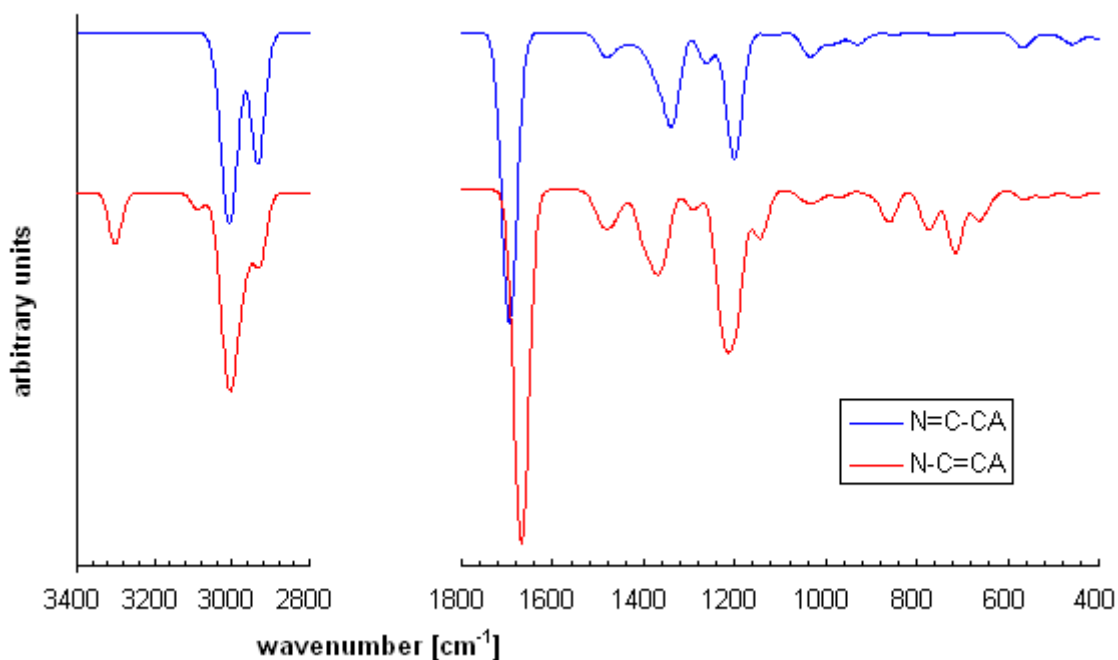


Fig. 39 The predicted IR spectrum of $N=C-CA$ at $B3LYP/6-31(d)$ level $\nu(\text{cm}^{-1})$: 454 (vw), 468 (vw), 571 (vw), 931 (vw), 1034 (vw), 1201 (m), 1340 (v), 1479 (vw), 1696 (vs), 2932 (m), 3004 (s) and the predicted IR spectrum of $N-C=CA$ at $B3LYP/6-31(d)$ level $\nu(\text{cm}^{-1})$: 451 (vw), 516 (vw), 562 (vw), 663 (vw), 716 (vw), 770 (vw), 861 (vw), 1033 (vw), 1142 (vw), 1212 (m), 1290 (vw), 1369 (w), 1483 (vw), 1669 (vs), 2929 (v), 3004 (m), 3089 (vw), 3001 (vw)

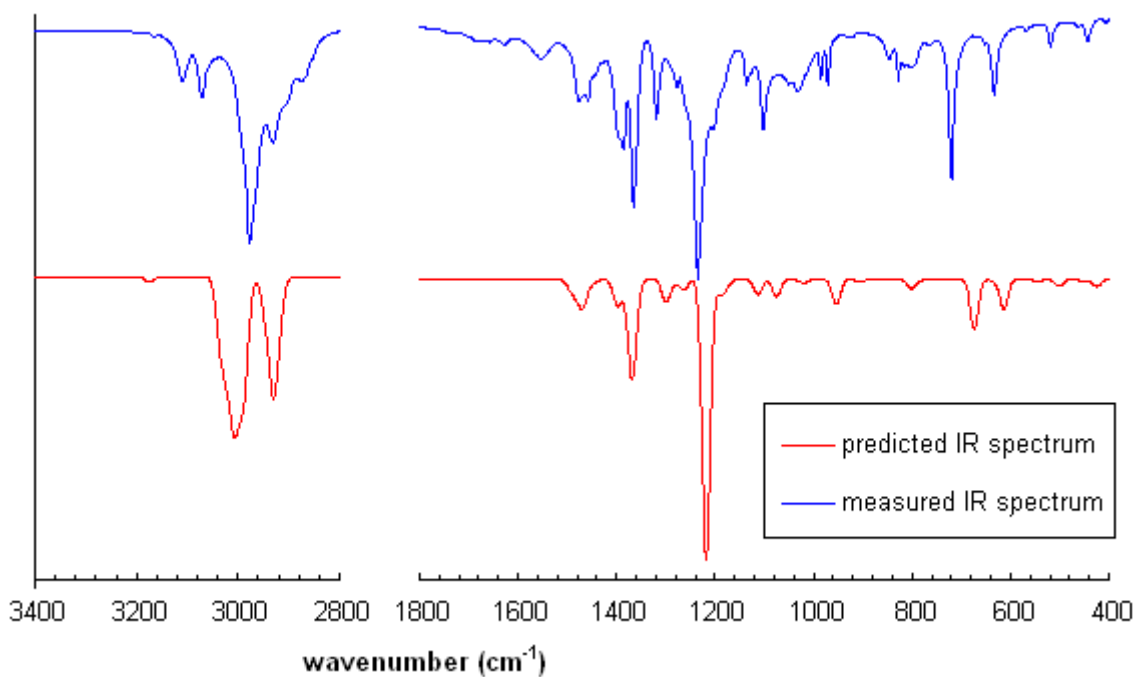


Fig. 40 The comparison of predicted ($B3LYP/6-31(d)$) and measured (2^{nd} synthesis) IR spectra of NC_1

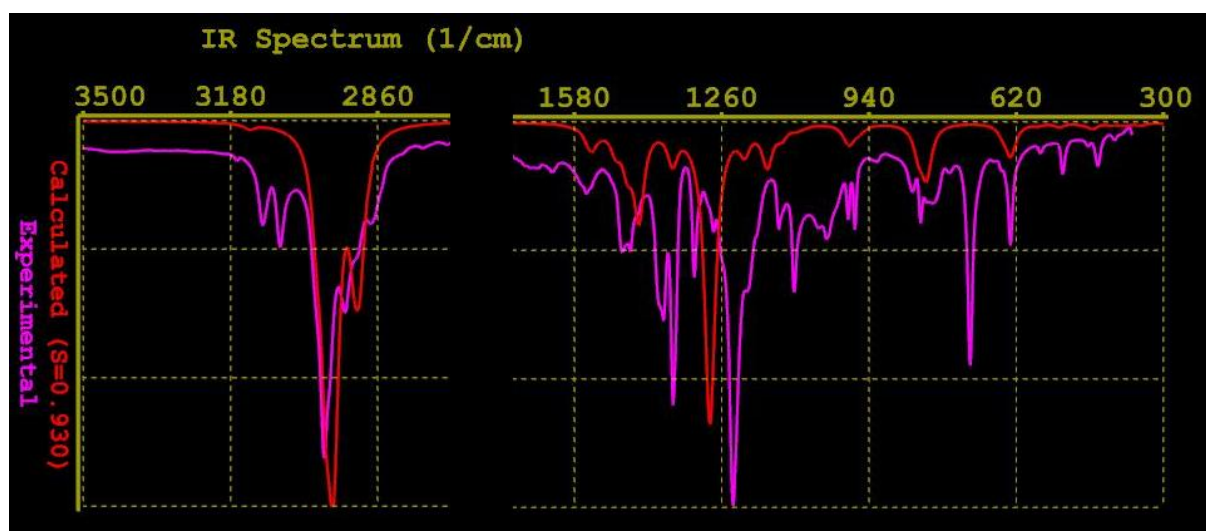


Fig. 41 The comparison of predicted and measured IR spectra of NC_1 in Spartan

4.4 Study on the mechanism of the ROP of lactide

Two mechanisms of ROP catalyzed by NHCs are widely accepted as it was discussed in Section 2.2.4. Initially, both mechanisms for system 1,3-di-*tert*-butylimidazol-2-ylidene, lactide and methanol S_1 were investigated. At first, nucleophilic monomer-activated mechanism was studied according to the proposed schema¹⁸ (Fig. 10). Energies of all reactants and their intermediates were computed. In this pathway the activation barrier was large and the simulation of the ring-opening of lactide was unsuccessful, therefore second possible mechanism was intensive studied (chain-end-activated mechanism).

Initially, all stationary points were optimized at AM1 and B3LYP/6-31G(d) level. Regarding the calculated energies the novel pathway of chain-end-activated mechanism was suggested (Fig. 42). This pathway was divided into two steps including an initiation and the ring-opening step. The crucial feature of the initiation step is the formation of H-bond and TS1 intermediate which could correspond with alcohol adduct (discussed in Section 2.2.5). Based on Tab. 3 it is obvious that both intermediates are located lower in energy than separated reactants. In the ring-opening step the four-centre bond in transition state TS2 is formed and methanol hydrogen causes the ring-opening of lactide. Chain-end-activated mechanism had the lower activation barrier than nucleophilic route and similar features as the known basic concerted route of the DMAP-catalyzed ring-opening of lactide with methanol²⁶ (Fig. 9). The energy profile of both mechanisms was presented in Fig. 43. For comparison the same method was applied for system 4-dimethylaminopyridine, lactide and methanol S_2 .

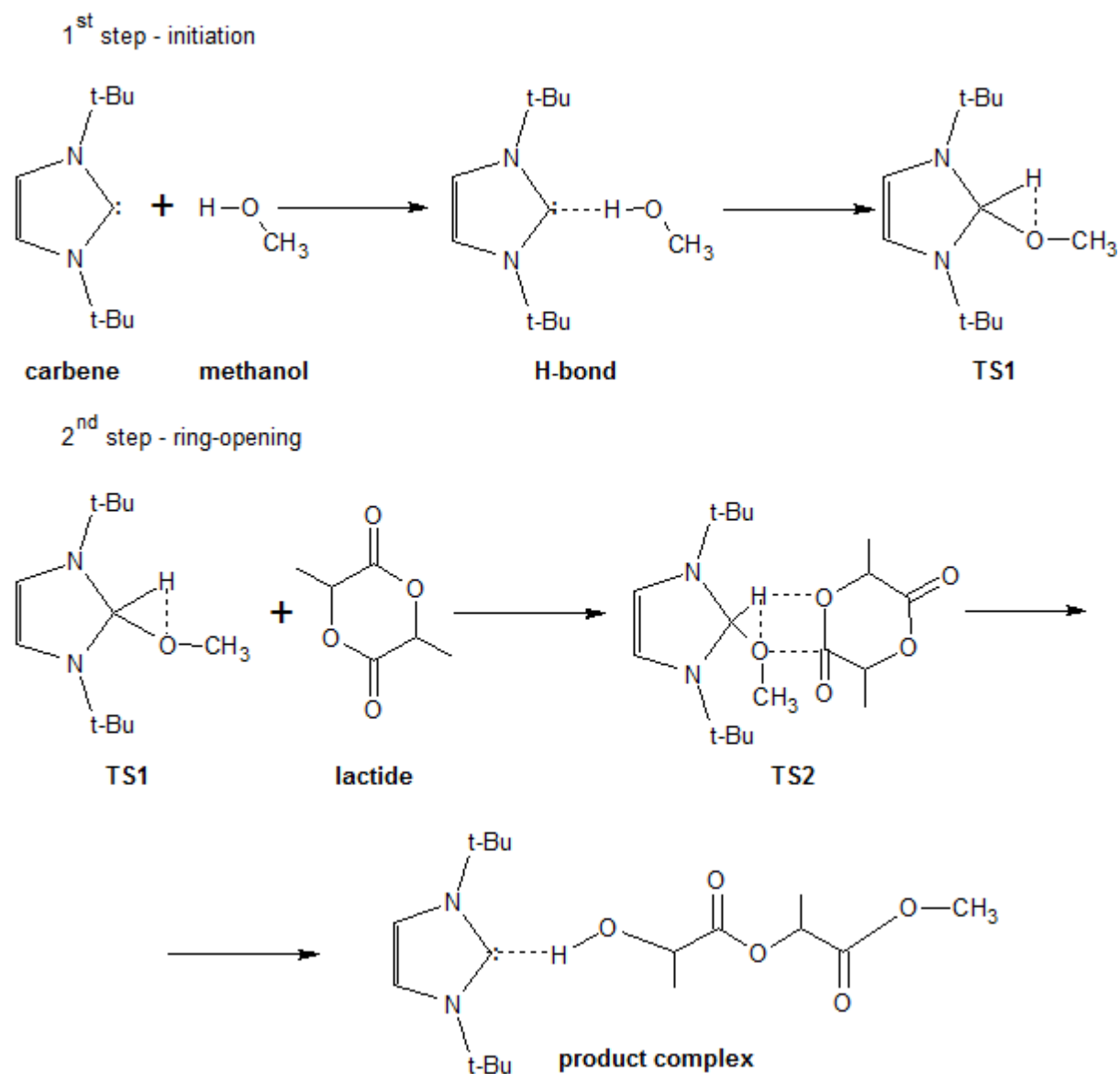


Fig. 42 Proposal of a novel chain-end-mechanism

Tab. 3 Calculated energies of all stationary points of the novel pathway

	B3LYP/6-31G(d)		
	E (au)	E rel. (au)	E rel. (kJ·mol ⁻¹)
Carbene +lactide + methanol	-1190.762667	0.000000	0.00
H-bond (+lactide)	-1190.784701	-0.022034	-57.84
TS1 (+lactide)	-1190.788041	-0.025374	-66.61
TS2 optimized	-1190.779200	-0.016533	-43.40
Product complex	-1190.803310	-0.040643	-106.69
Separated product	-1190.759300	0.003367	8.84

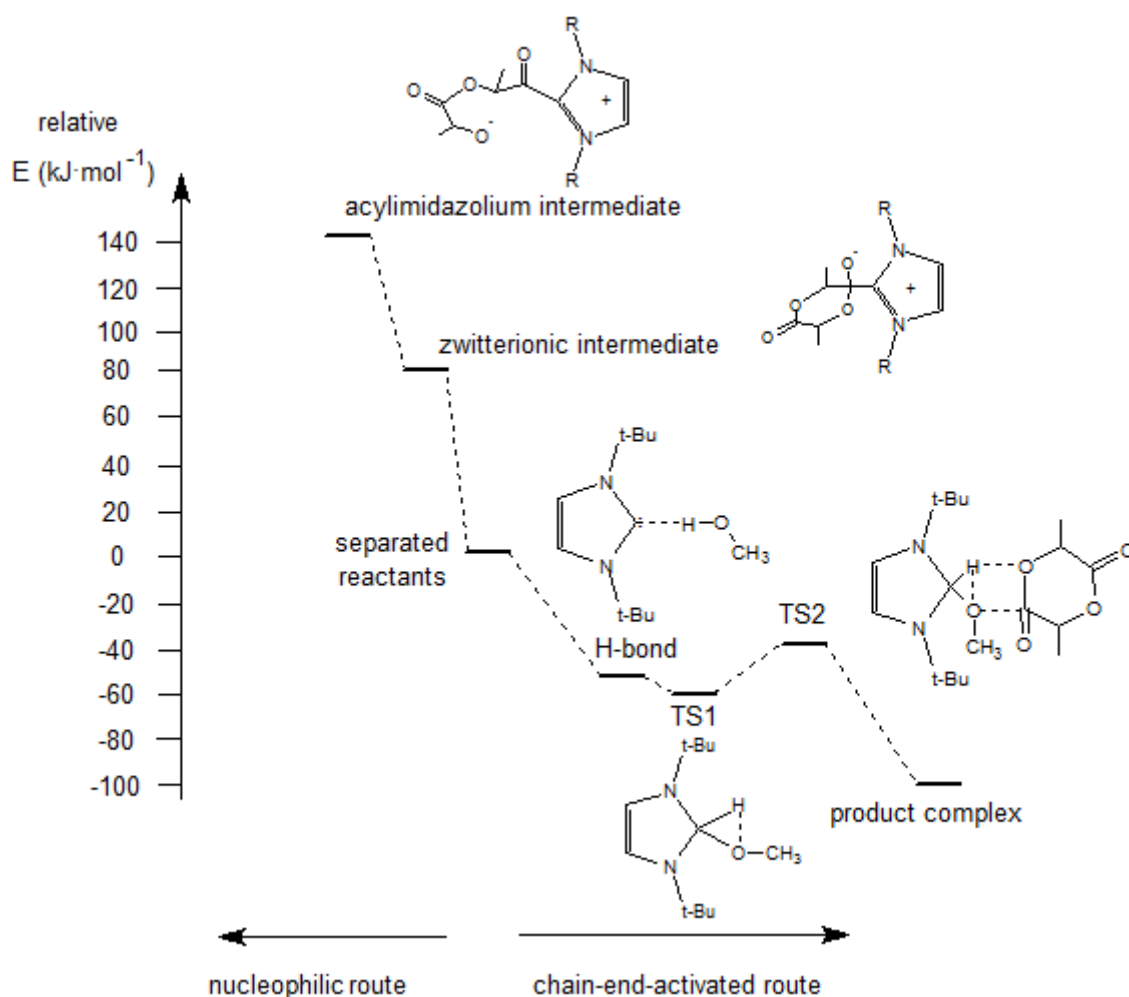


Fig. 43 The energy profile of both mechanisms

4.4.1 Simulation of the ring-opening of lactide

The process of the ring-opening of lactide was investigated by using Spartan computer program⁴⁶. An interaction between the carbene and the alcohol (H-bond) was simulated by using of a generation of transition state at molecular mechanics level. The proposed transition state was optimized at AM1 level. Subsequently the influence of modification of OH bond distance in alcohol on the changes of the energy of the whole molecule was studied (Fig. 44). Two best conformations (with the lowest energy) were optimized by the rotation around OH bond at AM1 level (12 steps after 30°). The best conformer (the lowest energy, right orientation) was optimized at B3LYP/6-31G(d) level.

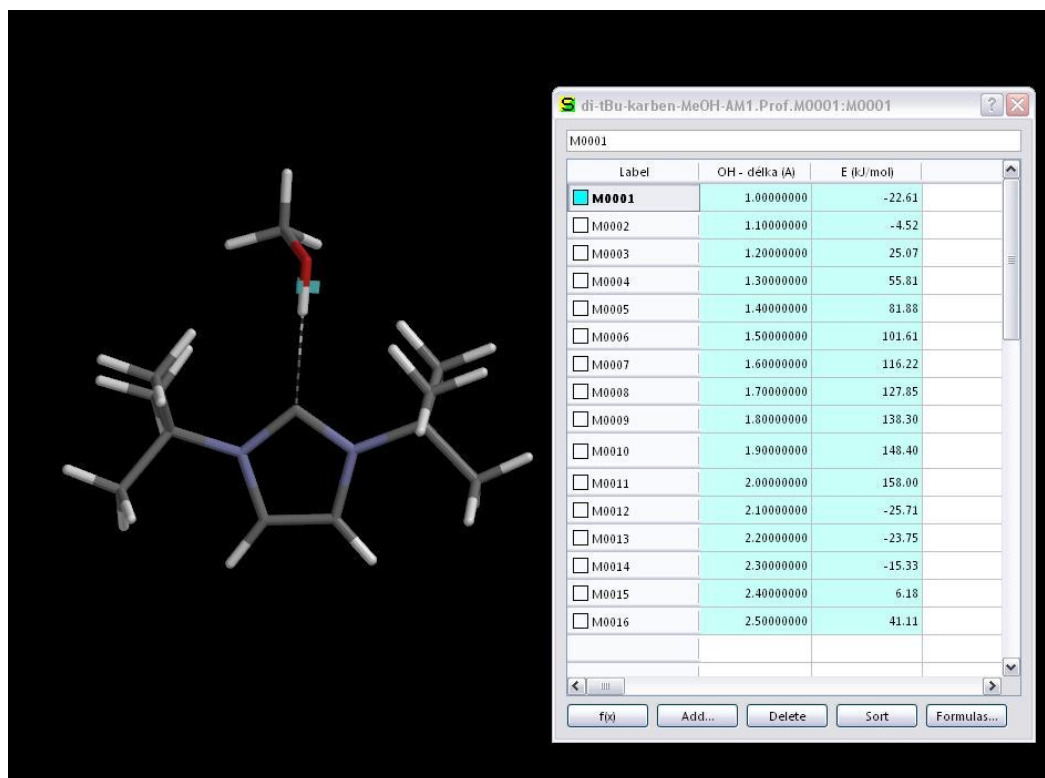


Fig. 44 The modelling of modification of bond distance OH in alcohol

Then transition state of foregoing best conformer and monomer (lactide) TS2 was generated at molecular mechanics level (Fig. 45). Subsequently, transition state was optimized at AM1 level and B3LYP/6-31G(d) level.

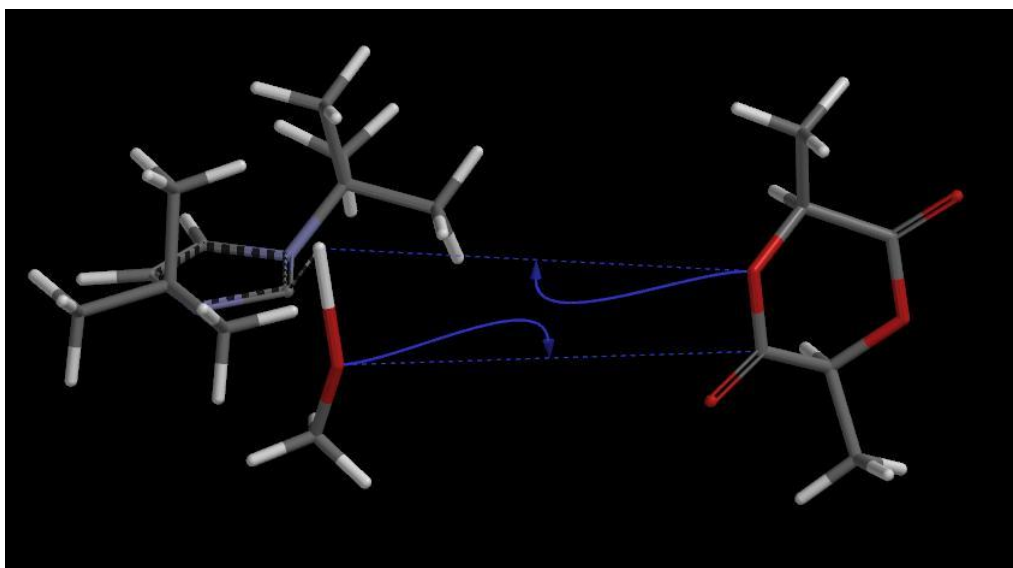


Fig. 45 The generation (blue arrows) of transition state at molecular mechanic level

The ring-opening was simulated by the modification of OH bond [O(lactide)---H-C(carbene)] at AM1 level (10 steps). All conformers were optimized at B3LYP/6-31G(d) level. The final product is the conformer with the lowest energy.

5 CONCLUSION

The energies and shapes of molecular orbitals and electrostatic potential maps of selected N-heterocyclic carbenes and their precursors based on chlorides were calculated. Titan⁴⁵ offers more possibilities of calculations than ArgusLab⁴⁴. These calculations are crucial for the prediction of properties. Both studied carbenes are very reactive due to a small HOMO-LUMO band gap. Moreover, electrostatic potential maps could be correlated with the catalytic activity, hence the suggestion of the better catalysts will be the subject for further study.

The geometry optimization of selected chloride precursors, similar precursors, NHCs and their possible hydrolysis products was made. Six compounds were calculated at DFT level using different seventeen functional. Three compounds were calculated at RHF level with five basis sets and at DFT level with three basis sets and with three functionals. The calculated structures were in good agreement with the published data and the more stable tautomer of hydrolysis products was determined. In next steps post-Hartree-Fock methods including electron correlation effect in addition and larger basis sets will be studied and accurate energies, enthalpies and entropies of these compounds will be calculated.

IR and RA spectra of selected imidazole compounds were obtained from data of geometry optimization. Subsequently, calculated spectra were compared with measured ones. For better spectra interpretation spectra of hydrolysis products were calculated. The finding of the efficient cause for the prediction of IR and RA spectra and subsequently their interpretation, eventually the obtaining of NMR spectra will be the subject for further study.

Two possible mechanisms of ROP of lactide catalyzed by NHCs were studied. In the first studied pathway, which is postulated by many authors, the activation barrier was too large. Therefore the second mechanism was investigated and the novel route was suggested. This novel route was more energetically favourable, which means more probable. Moreover the simulation of the ring-opening of lactide was successful and it was found out that methanol hydrogen causes the ring-opening of lactide. In next steps the experimental research such as *in situ* studies will be done and the influence of temperature and solvent effect on calculation will be account.

6 REFERENCES

- 1 *Molecular Electronic Structure* [online]. 2001 [ref. 2010-04-20]. Available from: <<http://www.chm.bris.ac.uk/pt/harvey/elstruct/introduction.html#menu>>.
- 2 HERRMANN, W. A., KÖCHER, C.: N-Heterocyclic Carbenes. *Angewandte Chemie International Edition in English*. 1997, vol. 35, p. 2162-2187.
- 3 WANZLICK, H.-W., SCHIKORA, E.: Ein neuer Zugang zur Carben-Chemie. *Angewandte Chemie*. 1960, vol. 70, p. 494.
- 4 ARDUENGO, A. J. III, HARLOW, R. L., KLINE, M.: A Stable Crystalline Carbene. *Journal of the American Chemical Society*. 1991, vol. 113, p. 361-363.
- 5 ENDERS, D., BREUER, K., RAABE, G., RUNSINK, J., TELES, J. H., MELDER, J. P., EBEL, K., BRODE, S.: Preparation, Structure, and Reactivity of 1,3,4-Triphenyl-4,5-dihydro-1H-1,2,4-triazol-ylidene, a New Stable Carbene. *Angewandte Chemie International Edition in English*. 1995, vol. 34, p. 1021-1023.
- 6 BOURISSOU, D., GUERRET, O., GABBAÏ, P., BERTRAND, G.: Stable Carbenes. *Chemical Reviews*. 2000, vol. 100, p. 39-91.
- 7 DENK, M. K., RODEZNO, J. M., GUPTA, S., LOUGH, A. J. Synthesis and reactivity of subvalent compounds: Part 11. Oxidation, hydrogenation and hydrolysis of stable diamino carbenes. *Journal of Organometallic Chemistry*. 2001, vol. 617-618, p. 242-253.
- 8 HOLLOCZKI, O., TERLECZKY, P., SZIEBERTH, D., MOURGAS, G., GUDAT, D., NYULASZI, L.: Hydrolysis of Imidazole-2-ylidenes. *Journal of the Chemical Society*. 2011, vol. 133, p. 780-789.
- 9 ARDUENGO, A. J. III: Looking for Stable Carbenes: The Difficulty in Starting Anew. *Accounts of Chemical Research*. 1999, vol. 32, p. 913-919.
- 10 ARDUENGO, A. J. III, BOCK, H., CHEN, H., DENK, M., DIXON, D. A., GREEN, J. C, HERRMANN, W. A., JONES, N. L., WAGNER, M., WEST, R.: Photoelectron Spectroscopy of a Carbene/Silene/Germylene Series. *Journal of the American Chemical Society*. 1994, vol. 116, p. 6641-6649.
- 11 HEINEMANN, C., MÜLLER, T., APELOIG, Y., SCHWARZ, H.: On the Question of Stability, Conjugation, and "Aromaticity" in Imidazol-2-ylidenes and Their Silicon Analogs. *Journal of the American Chemical Society*. 1996, vol. 118, p. 2023-2038.
- 12 TELES, J. H., MELDER, J.-P., EBEL, K., SCHNEIDER, R., GEHRER, E., HARDER, W., BRODE, S., ENDERS, D., BREUER, K., RAABE, G.: The Chemistry of Stable Carbenes: Benzoin-Type Condensations of Formaldehyde Catalyzed by Stable Carbenes. *Helvetica Chimica Acta*. 1996, vol. 79, p. 61-83.
- 13 ENDERS, D., BREUER, K., TELES, J. H.: A Novel Asymmetric Benzoin Reaction Catalyzed by a Chiral Triazolium Salt. Preliminary communication. *Helvetica Chimica Acta*. 1996, vol. 79, p. 1217-1221.
- 14 SINGH, R., NOLAN, S. P.: Synthesis of phosphorusesters by transesterification mediated by N-heterocyclic carbenes (NHCs). *Chemical Communications*, 2005, p. 5456-5458.
- 15 NYCE, G. W., LAMBOY, J. A., CONNOR, E. F., WAYMOUTH, R. M., HEDRICK, J. L.: Expanding the Catalytic Activity of Nucleophilic N-Heterocyclic Carbenes for Transesterification Reactions. *Organic Letters*. 2002, vol. 4, p. 3587-3590.

- 16 HEDRIK, J. L., KILICKIRAN, P., NYCE, G. W., WAYMOUTH, R. M.: United States
Patent 6911546B2, International Business Machines Corporation, 2005.
- 17 CONNOR, E. F., NYCE, G. W., MYERS, M., MCK, A., HEDRICK, J. L.: First
Example of N-Heterocyclic Carbenes as Catalysts for Living Polymerization:
Organocatalytic Ring-Opening Polymerization of Cyclic Esters. *Journal of the
American Chemical Society*. 2002, vol. 124, p. 914-915.
- 18 KAMBER, N. E., JEONG, W., WAYMOUTH, R. M.: Organocatalytic Ring-Opening
Polymerization. *Chemical Review*. 2007, vol. 107, p. 5813-5840.
- 19 DENK, K., SIRSCH, P., HERRMANN, W. A.: The first metal complexes of
bis(diisopropylamino)carbene: synthesis, structure and ligand properties. *Journal of
Organometallic Chemistry*. 2002, vol. 649, p. 219-224.
- 20 MAGILL, A. M., CAVELL, K. J., YATES, B. F.: Basicity of Nucleophilic Carbenes in
Aqueous and Nonaqueous Solvents – Theoretical Predictions. *Journal of the American
Chemical Society*. 2004, vol. 126, p. 0717-8724.
- 21 SPIVEY, A. C., ARSENIYADIS, S.: Nucleophilic Catalysis by 4-
(Dialkylamino)pyridines Revisited-The Search for Optimal Reactivity and Selectivity.
Angewandte Chemie International Edition in English. 2004, vol. 43, p. 5436-5441.
- 22 BRESLOW, R.: On the Mechanism of Thiamine Action. IV. Evidence from Studies on
Model Systems. *Journal of the American Chemical Society*. 1958, vol. 80, p. 3719-
3726.
- 23 MOVASSAGHI, M., SCHMIDT, M. A.: N-Heterocyclic Carbene-Catalyzed Amidation
of Unactivated Esters with Amino Alcohols. *Organic Letters*. 2005, vol. 7, p. 2453-
2456.
- 24 LAI, C. L., LEE, H. M., HU, C. H.: Theoretical study on the mechanism of N-
heterocyclic carbene catalyzed transesterification reactions. *Tetrahedron Letters*. Vol.
46, p. 6265-6270.
- 25 KIESEWETTER, M. K., SHIN, E. J., HEDRICK, J. L., WAYMOUTH, R. M.:
Organocatalysis: Opportunities and Challenges for Polymer Synthesis. *Macromolecules*.
2010, vol. 43., p. 2093-2107.
- 26 BONDUELLE, C., MARTIN-VACA, B., CASSIO, F. P., BOURISSOU, D.: Monomer
versus Alcohol Activation in the 4-Dimethylpyridine-Catalyzed Ring-Opening
Polymerization of Lactide and Lactic O-Carboxylic Anhydride. *Chemistry European
Journal*. 2008, vol. 14, p. 5304-5312.
- 27 CULKIN, D. A., JEONG, W., CSIHONY, S., GOMEZ, E. D., BALSARA, N. P.,
HEDRICK, J. L., WAYMOUTH, R. M.: Zwitterionic Polymerization of Lactide to
Cyclic Poly(Lactide) by Using N-Heterocyclic Carbene Organocatalysts. *Angewandte
Chemie International Edition in English*. 2007, vol. 46, p. 2627-2630.
- 28 NYCE, G. N., GLAUSER, T., CONNOR, E. F., MCK, A., WAYMOUTH, R. M.,
HEDRICK, J. L.: In Situ Generation of Carbenes: A General and Versatile Platform for
Organocatalytic Living Polymerization. *Journal of the American Chemical Society*.
2003, vol. 125, p. 3046-3056.
- 29 WELTON, T.: Room-Temperature Ionic Liquids. Solvent for Synthesis and Catalysis.
Chemical Reviews. 1999, vol. 99, p. 2071-2084.
- 30 SENTMAN, A. C., CSIHONY, S., WAYMOUTH, R. M., HEDRICK, J. L.: Silver(I)-
Carbene Complexes/Ionic Liquids: Novel N-Heterocyclic Carbene Delivery Agents for

- Organocatalytic Transformations. *Journal of Organic Chemistry*. 2005, vol. 70, p. 2391-2393.
- 31 NYCE, G. W., CSIHONY, S., WAYMOUTH, R. M., HEDRICK, J. L.: A general and Versatile Approach to Thermally Generated N-Heterocyclic Carbenes. *Chemistry – A European Journal*. 2004, vol. 10, p. 4073-4079.
- 32 CSIHONY, S., CULKIN, D. A., SENTMAN, A. C., DOVE, A. P., WAYMOUTH, R. M., HEDRICK, J. L.: Single-Component Catalyst/Initiators for the Organocatalytic Ring-Opening Polymerization of Lactide. *Journal of the American Chemical Society*. 2005, vol. 127, p. 9079-9084.
- 33 LEACH, A. R.: *Molecular Modelling: Principles and Application*. 2nd ed. Harlow: Pearson Education Limited, 2001. 744 p. ISBN 0-582-38210-6.
- 34 FORESMAN, J. B., FRISCH, AE.: *Exploring Chemistry with Electronic Structure Methods*. 2nd ed. Pittsburgh, PA: Gaussian, Inc., 1996. Li, 302 p. ISBN 0-9636769-3-8.
- 35 HEHRE, W. J.: *A Guide to Molecular Mechanics and Quantum Chemical Calculations*. USA: Wavfunction, Inc., 2003. 796 p. ISBN 1-890661-18-X.
- 36 KULOVANÁ, E. *Molecular modelling – structure and properties of carbene-based catalysts*. Brno: Vysoké učení technické v Brně, Fakulta chemická, 2010. 62 p. Vedoucí bakalářské práce RNDr. Lukáš Richtera, Ph.D.
- 37 *Basis sets* [online]. 2011 [ref. 2012-04-07]. Available from: <http://www.gaussian.com/g_tech/g_ur/m_basis_sets.htm>.
- 38 *Firefly (former PC GAMESS) Homepage* [online]. 1999 [ref. 2011-04-08]. Available from: <<http://classic.chem.msu.su/gran/gamess/index.html>>
- 39 NAKAMOTO, K.: *Infrared and Raman Spectra of Inorganic and Coordination Compounds, Part A: Theory and Applications in Inorganic Chemistry*. 6th ed. Hoboken, New Jersey: John Wiley & Sons, Inc., 2009, 419 p. ISBN 978-0-471-74339-2.
- 40 *Virtual Textbook of Organic Chemistry: Infrared spectroscopy* [online]. 1999 [ref. 2010-05-01]. Available from: <<http://www.cem.msu.edu/~reusch/VirtualText/Spectrpy/InfraRed/infrared.htm#ir1>>.
- 41 MERRICK, J. P., MORAN, D., RADOM, L.: An Evaluation of Harmonic Vibrational Frequency Scale Factors. *Journal of Physical Chemistry A*. 2007, vol. 111, p. 11683-11700.
- 42 GRANOVSKY, A. A. *PC GAMESS/Firefly* [computer program]. Ver. 7.1.F. 2005 [ref. 2009-5-20]. Available from: <<http://classic.chem.msu.su/gran/gamess/index.html>>.
- 43 SCHMIDT, M. W., BALDRIDGE, K. K., BOATZ, J. A., ELBERT, S. T., GORDON, M. S., JENSEN, J. H., KOSEKI, S., MATSUNAGA, N., NGUYEN, K. A., SU, S., WINDUS, T. L., DUPUIS, M., MONTGOMERY, A. J.: General atomic and molecular electronic structure system. *Journal of Computational Chemistry*. 1993, vol. 14, is. 11, 1347-1363.
- 44 *ArgusLab* [computer program]. Ver. 4.0.1. 1996 [ref. 2009-04-24]. Available from: <<http://www.arguslab.com/index.htm>>.
- 45 *Titan* [computer program, CD-ROM]. Ver. 1.0.5. 1999.
- 46 *Spartan '10* [computer program]. Demo Version. 2010.
- 47 *Gabedit* [computer program]. Ver. 2.2.8. 2002 [ref. 2010-01-28]. Available from: <<http://gabedit.sourceforge.net/>>.
- 48 *RUNpcg* [computer program]. Ver. March 07, 2009. 2009 [ref. 2010-5-20]. Available from: <<http://www.chemsoft.ch/qc/RUNpcg.htm>>.

- 49 *Microsoft Excel 2003* [computer program]. C1985-2001 [ref. 2007-04-27].
- 50 *WinSCP* [computer program]. Ver. 4.2.5. C2000-2009 [2010-02-15]. Available from:
<<http://winscp.net/eng/download.php>>.
- 51 *PuTTY* [computer program]. Ver. 0.60. C1997-2007 [ref. 2010-02-25]. Available from:
<<http://www.chiark.greenend.org.uk/~sgtatham/putty/download.html>>.
- 52 DENK, M. K., THADANI, A., HATANO, K., LOUGH, A. J.: Sterisch gehinderte
stabile nucleophile Carbene. *Angewandte Chemie*. 1997, vol. 109, p. 2719-2721.
- 53 RIJNBERG, E., RICHTER, B., THIELE, K. H., BOERSMA J., VELDMAN, N., SPEK,
A. L., KOTEN, G.: A Homologous Series of Homoleptic Zinc Bis(1,4-di-*tert*-butyl-1,4-
diaz-1,3-butadiene) Complexes: $K_x[Zn(t-BuNCHCHN-t-Bu)_2]$, $Zn(t-BuNCHCHN-t-$
 $Bu)_2$, and $[Zn(t-BuNCHCHN-t-Bu)_2](Otf)_x$ ($x = 1, 2$). *Inorganic Chemistry*. 1998, vol.
37, p. 56-63.
- 54 DENK, M. K., GUPTA, S., BROWNIE, J., TAJAMMUL, S., LOUGH, A. J.: C-H
Activation with Elemental Sulfur: Synthesis of Cyclic Thioureas from Formaldehyde
Aminals and S_8 . *Chemistry – A European Journal*. 2001, vol. 7, p. 4477-4486.
- 55 KULOVANÁ, E., RICHTERA, L., HERMANOVÁ, S., JANČÁŘ, J. Molecular
modeling – structure and properties of (un)saturated carbenes. In *5th Meeting on
Chemistry and Life. Brno, Czech Republic, 14th – 16th September 2011*. Ed. Chemické
listy. Praha: Česká společnost chemická, 2011, p. 919 – 920. ISSN 0009-2770.
- 56 LEITES, L. A., MAGDANUROV, G. I., BUKALOV, S. S., NOLAN, S. P., SCOTT, N.
M., WEST, R.: Vibrational and electronic spectra and the electronic structure of an
unsaturated Arduengo-type carbene. *Mendeleev Communications*. 2007, vol. 17, p. 92-
94.

7 LIST OF ABBREVIATIONS

AM1	Austin Model 1
aug-cc-pVDZ	Augmented cc-pVDZ
cc-pVDZ	Correlation Consistent-Polarized Valence Double Zeta
CCDC	Cambridge Crystallographic Data Centre
CI	Configural Interaction
DFT	Density Functional Theory
DZV	Double Zeta Valence
FTIR	Fourier Transform Infrared
FTP	File Transfer Protocol
GAMESS	General Atomic And Molecular Electronic Structure System
GTO	Gaussian Type Orbital
H-bonding	Hydrogen Bonding
HOMO	Highest Occupied Molecular Orbital
IR	Infrared
LCAO	Linear Combination Of Atomic Orbitals
LUMO	Lowest Unoccupied Molecular Orbital
MCSCF	Multi-Configurational Self-Consistent Field
MeCN	Acetonitrile
MNDO	Modified Neglet of Diatomic Overlap
MP2	Møller-Plesset Perturbation Theory (second-order)
MRDCI	Multireference Single And Double Configuration Interaction
NEVPT	N-electron Valence State Perturbation Theory
NHC	N-heterocyclic Carbene
PES	Potential Energy Surface
PM3	Third Parametrisation of MNDO
RA	Raman
RHF	Restricted Hartree Fock
ROHF	Restricted Open Shell Hartree Fock
S ₁	1,3-di- <i>tert</i> -butylimidazol-2-ylidene, lactide and methanol
S ₂	4-dimethylaminopyridine, lactide and methanol
SCF	Self-Consistent Field
SFTP	Secure File Transfer Protocol
SI	International System of Units
SSH	Secure Shell
STO	Slater Type Orbital
TCP	Transmission Control Protocol
THF	Tetrahydrofurane
UHF	Unrestricted Hartree Fock

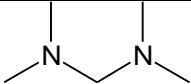
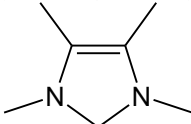
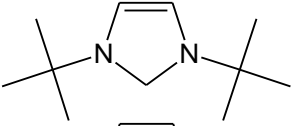
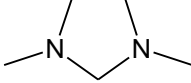
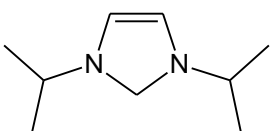
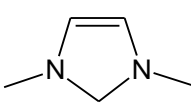
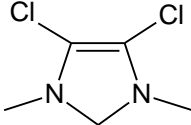
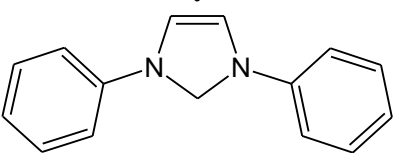
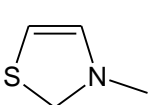
8 NOMENCLATURE LIST

DMAP	4-dimethylaminopyridine
DMSO	Dimethyl sulfoxide
IMes	1,3-dimesitylimidazol-2-ylidene
IMes	1,3-bis(2,4,6-trimethylphenyl)imidazol-2-ylidene
MeCN	Acetonitrile
NC ₁	1,3-di- <i>tert</i> -butylimidazol-2-ylidene
NC ₂	1,3-di- <i>tert</i> -butylimidazolin-2-ylidene
N=C-CA	[(2E)-2-(<i>tert</i> -butylimino)ethyl]formamide (1,4-di(<i>tert</i> -butyl)-4-formyl-1,4-diaza-but-1-ene)
N-C=CA	N- <i>tert</i> -butyl-N-[(Z)-2-(<i>tert</i> -butylamino)ethenyl]formamide
N-C-CA	N- <i>tert</i> -butyl-N-[2-(<i>tert</i> -butylamino)ethyl]formamide (N-formyl-N,N'-di- <i>tert</i> -butylethylenediamine)
NC ₁ H-Cl	1,3-di- <i>tert</i> -butylimidazolium chloride
NC ₁ H-F ₃ CSO ₃	1,3-di- <i>tert</i> -butylimidazolium trifluoromethanesulfonate
NC ₂ H-Cl	1,3-di- <i>tert</i> -butylimidazolinium chloride
NC ₂ H-SCN	1,3-di- <i>tert</i> -butylimidazolinium thiocyanate

Studied carbenes were marked **NC₁** and **NC₂**, where NC reflects N-heterocyclic carbenes and numbers differ unsaturated (1) and saturated analogue (2). Their precursors contain hydrogen (H) and anion (Cl⁻, F₃CSO₃⁻ or SCN⁻) in addition. All hydrolysis products are based on formamide (A abbreviates formamide) and differ in single (-) and double bonds (=) in the sequence NCN. Their nomenclatures were generated in chemical software. N=C-CA and N-C-CA have second names, because these names were used in some publications. The IMes abbreviates 1,3-dimesitylimidazol-2-ylidene, however mesityl means 2,4,6-trimethylphenyl, hence both names were mentioned.

9 APPENDIX

Tab. 4 Examples of pKa's of nucleophilic carbenes in DMSO, MeCN and water

Carbene	DMSO	MeCN	Water
	27.9 ± 0.23	39.1 ± 0.25	34.0 ± 0.3
	23.7 ± 0.21	34.9 ± 0.21	29.5 ± 0.3
	22.6 ± 0.09	33.0 ± 0.09	28.3 ± 0.1
	22.3 ± 0.25	33.6 ± 0.25	28.5 ± 0.4
	22.0 ± 0.21	33.3 ± 0.21	28.2 ± 0.3
	21.1 ± 0.23	32.4 ± 0.22	27.4 ± 0.4
	16.2 ± 0.10	27.4 ± 0.10	23.4 ± 0.2
	16.1 ± 0.05	27.4 ± 0.07	22.0 ± 0.1
	14.5 ± 0.16	25.6 ± 0.15	21.2 ± 0.2

Tab. 5 Types and descriptions of functionals

Type	Functional	Description
Pure exchange	SLATER	Slater exchange, no correlation
Pure correlation	LYP	Hartree-Fock exchange, Lee-Yang-Parr 1988 correlation
Exchange-correlation	SLYP	Slater exchange, Lee-Yang-Parr 1988 correlation
Exchange-correlation	BLYP	Becke 1988 exchange, Lee-Yang-Parr 1988 correlation
Exchange-correlation	GLYP	Gill 1996 exchange, Lee-Yang-Parr 1988 correlation
Exchange-correlation	XLYP	Extended exchange functional of Xu and Goddard III, Lee-Yang-Parr 1988 correlation
Exchange-correlation	OLYP	OPTX exchange, Lee-Yang-Parr 1988 correlation
Exchange-correlation	SVWN1RPA	Slater exchange, VWN formula 1 RPA correlation
Exchange-correlation	BVWN1RPA	Becke 1988 exchange, VWN formula 1 RPA correlation
Exchange-correlation	SVWN5	Slater exchange, VWN formula 5 RPA correlation
Exchange-correlation	BVWN5	Becke 1988 exchange, VWN formula 5 RPA correlation
Exchange-correlation	PBE96	Perdew-Burke-Ernzerhof 1996 exchange, Perdew-Burke-Ernzerhof nonlocal + Perdew-Wang 1991 LDA correlation
Exchange-correlation	PBEPW91	Perdew-Burke-Ernzerhof 1996 exchange, Perdew 1991 nonlocal + Perdew-Wang 1991 LDA correlation
Exchange-correlation	PW91	Perdew-Wang 1991 exchange, Perdew 1991 nonlocal + Perdew-Wang 1991 LDA correlation
Hybrid	B3LYP	Becke-style three-parameter functional, using VWN formula 5 RPA correlation
Hybrid	X3LYP	Extended exchange functional of Xu and Goddard III + Hartree-Fock exchange
Hybrid	O3LYP	Slater + OPTX + Hartree-Fock exchange, VWN formula 5 + Lee-Yang-Parr 1988 correlation
Hybrid	BHHLYP	Becke 1988 + Hartree-Fock exchange, Lee-Yang-Parr 1988 correlation
Hybrid	PBE0	Perdew-Burke-Ernzerhof 1996 + Hartree-Fock exchange, Perdew-Burke-Ernzerhof nonlocal + Perdew-Wang 1991 LDA correlation
Hybrid	PBE1PW91	Perdew-Burke-Ernzerhof 1996 + Hartree-Fock exchange, Perdew 1991 nonlocal + Perdew-Wang 1991 LDA correlation
Hybrid	B3PW91	Slater + Becke 1988 + Hartree-Fock exchange, Perdew 1991 nonlocal + Perdew-Wang 1991 LDA correlation

```

$CONTRL SCFTYP=RHF  RUNTYP=OPTIMIZE  MAXIT=200  DFTTYP=B3LYP  NZVAR=99  $END
$SYSTEM MWORDS=100  $END
$SCF DIRSCF=.True.  $END
$GUESS GUESS=HUCKEL  $END
$BASIS GBASIS=N31  NGAUSS=6  NDFUNC=1  $END
$ZMAT  DLC=.TRUE.  AUTO=.TRUE.  $end
$STATPT NSTEP=100000  $END
$DATA
B3LYP/6-31G(d)
C1
NITROGEN  7.0  29.2044828342  -19.5710300026  -1.9390650357
CARBON    6.0  28.1115395843  -20.3413378590  -2.0509731194
NITROGEN  7.0  27.0552734180  -19.5222015703  -2.1661542574
CARBON    6.0  27.4027338822  -18.1130339560  -1.9877570611
CARBON    6.0  28.9225153335  -18.1481702059  -2.1230751225
CARBON    6.0  25.6653774482  -19.9924939797  -2.0429607455
CARBON    6.0  30.5711900370  -20.1053934032  -2.0589251858
CARBON    6.0  31.5449831283  -19.1759440619  -1.3210859838
CARBON    6.0  30.6430353343  -21.4953998429  -1.4193831165
CARBON    6.0  30.9678919188  -20.2061849872  -3.5399415403
CARBON    6.0  24.7343685314  -19.0197574995  -2.7796069445
CARBON    6.0  25.5264572976  -21.3781624108  -2.6808983554
CARBON    6.0  25.2667883997  -20.0732960726  -0.5610241401
HYDROGEN  1.0  26.9408636900  -17.4828828336  -2.7357090169
HYDROGEN  1.0  29.4130047939  -17.5371134611  -1.3775480124
HYDROGEN  1.0  31.6159896821  -18.1986255129  -1.7871854599
HYDROGEN  1.0  32.5401023309  -19.6076847968  -1.3258172629
HYDROGEN  1.0  31.2417538464  -19.0407142086  -0.2874697622
HYDROGEN  1.0  30.0008125795  -22.1993714489  -1.9278931821
HYDROGEN  1.0  31.6655424009  -21.8589247465  -1.4676090378
HYDROGEN  1.0  30.3400874367  -21.4573269956  -0.3786373658
HYDROGEN  1.0  30.2958895204  -20.8783728541  -4.0622078049
HYDROGEN  1.0  30.9309315918  -19.2391457092  -4.0323275409
HYDROGEN  1.0  31.9798100102  -20.5882207051  -3.6426422356
HYDROGEN  1.0  23.7201942357  -19.4048422261  -2.7716844836
HYDROGEN  1.0  24.7099728491  -18.0395302083  -2.3146186414
HYDROGEN  1.0  25.0404425580  -18.8999153836  -3.8143351242
HYDROGEN  1.0  24.4881410668  -21.6931618038  -2.6286899963
HYDROGEN  1.0  26.1365237788  -22.1116891973  -2.1740583587
HYDROGEN  1.0  25.8266510976  -21.3554199369  -3.7229823952
HYDROGEN  1.0  25.3492775240  -19.1085464195  -0.0696240504
HYDROGEN  1.0  25.9071642566  -20.7755643518  -0.0384168800
HYDROGEN  1.0  24.2383435971  -20.4076183585  -0.4570090783
HYDROGEN  1.0  27.0976057720  -17.7531055868  -1.0085597662
HYDROGEN  1.0  29.2439153468  -17.8064804771  -3.1033639355
$END

```

Fig. 46 *The example of the input file for PC GAMESS/Firefly*

Tab. 6 Selected bond distances and bond angles of NC₁ and comparison

6-31G(d)	Bond distance (Å)			Bond angle (°)	E ₀ (%)	E (au)	CPU time	
	C(1)-N(1)	C(2)-C(3)	N(1)-C(2)	N(1)-C(1)-N(2)				
exp. data ⁷	1.366(2)	1.341(2)	1.380(2)	102.19(12)	-	-	-	
DFT	SLATER	1.381	1.375	1.401	101.99	1.27	-529.46	93 min
	LYP	1.386	1.368	1.407	102.30	1.35	-540.36	115 min
	BLYP	1.386	1.368	1.407	102.30	1.35	-540.38	83 min
	SLYP	1.360	1.362	1.381	101.95	0.61	-532.77	84 min
	GLYP	1.384	1.367	1.402	102.32	1.24	-540.34	85 min
	OLYP	1.378	1.363	1.393	102.40	0.92	-540.43	84 min
	SVWN1RPA	1.360	1.359	1.377	102.15	0.51	-537.71	201 min
	SVWN5	1.362	1.360	1.380	102.11	0.45	-535.78	87 min
	PBE96	1.379	1.367	1.395	102.07	1.02	-539.95	127 min
	PW91	1.377	1.365	1.394	102.13	0.92	-540.44	134 min
	B3LYP	1.371	1.356	1.392	102.62	0.69	-540.68	235 min
	BHLYP	1.358	1.341	1.383	103.00	0.40	-540.33	97 min
	X3LYP	1.370	1.355	1.391	102.61	0.64	-540.41	241 min
	O3LYP	1.363	1.354	1.380	102.47	0.37	-539.46	251 min
	PBE0	1.365	1.354	1.384	102.48	0.40	-540.04	239 min
PBE1PW91	1.365	1.353	1.384	102.46	0.38	-540.25	243 min	
B3PW91	1.367	1.356	1.387	102.50	0.50	-540.49	244 min	

* Three best results are marked in bold italic

Tab. 7 Selected bond distances and bond angles of NC₁H-Cl

6-31G(d)	Bond distance (Å)			Bond angle (°)	E (au)	CPU time	
	C(1)-N(1)	C(2)-C(3)	N(1)-C(2)	N(1)-C(1)-N(2)			
DFT	SLATER	1.347	1.385	1.382	109.26	-987.39	108 min
	LYP	1.296	1.332	1.355	110.53	-1001.17	122 min
	BLYP	1.348	1.377	1.389	109.86	-1001.16	202 min
	SLYP	1.331	1.370	1.363	108.82	-991.43	132 min
	GLYP	1.345	1.375	1.387	109.97	-1001.16	187 min
	OLYP	1.340	1.372	1.379	110.08	-1001.25	192 min
	SVWN1RPA	1.359	1.367	1.362	109.10	-997.39	116 min
	SVWN5	1.331	1.369	1.364	109.13	-995.10	113 min
	PBE96	1.341	1.376	1.380	109.71	-1000.57	159 min
	PW91	1.340	1.375	1.379	109.61	-1001.23	164 min
	B3LYP	1.332	1.366	1.376	110.06	-1001.50	83 min
	BHLYP	1.318	1.352	1.368	110.18	-1001.14	77 min
	X3LYP	1.331	1.365	1.376	110.04	-1001.18	77 min
	O3LYP	1.326	1.362	1.366	109.83	-1000.05	102 min
	PBE0	1.327	1.364	1.369	109.85	-1000.69	83 min
	PBE1PW91	1.327	1.364	1.369	109.83	-1000.96	81 min
	B3PW91	1.330	1.365	1.371	109.88	-1001.25	82 min

Tab. 8 Selected bond distances and bond angles of NC₂ and comparison

6-31G(d)	Bond distance (Å)			Bond angle (°)	E ₀ (%)	E (au)	CPU time	
	C(1)-N(1)	C(2)-C(3)	N(1)-C(2)	N(1)-C(1)-N(2)				
exp. data ⁵²	1.348(1)	1.542(2)	1.476(1)	106.44(9)	-	-	-	
DFT	SLATER	1.361	1.537	1.489	106.31	0.91	-530.53	58 min
	LYP	1.326	1.505	1.440	106.81	1.22	-541.57	52 min
	BLYP	1.363	1.541	1.504	106.78	1.31	-541.56	57 min
	SLYP	1.343	1.513	1.462	105.99	0.45	-533.89	69 min
	GLYP	1.361	1.541	1.502	106.79	1.24	-541.53	85 min
	OLYP	1.356	1.533	1.487	106.72	0.75	-541.62	49 min
	SVWN1RPA	1.342	1.514	1.464	106.25	0.39	-538.92	57 min
	SVWN5	1.343	1.517	1.466	106.24	0.39	-536.95	57 min
	PBE96	1.356	1.533	1.489	106.45	0.72	-541.14	58 min
	PW91	1.356	1.533	1.489	106.52	0.73	-541.63	57 min
	B3LYP	1.352	1.532	1.483	106.80	0.61	-541.89	55 min
	BHLYP	1.342	1.523	1.465	106.83	0.57	-541.54	44 min
	X3LYP	1.351	1.531	1.481	106.76	0.53	-541.60	56 min
	O3LYP	1.343	1.520	1.468	106.59	0.40	-540.65	51 min
	PBE0	1.347	1.524	1.470	106.59	0.33	-540.65	56 min
	PBE1PW91	1.347	1.525	1.470	106.47	0.35	-541.23	56 min
B3PW91	1.349	1.528	1.475	106.52	0.34	-541.45	55 min	

* Three best results are marked in bold italic

Tab. 9 Selected bond distances and bond angles of NC₂H-Cl

6-31G(d)	Bond distance (Å)			Bond angle (°)	E (au)	CPU time	
	C(1)-N(1)	C(2)-C(3)	N(1)-C(2)	N(1)-C(1)-N(2)			
DFT	SLATER	1.356	1.544	1.477	111.66	-988.50	450 min
	LYP	1.294	1.514	1.442	113.88	-1002.43	150 min
	BLYP	1.350	1.552	1.488	113.05	-1002.39	540 min
	SLYP	1.346	1.520	1.451	110.20	-992.60	540 min
	GLYP	1.341	1.546	1.490	113.00	-1002.37	186 min
	OLYP	1.336	1.535	1.477	112.95	-1002.46	208 min
	SVWN1RPA	1.343	1.522	1.452	110.78	-998.64	450 min
	SVWN5	1.344	1.524	1.455	110.88	-996.31	450 min
	PBE96	1.350	1.542	1.475	112.14	-1001.79	560 min
	PW91	1.349	1.541	1.475	112.07	-1002.46	578 min
	B3LYP	1.328	1.539	1.477	113.22	-1002.73	180 min
	BHLYP	1.315	1.530	1.464	113.36	-1002.37	180 min
	X3LYP	1.328	1.537	1.475	113.18	-1003.01	540 min
	O3LYP	1.323	1.525	1.461	112.62	-1001.27	210 min
	PBE0	1.323	1.530	1.466	112.83	-1001.92	210 min
	PBE1PW91	1.324	1.530	1.466	112.83	-1002.19	210 min
B3PW91	1.326	1.533	1.470	112.92	-1002.49	180 min	

Tab. 10 Symmetry and energy of NC₁

	Symmetry	Energy		
		AM1 (kJ·mol ⁻¹)	RHF/6-31G(d) (au)	B3LYP/6-31(d) (au)
NC ₁	C _s	238.36	-537.04829	-540.681976
NC ₁	C _{2v}	238.39	-537.04762	-540.682946

Tab. 11 Selected bond distances and bond angles of NC₁H-F₃CSO₃ and comparison

6-31G(d)	Bond distance (Å)			Bond angle (°)	E _∅ (%)	E (au)	CPU time	
	C(1)-N(1)	C(2)-C(3)	N(1)-C(2)	N(1)-C(1)-N(2)				
exp. data ⁵³	1.336(5)	1.345(5)	1.375(5)	109.8(4)	-	-	-	
DFT	SLATER	1.344	1.382	1.385	109.17	1.11	-1481.02	509 min
	LYP	1.300	1.332	1.356	110.56	1.49	-1502.04	580 min
	BLYP	1.347	1.377	1.390	109.90	1.04	-1502.35	414 min
	SLYP	1.329	1.368	1.365	108.73	1.04	-1487.18	306 min
	GLYP	1.346	1.376	1.387	109.91	0.95	-1502.31	432 min
	OLYP	1.341	1.370	1.380	110.11	0.67	-1502.34	411 min
	SVWN1RPA	1.328	1.365	1.366	109.07	0.91	-1496.12	443 min
	SVWN5	1.330	1.367	1.368	109.01	0.88	-1492.71	441 min
	PBE96	1.343	1.375	1.380	109.62	0.77	-1501.29	221 min
	PW91	1.343	1.374	1.380	109.63	0.75	-1502.33	208 min
	B3LYP	1.333	1.366	1.378	109.99	0.49	-1502.73	441 min
	BHLYP	1.319	1.353	1.368	110.11	0.72	-1502.13	446 min
	X3LYP	1.333	1.365	1.377	109.94	0.48	-1502.24	228 min
	O3LYP	1.328	1.362	1.367	109.75	0.68	-1500.45	474 min
	PBE0	1.329	1.363	1.370	109.77	0.62	-1501.39	451 min
PBE1PW91	1.329	1.362	1.370	109.82	0.60	-1501.82	458 min	
B3PW91	1.332	1.364	1.373	109.88	0.54	-1502.28	448 min	

* Three best results are marked in bold italic

Tab. 12 Selected bond distances and bond angles of NC₂H-SCN and comparison

6-31G(d)		Bond distance (Å)			Bond angle (°)	E _∅ (%)	E (au)	CPU time
		C(1)-N(1)	C(2)-C(3)	N(1)-C(2)	N(1)-C(1)-N(2)			
exp. data ⁵⁴		1.313(2)	1.517(3)	1.473(2)	113.80(16)	-	-	-
DFT	SLATER	1.333	1.553	1.483	113.95	1.18	-1017.90	361 min
	LYP	1.289	1.519	1.447	114.84	1.16	-1033.17	375min
	BLYP	1.333	1.557	1.496	114.86	1.66	-1033.21	262 min
	SLYP	1.318	1.530	1.458	113.30	0.67	-1022.41	492 min
	GLYP	1.331	1.556	1.493	114.86	1.56	-1033.18	257 min
	OLYP	1.326	1.547	1.481	115.09	1.16	-1033.27	308 min
	<i>SVWNIRPA</i>	<i>1.317</i>	<i>1.531</i>	<i>1.459</i>	<i>113.68</i>	<i>0.57</i>	<i>-1029.05</i>	<i>457 min</i>
	<i>SVWN5</i>	<i>1.318</i>	<i>1.532</i>	<i>1.461</i>	<i>113.77</i>	<i>0.55</i>	<i>-1026.49</i>	<i>447 min</i>
	PBE96	1.328	1.548	1.481	114.44	1.07	-1032.54	263 min
	PW91	1.328	1.548	1.481	114.43	1.07	-1033.27	271 min
	B3LYP	1.320	1.546	1.481	114.93	1.00	-1033.57	264 min
	BHLYP	1.307	1.536	1.468	114.90	0.75	-1033.15	274 min
	X3LYP	1.319	1.545	1.479	114.85	0.91	-1033.20	265 min
	<i>O3LYP</i>	<i>1.314</i>	<i>1.533</i>	<i>1.465</i>	<i>114.55</i>	<i>0.58</i>	<i>-1031.93</i>	<i>269 min</i>
	PBE0	1.315	1.538	1.469	114.54	0.61	-1032.66	277 min
PBE1PW91	1.315	1.538	1.470	114.61	0.61	-1032.96	278 min	
B3PW91	1.318	1.541	1.473	114.62	0.67	-1033.29	265 min	

* Three best results are marked in bold italic

Tab. 13 Selected bond distances and bond angles of N=C-CA

Method	Bond distance (Å)			Bond angle (°)	E (au)	CPU time
	N(1)-C(2)	C(2)-C(3)	C(3)-N(2)	O=C(1)-N(1)		
RHF/6-31G(d)	1.464	1.508	1.249	124.25	-613.11	35 min
RHF/6-31G+(d)	1.465	1.510	1.249	115.74	-613.12	111 min
RHF/6-311G+	1.470	1.504	1.259	123.91	-612.97	122 min
RHF/6-31G+(d,p)	1.464	1.510	1.249	124.24	-613.16	146 min
RHF/ 6-311G+(d,p)	1.465	1.511	1.246	124.56	-613.27	277 min
B3LYP/6-31G(d)	1.473	1.512	1.269	124.12	-617.15	59 min
B3LYP/ 6-31G+(d,p)	1.473	1.513	1.270	124.21	-617.20	73 min
B3LYP/ 6-311G+(d,p)	1.473	1.512	1.264	124.36	-617.33	112 min
O3LYP/6-31G(d)	1.457	1.501	1.265	124.07	-615.79	62 min
O3LYP/ 6-31G+(d,p)	1.456	1.502	1.266	124.17	-615.84	162 min
O3LYP/ 6-311G+(d,p)	1.455	1.500	1.261	124.37	-615.96	327 min
B3PW91/ 6-31G(d)	1.465	1.508	1.268	124.07	-616.92	54 min
B3PW91/ 6-31G+(d,p)	1.465	1.508	1.268	124.22	-616.96	151 min
B3PW91/ 6-311G+(d,p)	1.463	1.507	1.264	124.32	-617.09	267 min

Tab. 14 Selected bond distances and bond angles of N-C=CA

Method	Bond distance (Å)			Bond angle (°)	E (au)	CPU time
	N(1)-C(2)	C(2)-C(3)	C(3)-N(2)	O=C(1)-N(1)		
RHF/6-31G(d)	1.430	1.326	1.380	125.78	-613.10	75 min
RHF/6-31G+(d)	1.430	1.328	1.380	125.75	-613.11	289 min
RHF/6-311G+	1.434	1.331	1.377	125.32	-612.97	226 min
RHF/6-31G+(d,p)	1.430	1.329	1.378	125.70	-613.15	364 min
RHF/ 6-311G+(d,p)	1.429	1.326	1.379	125.90	-613.26	132 min
B3LYP/6-31G(d)	1.430	1.351	1.377	125.69	-617.14	49 min
B3LYP/ 6-31G+(d,p)	1.429	1.353	1.376	125.50	-617.20	172 min
B3LYP/ 6-311G+(d,p)	1.429	1.349	1.475	125.64	-617.33	180 min
O3LYP/6-31G(d)	1.415	1.350	1.365	125.65	-615.78	52 min
O3LYP/ 6-31G+(d,p)	1.415	1.351	1.364	125.38	-615.84	189 min
O3LYP/ 6-311G+(d,p)	1.413	1.348	1.361	125.62	-615.97	265 min
B3PW91/ 6-31G(d)	1.423	1.351	1.372	125.64	-616.92	49 min
B3PW91/ 6-31G+(d,p)	1.423	1.353	1.371	125.45	-616.96	164 min
B3PW91/ 6-31G+(d,p)	1.422	1.348	1.369	125.65	-617.09	262 min

Tab. 15 Selected bond distances and bond angles of N-C-CA and comparison

Method	Bond distance (Å)			Bond angle (°)	E ₀ (%)	E (au)	CPU time
	N(1)-C(2)	C(2)-C(3)	C(3)-N(2)	O=C(1)-N(1)			
exp. data ⁵⁴	1.4729(17)	1.5250(2)	1.4586(18)	123.98(14)	-	-	-
RHF/6-31G(d)	1.471	1.527	1.453	124.75	0.32	-614.28	67 min
RHF/6-31G+(d)	1.472	1.528	1.454	124.88	0.32	-614.29	226 min
RHF/6-31G+	1.478	1.529	1.460	124.48	0.28	-614.02	113 min
RHF/6-311G+	1.478	1.527	1.460	124.44	0.24	-614.14	245 min
RHF/6-31G+(d,p)	1.472	1.528	1.453	124.80	0.32	-614.33	306 min
RHF/ 6-311G+(d,p)	1.472	1.528	1.453	125.01	0.37	-614.44	596 min
B3LYP/6-31G(d)	1.478	1.535	1.464	124.42	0.43	-618.36	227 min
B3LYP/ 6-31G+(d,p)	1.481	1.534	1.466	124.50	0.50	-618.41	261 min
B3LYP/ 6-311G+(d,p)	1.479	1.534	1.465	124.67	0.50	-618.55	489 min
O3LYP/6-31G(d)	1.462	1.523	1.449	124.37	0.46	-616.99	116 min
O3LYP/ 6-31G+(d,p)	1.464	1.523	1.451	124.32	0.39	-617.04	286 min
O3LYP/ 6-311G+(d,p)	1.463	1.521	1.448	124.62	0.54	-617.17	536 min
<i>B3PW91/ 6-31G(d)</i>	<i>1.471</i>	<i>1.529</i>	<i>1.458</i>	<i>124.42</i>	<i>0.20</i>	<i>-618.13</i>	<i>75 min</i>
<i>B3PW91/ 6-31G+(d,p)</i>	<i>1.473</i>	<i>1.529</i>	<i>1.458</i>	<i>124.43</i>	<i>0.17</i>	<i>-618.18</i>	<i>261 min</i>
<i>B3PW91/ 6-311G+(d,p)</i>	<i>1.471</i>	<i>1.528</i>	<i>1.458</i>	<i>124.62</i>	<i>0.22</i>	<i>-618.31</i>	<i>509 min</i>

* Three best results are marked in bold italic

Tab. 16 The notation of intensities

Intensity	Abbreviations
very strong	vs
strong	s
medium	m
weak	w
very weak	vw

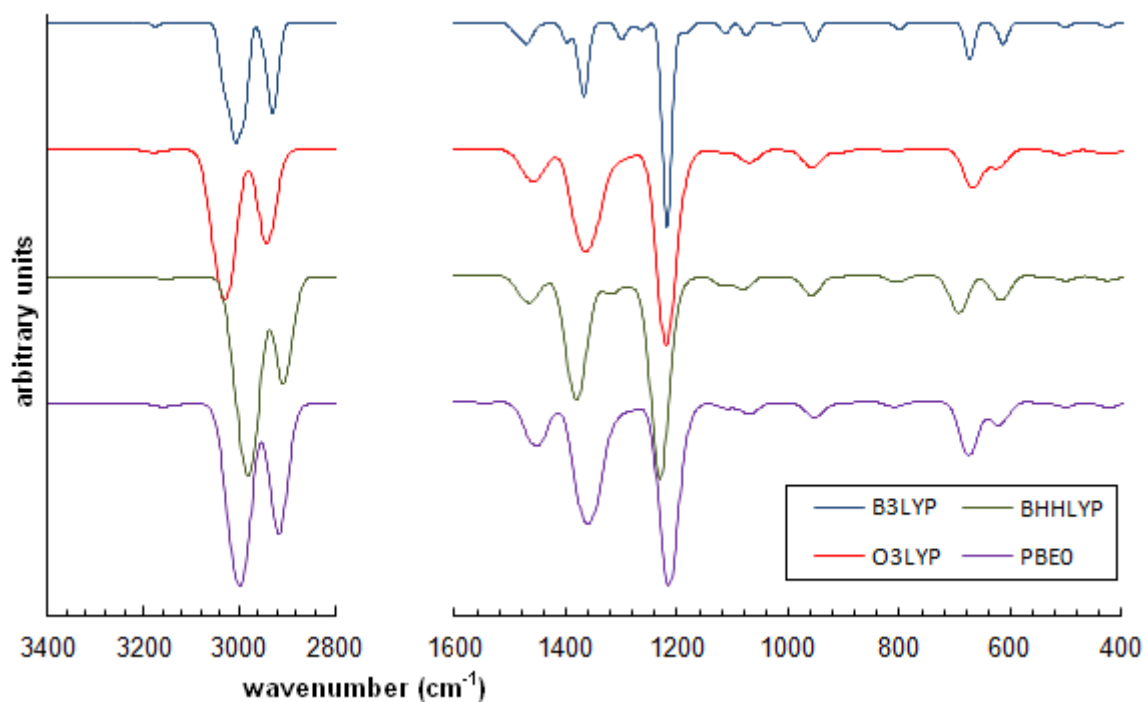


Fig. 47 The predicted IR spectra of NC_1 at B3LYP/6-31(d) level ν (cm^{-1}): 425 (vw), 500 (vw), 546 (vw), 614 (vw), 673 (vw), 800 (vw), 907 (vw), 955 (vw), 1021 (vw), 1076 (vw), 1115 (vw), 1183 (vw), 1218 (s), 1265 (vw), 1301 (vw), 1366 (w), 1397 (vw), 1470 (vw), 2931 (m), 3009 (m), 3180 (vw), at O3LYP/6-31(d) level ν (cm^{-1}): 426 (vw), 508 (vw), 621 (vw), 667 (vw), 814 (vw), 910 (vw), 958 (vw), 1069 (vw), 1113 (vw), 1221 (vs), 1364 (m), 1460 (vw), 2941 (m), 3029 (s), 3180 (vw), at BHHLYP/6-31(d) level ν (cm^{-1}): 421 (vw), 501 (vw), 617 (vw), 693 (vw), 807 (vw), 956 (vw), 1077 (vw), 1120 (vw), 1232 (vs), 1317 (vw), 1381 (s), 1467 (vw), 2906 (m), 2980 (vs), 3155 (vw) and at PBE0/6-31(d) level ν (cm^{-1}): 423 (vw), 500 (vw), 617 (vw), 675 (w), 809 (vw), 952 (vw), 1069 (vw), 1115 (vw), 1215 (vs), 1359 (s), 1454 (w), 1548 (vw), 2916 (s), 2998 (vs), 3159 (vw)

Tab. 17 Measured IR spectra of NC₁

1st synthesis	2nd synthesis	Leites⁵⁶	Assignment⁵⁶
Wavenumber (cm⁻¹)	Wavenumber (cm⁻¹)	Wavenumber (cm⁻¹)	
3109(w)	3109(w)	3110(w)	$\nu_{=CH}^{as}$
3073(w)	3073(w)	3072(w)	$\nu_{=CH}^s$
2976(vs)	2976(vs)	2972(vs)	ν_{CH}^{as} in Me
2932(m)	2931(m)	2927(m)	ν_{CH}^s in Me
2909(sh)	2901(sh)	2904(sh)	$2\delta_{Me}^{as}$
2876(w)	2875(w)	2870(w)	δ_{Me}^s
1686(w)			$\nu_{C=O}$
1672(w)			
1657(w)			
1555(w)	1554(vw)		$\nu_{C=C}$
1476(m)	1475(w)		
1458(m)	1458(w)	1462(s)	δ_{Me}^{as}
1387(s)	1387(s)	1396(m)	δ_{Me}^s
1366(vs)	1365(s)	1366(vs)	$\delta_{=CH}^{as} + \nu_{=C-N}^{as}$
1319(m)	1319(w)	1319(s)	$\nu_{=C-N}^{as} + \delta_{Me}$
1277(m)	1279(w)	1280(m)	$\nu_{=C(II)-N}^{as} + \delta_{Me}$
1234(vs)	1234(vs)	1237(vs)	$\delta_{Me}^s + \delta_{CH} + \nu_{C-C}$
1202(m)	1203(m)	1203(w)	$\nu_{=C(II)-N}^{as}$
1186(sh)	1186(sh)	1186(sh)	$\nu_{=C(II)-N}^s$
1136(w)	1136(w)	1132(w)	$\delta_{=CH}^{as} + \delta_{Me}$
1101(m)	1101(m)	1094(m)	$\delta_{=CH}^s + \nu_{C-C}$
1031(w)	1031(w)	1031(w)	r_{Me}
986(w)	985(w)	985(w)	$\delta_{=CH}^s + \delta_{=C-N}^s$
970(w)	970(w)	969(m)	$\delta_{=CH}^{as} + \delta_{=C-N}^{as}$
922(vw)	922(vw)		
847(w)	847(w)		
827(w)	827(w)	827(m)	r_{Me}
816(w)	816(w)	816(vw)	$\delta_{=CH} + \delta_{N-C(exo)}$
719(s)	719(s)	721(s)	$\rho_{=CH}^{as}$
633w	633w	632(s)	$\rho_{=CH}^s$
567(vw)	567(vw)	568(vw)	ring puckering
519(vw)	519(vw)	518(m)	ring puckering
463(vw)	462(vw)	466(vw)	
444(vw)	444(vw)	443(m)	

HYDROLYSIS OF (UN)SATURATED N-HETEROCYCLIC CARBENES

Eva Kulovaná, Lukáš Richtera, Soňa Hermanová, Josef Jančář

Institute of Materials Chemistry, Faculty of Chemistry, Brno University of Technology, Purkyňova 118, 602 00 Brno, Czech Republic (richtera@fch.vutbr.cz)



Central European Institute of Technology
BRNO | CZECH REPUBLIC

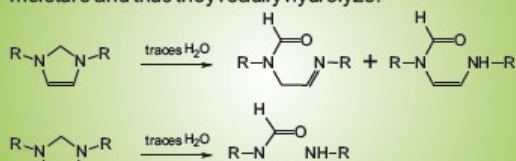


BRNO UNIVERSITY OF TECHNOLOGY
FACULTY OF CHEMISTRY
Purkyňova 118, 602 00 Brno, CZECH REPUBLIC
phone: +420 541 14 91 11, fax: +420 541 21 16 97
http://www.fch.vutbr.cz



INTRODUCTION

Thermally stable heterocyclic diaminocarbenes (NHCs) represent versatile green catalysts for a variety of reactions. Such compounds are very sensitive to moisture and thus they readily hydrolyze.



A new approach towards characterization of reaction components includes a computational study of these compounds and their possible by-products. The results obtained represent a background for interpretation of experimental data.

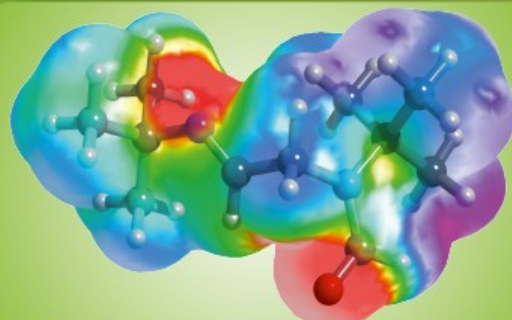
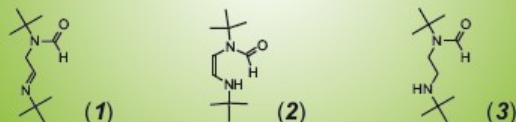


Fig. 1: The electrostatic potential-mapped electron density surface in ArgusLab

EXPERIMENTAL

In this work, the prediction of the structures of *N-tert-butyl-N-[(2E)-2-(tert-butylimino)ethyl]formamide* (**1**), *N-tert-butyl-N-[(Z)-2-(tert-butylamino)ethyl]formamide* (**2**) and *N-tert-butyl-N-[2-(tert-butylamino)ethyl]formamide* (**3**) as possible NHCs hydrolysis products was performed. All structures were optimized at RHF and at DFT level with B3LYP, O3LYP and B3PW91 functional.



RESULTS

Well correlation between experimental and theoretical data was found out for **3** by using B3PW91/6-31+G(d,p).

Tab. 1: Selected bond distances and bond angle calculated at B3PW91/6-31+G(d,p) level

B3PW91/6-31+G(d,p)	Selected bond distance (Å)			Bond angle (°)
	N-C	C-C	N-C	O=C-N
	1.4652	1.5078	1.2676	124.22
	1.4227	1.3528	1.3711	125.45
	1.4725	1.5291	1.4581	124.43

From optimized structures **1-3** vibrational frequencies calculation at RHF and DFT level were performed. All predictions were computed by using PC GAMESS/Firefly.

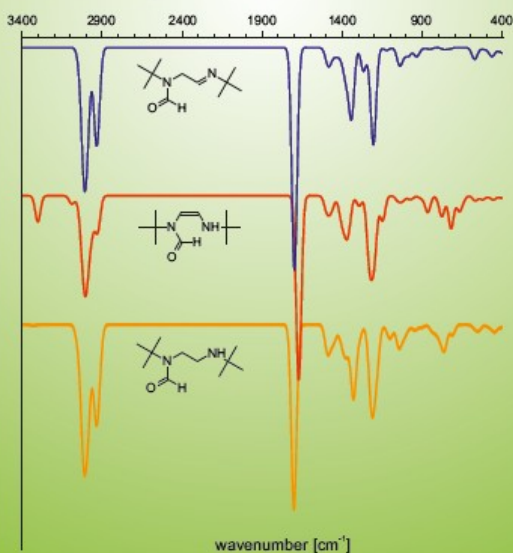
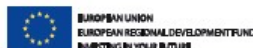


Fig. 2: Predicted IR spectra at B3LYP/6-31G(d) level

ACKNOWLEDGEMENT

This work was supported by the Ministry of Education of the Czech Republic under project no. MSM0021630501.



DONOR-ACCEPTOR COMPLEXES OF TETRAHYDROFURAN WITH SULFUR TRIOXIDE AND SELENIUM TRIOXIDE

Lukáš Richtera¹, Eva Kulovaná¹, Jiří Toužín²

¹Institute of Materials Chemistry, Faculty of Chemistry, Brno University of Technology, Purkyňova 159, 612 00 Brno, Czech Republic (lrichtera@fch.vutbr.cz)

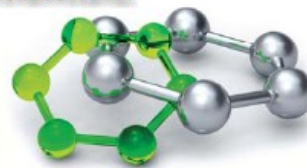
²Department of Chemistry, Faculty of Science, Masaryk University, Kofrova 42, 61137 Brno, Czech Republic



Central European Institute of Technology
BRNO | CZECH REPUBLIC



BRNO UNIVERSITY OF TECHNOLOGY
FACULTY OF CHEMISTRY
Purkyňova 118, 612 00 Brno, CZECH REPUBLIC
phone: +420 541 14 01 11, fax: +420 541 21 16 97
http://www.fch.vutbr.cz



INTRODUCTION

Sulfur and selenium trioxides react as Lewis acids with dialkyl and cyclic ethers to form donor-acceptor complexes having various degree of stability as primary products of this interaction. Quick rearrange of dialkyl ethers complexes to corresponding dialkyl sulfates or dialkyl selenates makes the isolation and subsequent structural characterization of these products more difficult.

In our previous work, donor-acceptor complexes with the formula $\text{Et}_2\text{O} \cdot \text{SeO}_3$ and $(\text{Me}_2\text{O})_2 \cdot \text{SeO}_3$ were synthesized by the reaction of selenium trioxide with dialkyl ethers (R_2O , where $\text{R} = \text{Me}, \text{Et}$)¹. The crystal and molecular structures of both complexes, which are stable only below their melting points, was determined by X-ray structure analysis. Further, crystal and molecular structures of adducts with 1,4-dioxane: $\text{C}_4\text{H}_8\text{O}_2 \cdot \text{SO}_3$ and $\text{C}_4\text{H}_8\text{O}_2 \cdot 2\text{SO}_3$ were determined by X-ray structure analysis and Raman spectroscopy².

Donor-acceptor complexes with cyclic ethers as for example 1,4-dioxane supposed to be more stable towards rearrangement to sulfates or selenates but further reactions such as the ring-opening polymerization could take place.

OBJECTIVE

Some representatives of these intermediates found their application also on industrial scale. Dimethyl sulfate can be manufactured and obtained in an excellent yield and purity on a continuous basis from dimethyl ether and liquid sulfur trioxide³. Complexes of sulfur trioxide with 1,4-dioxane were used in the sulfonation of olefins⁴ and aromatic compounds^{4,5}.

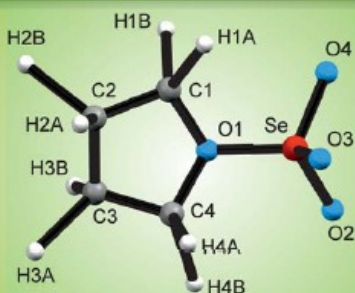


Fig. 1: Simulation of $\text{C}_4\text{H}_8\text{O} \cdot \text{SeO}_3$ structure in HyperChem

EXPERIMENTAL AND RESULTS

In this work, the synthesis of donor-acceptor complexes with the formula $\text{C}_4\text{H}_8\text{O} \cdot \text{SO}_3$ and $\text{C}_4\text{H}_8\text{O} \cdot \text{SeO}_3$ was performed. Tetrahydrofuran (THF) was used in a high excess with respect to trioxide since it functions as solvent for the reaction as well.

The reaction of sulfur trioxide with THF was carried out at -30°C to prevent the decomposition of organic component. Further, the solubility of sulfur trioxide was still sufficient to form a clear solution. Even at this low temperature the concomitant formation of gelous polymeric substance along with white crystalline solid was immediately observed. Unfortunately, all attempts to detect $\text{C}_4\text{H}_8\text{O} \cdot \text{SO}_3$ in reaction mixture failed.

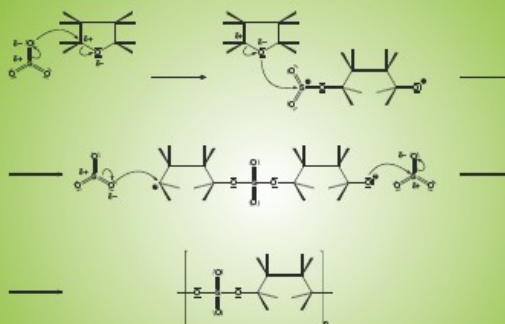


Fig. 2: Proposed mechanism of $\text{C}_4\text{H}_8\text{O} \cdot \text{SO}_3$ decomposition

The reaction of selenium trioxide with THF was carried out under same conditions. Long colourless needle crystals were isolated in a quantitative yield. However, regarding the extreme instability of these adduct, all attempts to isolate the crystals of $\text{C}_4\text{H}_8\text{O} \cdot \text{SeO}_3$ suitable for X-ray structure analysis failed. The identification of the product $\text{C}_4\text{H}_8\text{O} \cdot \text{SeO}_3$ was performed by means of Raman spectroscopy.

References

1. Richtera L., Taraba J., Toužín J.: *Z. Anorg. Allg. Chem.* **629**, 716 (2003).
2. Richtera L., Taraba J., Toužín J.: *Collect. Czech. Chem. Commun.* **71**, 155 (2006).
3. Gilbert E. E.: *Chem. Rev.* **62**, 549 (1962).
4. Suter C. M., Evans P. B., Kiefer J. M.: *J. Am. Chem. Soc.* **60**, 538 (1938).
5. Hurd C. D., Kharasch N.: *J. Am. Chem. Soc.* **69**, 2113 (1947).

ACKNOWLEDGEMENT

This work was supported by the Ministry of Education of the Czech Republic under project no. MSM0021630501.

